ผลของตัวให้อิเล็กตรอนต่อการเกิดพอลิเมอร์ของเอทิลีนและการเกิดโคพอลิเมอร์กับ 1-เฮกซีนเร่งปฏิกิริยาด้วยซีเกลอร์-นัตตาโดยการคำนวณเชิงเคมีควอนตัม

นายสุเทียม เครือวัลย์

จุฬาลงกรณ์มหาวิทยาลัย
Chulalongkorn University

บทคัดย่อและแฟ้มข้อมูลฉบับเต็มของวิทยานิพนธ์ตั้งแต่ปีการศึกษา 2554 ที่ให้บริการในคลังปัญญาจุฬาฯ (CUIR)
เป็นแฟ้มข้อมูลของนิสิตเจ้าของวิทยานิพนธ์ ที่ส่งผ่านทางบัณฑิตวิทยาลัย
The abstract and full text of theses from the academic year 2011 in Chulalongkorn University Intellectual Repository (CUIR)
are the thesis authors' files submitted through the University Graduate School.

วิทยานิพนธ์นี้เป็นส่วนหนึ่งของการศึกษาตามหลักสูตรปริญญาวิทยาศาสตรดุษฎีบัณฑิต
สาขาวิชาเคมี ภาควิชาเคมี
คณะวิทยาศาสตร์ จุฬาลงกรณ์มหาวิทยาลัย
ปีการศึกษา 2558
ลิขสิทธิ์ของจุฬาลงกรณ์มหาวิทยาลัย

EFFECTS OF ELECTRON DONORS ON ZIEGLER-NATTA CATALYZED ETHYLENE POLYMERIZATION AND COPOLYMERIZATION WITH 1-HEXENE BY QUANTUM CHEMICAL CALCULATIONS

Mr. Sutiam Kruawan

A Dissertation Submitted in Partial Fulfillment of the Requirements
for the Degree of Doctor of Philosophy Program in Chemistry
Department of Chemistry
Faculty of Science
Chulalongkorn University
Academic Year 2015
Copyright of Chulalongkorn University

Thesis Title	EFFECTS OF ELECTRON DONORS ON ZIEGLER-NATTA CATALYZED ETHYLENE POLYMERIZATION AND COPOLYMERIZATION WITH 1-HEXENE BY QUANTUM CHEMICAL CALCULATIONS
By	Mr. Sutiam Kruawan
Field of Study	Chemistry
Thesis Advisor	Professor Supot Hannongbua, Dr.rer.nat.
Thesis Co-Advisor	Associate Professor Vudhichai Parasuk, Ph.D.
	Thanyada Rungrotmongkol, Ph.D.

Accepted by the Faculty of Science, Chulalongkorn University in Partial Fulfillment of the Requirements for the Doctoral Degree

.....Dean of the Faculty of Science
(Associate Professor Polkit Sangvanich, Ph.D.)

THESIS COMMITTEE

.....Chairman
(Associate Professor Sirirat Kokpol, Ph.D.)

.....Thesis Advisor
(Professor Supot Hannongbua, Dr.rer.nat.)

.....Thesis Co-Advisor
(Associate Professor Vudhichai Parasuk, Ph.D.)

.....Thesis Co-Advisor
(Thanyada Rungrotmongkol, Ph.D.)

.....Examiner
(Dr.Duangamol Tungasmita, Ph.D.)

.....Examiner
(Assistant Professor Dr.Kanet Wongravee, Ph.D.)

.....External Examiner
(Dr.Oraphan Saengsawang, Dr.rer.nat.)

สุเทียม เครือวัลย์ : ผลของตัวให้อิเล็กตรอนต่อการเกิดพอลิเมอร์ของเอทิลีนและการเกิดโคพอลิเมอร์กับ 1-เฮกซีนเร่งปฏิกิริยาด้วยซีเกลอร์-นัตตาโดยการคำนวณเชิงเคมีควอนตัม (EFFECTS OF ELECTRON DONORS ON ZIEGLER-NATTA CATALYZED ETHYLENE POLYMERIZATION AND COPOLYMERIZATION WITH 1-HEXENE BY QUANTUM CHEMICAL CALCULATIONS) อ.ที่ปรึกษาวิทยานิพนธ์หลัก: ศ. ดร.สุพจน์ หารหนองบัว, อ.ที่ปรึกษาวิทยานิพนธ์ร่วม: รศ. ดร.วุฒิชัย พาราสุข, อ. ดร.ธัญญดา รุ่งโรจน์มงคล, 101 หน้า.

การตรวจสอบเส้นทางของปฏิกิริยาการแทรกสอดของเอทิลีนโดยใช้ตัวเร่งซีเกลอร์-นัตตาในระบบที่มีและไม่มีตัวให้อิเล็กตรอนบนผิวของระนาบผลึก(110) แมกนีเซียมคลอไรด์ของปฏิกิริยาเอทิลีนโฮโมพอลิเมอไรเซชันและเอทิลีนกับ1-เฮกซีนโคพอลิเมอไรไซชันถูกทำให้สำเร็จได้ด้วยวิธีการคำนวณภายในทฤษฎีฟังก์ชันของความหนาแน่น สิ่งแรกคือทำการติดตามปฏิกิริยาการเกิดเอทิลีนโฮโมพอลิเมอไรเซชัน ซึ่งตัวให้อิเล็กตรอนถูกทำให้เกิดจากการผสมแมกนีเซียมเอทอกซีเลท+ซิลิคอนเตตระ คลอไรด์+ไทเทเนียมเตตระคลอไรด์ ได้แก่ $Si(OEt)_mCl_n$ (เมื่อ $m + n = 4$)ในระบบตัวเร่ง การดูดซับของตัวให้อิเล็กตรอนที่ต่างกันทั้งสี่ชนิดบนอะตอมแมกนีเซียมของผิวตัวเร่งถูกตรวจสอบจากพลังงานการดูดซับจากคำนวณแสดงให้เห็นว่าการดูดซับที่แข็งแรงที่สุดของซิลิคอนเตตระเอทอกซีบนผิวระนาบผลึก(110)แมกนีเซียมคลอไรด์ด้วยรูปแบบที่ชอบมากแบบไบเดนเทต จากแผนผังของพื้นผิวพลังงานศักย์ได้บ่งชี้ถึงกลไกของปฏิกิริยาการแทรกสอดของเอทิลีนที่พันธะไทเทเนียม-คาร์บอนศูนย์เร่งว่าเป็นกลไกคอนเซิดเต็ดแบบไม่แท้ เราพบว่าตัวให้อิเล็กตรอนไม่ได้มีแนวโน้มที่จะลดค่าพลังงานก่อกัมมันต์แต่อย่างใดแต่เขาช่วยทำให้สารประกอบเชิงซ้อนที่มีตัวให้อิเล็กตรอนและสารประกอบเชิงซ้อนพายมีความเสถียรมากขึ้นจากการลดพลังงานกระตุ้นปรากฏ ค่าพลังงานกระตุ้นปรากฏที่ได้รับเมื่อเรียงตามลำดับพบว่า ระบบที่ไม่มีตัวให้อิเล็กตรอนมีค่ามากกว่าซิลิคอนเตตระคลอไรด์มอนอเอทอกซีมากกว่าซิลิคอนไดคลอไรด์ไดเอทอกซีมากกว่าซิลิคอนมอนอคลอไรด์ไทรเอทอกซีมากกว่าซิลิคอนเตตระเอทอกซีตามลำดับ ดังนั้นการที่มีตัวให้อิเล็กตรอนในระบบตัวเร่งซีเกลอร์-นัตตาสามารถที่จะลดค่าพลังงานกระตุ้นปรากฏได้ ซึ่งพบว่าซิลิคอนเตตระเอทอกซีคือตัวให้อิเล็กตรอนที่เหมาะสมที่สุดสำหรับปฏิกิริยาของเอทิลีนโฮโมพอลิเมอไรเซชัน ส่วนที่สองคือ การตรวจสอบเส้นทางการแทรกสอดของเอทิลีนที่พันธะไทเทเนียม-คาร์บอนบริเวณไทเทเนียม-เฮกซีนเอทิลีนสายโซ่กำลังโตทั้งระบบที่มีและไม่มีตัวให้อิเล็กตรอนในปฏิกิริยาการเกิดโคพอลิเมอร์เอทิลีนกับ1-เฮกซีน ข้อมูลที่ได้การทดลองพบว่า ระบบตัวเร่งซีเกลอร์-นัตตาที่มีตัวให้ซิลิคอนเทอร์เชียรีมอนอบิวทิลเอทอกซีไดเอทอกซีมอนอไอโซโพรพิลเอทอกซีเป็นตัวเร่งที่มีความว่องไวมากที่สุด ซึ่งโครงสร้างที่เหมาะสมที่ได้จากการคำนวณพบว่าในการจับที่ชอบที่สุดคือแบบไบเดนเทตที่ผิวระนาบผลึก(110)แมกนีเซียมคลอไรด์ จากการคำนวณที่นี่ยังเปิดเผยให้เห็นว่าพันธะคู่ของคาร์บอน-คาร์บอนจากโมเลกุลเอทิลีนที่เคลื่อนที่สามารถสร้างสารประกอบเชิงซ้อนพายที่เสถียรได้ทั้งแบบขนานและแบบตั้งฉากกับพันธะไทเทเนียม-คาร์บอน ในที่สุด สารประกอบเชิงซ้อนซิลิคอนเทอร์เชียรีมอนอบิวทิลเอทอกซีไดเอทอกซีมอนอไอโซโพรพิลเอทอกซี คือ ระบบตัวเร่งที่มีความว่องไวมากที่สุดจากการพบพลังงานก่อกัมมันต์ที่ต่ำที่สุดจากการแทรกสอดของเอทิลีนทั้งจากด้านหน้าและด้านหลังของพันธะไทเทเนียม-คาร์บอนที่ศูนย์เร่ง

ภาควิชา เคมี	ลายมือชื่อนิสิต .....
สาขาวิชา เคมี	ลายมือชื่อ อ.ที่ปรึกษาหลัก .....
ปีการศึกษา 2558	ลายมือชื่อ อ.ที่ปรึกษาร่วม .....
	ลายมือชื่อ อ.ที่ปรึกษาร่วม .....

5273905623 : MAJOR CHEMISTRY
KEYWORDS: ZIEGLER-NATTA CATALYST / DFT CALCULATION / MGCL2 SURFACE / POLYETHYLENE

SUTIAM KRUAWAN: EFFECTS OF ELECTRON DONORS ON ZIEGLER-NATTA CATALYZED ETHYLENE POLYMERIZATION AND COPOLYMERIZATION WITH 1-HEXENE BY QUANTUM CHEMICAL CALCULATIONS. ADVISOR: PROF. SUPOT HANNONGBUA, Dr.rer.nat., CO-ADVISOR: ASSOC. PROF. VUDHICHAI PARASUK, Ph.D., THANYADA RUNGROTMONGKOL, Ph.D., 101 pp.

The investigation of ethylene insertion reaction pathway using Ziegler-Natta catalyst (ZNc) with the presence and absence of electron donors (EDs) systems on the (110) $MgCl_2$ surface of the ethylene homopolymerization and ethylene/1-hexene copolymerization was carried out within the density functional theory (DFT) calculations. Firstly, the ethylene homopolymerization where EDs generated from mixing $Mg(OEt)_2$ + $SiCl_4$ + $TiCl_4$ are $Si(OEt)_mCl_n$ (m + n = 4) in the catalytic system was considered. The coadsorption of four different EDs on the Mg atoms of catalyst surface was also investigated by the adsorption energy (E_{ads}). The calculation shows the strongest coadsorption of $Si(OEt)_4$ on (110) $MgCl_2$ surface with the preferential bidentate mode. The potential energy surface (PES) maps indicated that the reaction mechanism of ethylene insertion to Ti-C bond at active center is pseudo-concerted mechanism. We found that the EDs are not tended to decrease the (intrinsic) activation energy (E_a) but they stabilize the electron donor complexes and π-complexes by decreasing the apparent activation energy (E_{aa}). The obtained E_{aa} values found in the order of absence-ED > $SiOEtCl_3$ > $Si(OEt)_2Cl_2$ > $Si(OEt)_3Cl$ > $Si(OEt)_4$, respectively. Therefore, presence EDs in ZNc system can be lowered the E_{aa} where $Si(OEt)_4$ is found to be the most suitable ED for ethylene homopolymerization. Secondly, the ethylene insertion pathway to the Ti-C bond at the Ti-HE (H=hexane, E=ethylene) growing chain with presence and absence of EDs systems in the ethylene/1-hexene copolymerization was investigated. Based on experimental data, the presence of $Si(OEt)_2$(O*t*Bu)(O*i*Pr) donor molecule is the most active catalyst in which the strongest coadsorption was found. The optimized geometry was found in the preferential bidentate binding mode on (110) $MgCl_2$ surface. The calculation here revealed that the C-C double bond of dynamic ethylene molecule can formed the stable π-complexes either orthogonal or parallel orientation to the Ti-C bond. Finally, the $Si(OEt)_2$(O*t*Bu)(O*i*Pr) complex is the most active catalyst system due to the lowest E_a found from insertion of dynamic ethylene to either back and front side to the Ti-C bond at active center.

Department:	Chemistry	Student's Signature	.....
Field of Study:	Chemistry	Advisor's Signature	.....
Academic Year:	2015	Co-Advisor's Signature	.....
		Co-Advisor's Signature	.....

ACKNOWLEDGEMENTS

Suggestions, encouragement and all assistances from my kind thesis supervisor, Professor Dr.Supot Hannongbua, are gratefully acknowledged. Particular thanks are also given to my thesis co-advisor, Associate Profressor Vudhichai Parakuk and Dr.Thanyada Rungrotmongkol for their suggestions, assistance and personal friendship. I would like to thank Dr.Oraphan Saengsawang from IRPC for experimental data and many useful suggestions. In addition I would like to thank Associate Professor Dr.Sirirat Kokpol, Dr.Duangkamol Tungasmita, and Assistant Professor Dr.Kanet Wongravee for their inputs, interests, valuable suggestions, and comments as committee members and thesis examiners. This would not be successful without kindness and helps from a number people in computational chemistry unit cell (CCUC). I would like to express my gratitude to the former and current members in this research unit.

My deepest gratitude goes to IRPC company for financial support and The 90th year Chulalongkorn university for student scholarship.

จุฬาลงกรณ์มหาวิทยาลัย
Chulalongkorn University

CONTENTS

Page

THAI ABSTRACT iv

ENGLISH ABSTRACT v

ACKNOWLEDGEMENTS vi

CONTENTS vii

LIST OF FIGURES 1

LIST OF TABLES 4

LIST OF ABBREVIATEDS 5

CHAPTER I INTRODUCTION 7

1.1 Introduction of Ziegler-Natta catalyst 7

1.2 α-Olefin polymerization via heterogeneous Ziegler-Natta catalyst 8

1.2.1 Ethylene homopolymerization 8

1.2.2 Ethylene/1-hexene copolymerization 9

1.3 Ziegler-Natta catalytic systems 10

1.3.1 Ziegler-Natta catalyst for ethylene homopolymerization system 11

1.3.2 Ziegler-Natta catalyst for ethylene/1-hexene copolymerization system 13

CHAPTER II THEORETICAL BACKGROUND 15

2.1 Character of Ziegler-Natta Species 15

2.1.1 Characteristic of $MgCl_2$ 15

2.1.2 Characteristic of $MgCl_2$ supported $TiCl_4$ 16

2.1.3 Characteristic of $MgCl_2.TiCl_4$ with AlR_3 21

2.1.4 Characteristic of $MgCl_2/TiCl_4/AlR_3$/electron donor 24

2.2 α-Olefin polymerization mechanism 26

2.2.1 The mechanism of ethylene homopolymerization 26

2.2.2 The mechanism of ethylene /1-hexene copolymerization 27

2.3 Introduction to quantum mechanics 28

2.4 Born-Oppenheimer approximation 31

2.5 Spatial orbital and spin orbitals 32

2.6 The Hartree-Fock approximation 33

Chulalongkorn University

Page

2.7 Density functional theory (DFT) 35
2.8 Basis sets 38
CHAPTER III CALCULATION DETAIL 41
3.1 Model of active Ziegler-Natta catalyst structure 41
3.2 Electron donor systems 42
3.2.1 Electron donors for ethylene homopolymerization 42
3.2.2 Electron donors for ethylene/1-hexene copolymerization 44
3.3 Geometry optimization 44
3.3.2 $MgCl_2$/Donor coadsorption 46
3.3.3 Insertion of ethylene 48
3.3.3.1 Ethylene insertion for ethylene homopolymerization 49
3.3.3.2 Ethylene insertion for ethylene/1-hexene copolymerization 50
3.4 The reaction barrier 51
CHAPER IV RESULTS AND DISCUSSION 52
4.1 Ethylene homopolymerization 52
4.1.1 Conformation of ethyl group 52
4.1.2 $MgCl_2$/donor coadsorption 53
4.1.3 Insertion of ethylene 56
4.2 Ethylene/1-hexene copolymerization 71
4.2.1 MgC_{l2}/Donor coadsorption 71
4.2.2 Ethylene insertion 76
4.2.2.1 Conformation of alkyl group 76
4.2.2.2 PES for absence of electron donor 78
4.2.2.3 Ethylene insertion to Ti-HE 80
CHAPTER V CONCLUSIONS 92
REFERENCES 94
VITA 101

จุฬาลงกรณ์มหาวิทยาลัย
CHULALONGKORN UNIVERSITY

LIST OF FIGURES

Figure 1.1 Ethylene homopolymerization catalyzed by heterogeneous ZNc 9

Figure 1.2 Ethylene/1-hexene copolymerization catalyzed by heterogeneous ZNc ...10

Figure 2.1 Model for a monolayer of $MgCl_2$ crystal showing the most probable surfaces 16

Figure 2.2 Model for a monolayer of a $TiCl_3$ crystal.....17

Figure 2.3 Dinuclear Ti(IV) species on the (104) $MgCl_2$ surface and great separated mononuclear Ti(IV) species on the (110) $MgCl_2$ surface.....18

Figure 2.4 Models obtained from the Raman spectra evidences: $TiCl_4$ molecule absorbed on the (110) $MgCl_2$ surface in an octahedral coordination (model 1), $TiCl_4$ molecule absorbed on the (110) $MgCl_2$ surface in a tetrahedral coordination (model 2), dinuclear $TiCl_4$ species (Ti_2Cl_8) on the (104) $MgCl_2$ surface (model 3)....19

Figure 2.5 Active model of $TiCl_3$ supported on $MgCl_2$ surfaces 21

Figure 2.6 The possible reduction of Ti(IV) to Ti (III) active site by $AlEt_3$ on (110) $MgCl_2$ surface.....22

Figure 2.7 The possible mechanism for active site formation schematically illustrated mononuclear $TiCl_4$ species on the (110) $MgCl_2$ surface.....23

Figure 2.8 Possible binding modes at (110) and (104) $MgCl_2$ surfaces 25

Figure 2.9 Reaction mechanism of ethylene insertion by classical ZNc derived by Cossee-Arlman mechanism 27

Figure 3.1 Titanium configuration relevant as the Corradini model (**a**) and reduction form : Ti(III), $TiCl_2$-CH_2CH_3 **(b)**.....42

Figure 3.2 Assignment of four atoms for dihedral angles for (101) $Mg_{13}Cl_{26}.TiCl_2$-CH_2CH_3.....46

Figure 3.3 Structure of electron donors considered in this investigation for ethylene homopolymerization and ethylene/1-hexene copolymerization.....47

Figure 3.4 Label the adsorption sites at the (110) $Mg_{13}Cl_{26}.TiCl_2$-CH_2CH_3 surface **(a)** binding modes of electron donors to Mg atom: monodentate (**a**), bidentate (**b**) and bridging (**c**).....48

Figure 3.5 Definitions of the two intermolecular distances (*D1* and *D2*) between the incoming ethylene and the (110) $MgCl_2$ surface where the atoms (C_α, Ti, C1

and C2) involved in the ethylene insertion reaction are labeled for homopolymerization **(a)** and copolymerization **(b)**.....51

Figure 4.1 Relative energy profile vs dihedral angles of ethyl on (110) $MgCl_2$ surface and optimum structure (inset).....53

Figure 4.2 The lowest adsorption energy binding mode structures of (110) ED.$Mg_{13}Cl_{26}$.$TiCl_2$-CH_2CH_3 complexes: 1OEt(**a**), 2OEt(**b**), 3OEt(**c**) and 4OEt(**d**)..56

Figure 4.3 PES for ethylene insertion of EA system and covalent complex formation (**a**), The geometries of reactant (R), transition state complex (TS) and product (P) determined from PES of the EA system (**b**), Fully optimized structures of reactant and product for the EA system (**c**) running by MS.....58

Figure 4.4 PES of the ethylene insertion for the EAS systems with presence electron donors:1OEt(**a**), 2OEt(**b**), 3OEt(**c**) and 4OEt(**d**).....61

Figure 4.5 The (**a**) constraint and (**b**) fully optimized structures of reactant (R), transition state complex (TS) and product (P) taken from PES for 1OEt running by MS.....62

Figure 4.6 The (**a**) constraint and (**b**) fully optimized structures of reactant (R), transition state complex (TS) and product (P) taken from PES for 2OEt running by MS.....63

Figure 4.7 The (**a**) constraint and (**b**) fully optimized structures of reactant (R), transition state complex (TS) and product (P) taken from PES for 3OEt running by MS.....64

Figure 4.8 The (**a**) constraint and (**b**) fully optimized structures of reactant (R), transition state complex (TS) and product (P) taken from PES for 4OEt running by MS.....65

Figure 4.9 The optimized structures of reactant (R), transition state complex (TS) and product (P) for **(a)** the 1OEt system **(b)** the 1OEt and (**c**) 2OEt systems running by GAUSSIAN09.....67

Figure 4.10 (a) The optimized structures of reactant (R), transition state complex (TS) and product (P) for the 3OEt and 4OEt systems running by GAUSSIAN09....68

Figure 4.11 Label the bidentate mode at Mg-*B* on the (110) $MgCl_2$ surface (denoted OR_1/OR_3).....72

Figure 4.12 The most stable structures of (110) ED.$Mg_{13}Cl_{26}$.$TiCl_2$-CH_2CH_3 complexes :(**a**) ED2, (**b**)ED3, (**c**) ED4.....75

Figure 4.13 Relative energy profile vs dihedral angles of –CH_2CH_2(CH_2CH_3)(*n*-But) on (110) $MgCl_2$ surface and assignment of four atoms for dihedral angles for

(110) $Mg_{13}Cl_{26}.TiCl_2$- $CH_2CH(CH_2CH_3)$(*n*-But) surfaces (inset) **(a)**, Fully optimized geometry of (110) $Mg_{13}Cl_{26}.TiCl_2$- $CH_2CH(CH_2CH_3)$(*n*-But) front view (**b)**, side view (**c)** running by MS 77

Figure 4.14 (a) Potential energy surface for ethylene insertion of ED0 (110)-$MgCl_2$ and covalent complex formation**, (b-1)** The constraint distance of reactant (R), transition state complex (TS) and product (P) taken from PES and **(b-2)** fully optimized structures of reactant (R_{opt}) and product (P_{opt}) running by MS.....79

Figure 4.15 Definitions of the two intermolecular distances (*D1* and *D2*) between the incoming ethylene and the (110) $MgCl_2.TiCl_2$-$CH_2CH(CH_2CH_3)$(*n*-Bu) surface where the atoms (C_α, Ti, C1 and C2) involved in the ethylene insertion reaction are labeled (**a)** back (**b**) front 80

Figure 4.16 The various states of the ethylene insertion of **ED0** system. The approaching of an ethylene to the Ti active center on $Mg_{13}Cl_{26}.TiCl_2.CH_2CH(Et)$(*n*-But) (**$R_{ED0}$**), the π-complex form as the reactant state, (**TS_{ED0}**) the 4-center covalent bond shortening and elongation as the transition state and (**P_{ED0}**) the product state running by GASSIAN09.....84

Figure 4.17 The various states of the back and front ethylene insertion of ED1 system. The approaching of an ethylene to the Ti active center on $Si(OEt)_4.Mg_{13}Cl_{26}.TiCl_2.CH_2CH_2(CH_2CH_3)$(*n*-Bu) complex, the π-complex form as the reactant state (**R_{ED1}**), the 4-center covalent bond transition state (**TS_{ED1}**) and as the product state (**P_{ED1}**) running by GAUSSIAN09 88

Figure 4.18 The various states of the back and front ethylene insertion of ED2 system. The approaching of an ethylene to the Ti active center on $Si(OEt)_3$(O*i*Pr).$Mg_{13}Cl_{26}.TiCl_2.CH_2CH_2$(Et)(*n*-Bu) complex, the π-complex form as the reactant state (**R_{ED2}**), the 4-center covalent bond as the transition state (**TS_{ED2}**) and as the product state (**P_{ED2}**) running by GAUSSIAN09.....89

Figure 4.19 The various states of the back and front ethylene insertion of **ED3** system. The approaching of an ethylene to the Ti active center on $Si(OEt)_3$(O*t*Bu).$Mg_{13}Cl_{26}.TiCl_2.CH_2CH_2(CH_2CH_3)$(*n*-Bu) complex, the π-complex form as the reactant state (**R_{ED3}**), the 4-center covalent bond as the transition state (**TS_{ED3}**) and as the product (**P_{ED3}**) running by GASSIAN09.....90

Figure 4.20 The various states of the back and front ethylene insertion of **ED4** system. The approaching of an ethylene to the Ti active center on $Si(OEt)_2$(O*t*Bu)(O*i*Pr).$Mg_{13}Cl_{26}.TiCl_2.TiCl_2.CH_2CH_2(CH_2CH_3)$(*n*-Bu) complex, the π-complex form as the reactant state (**R_{ED4}**), the 4-center covalent bond as the transition state (**TS_{ED4}**) and as the product state (**P_{ED4}**) running by GAUSSIAN09 ...91

LIST OF TABLES

Table 4.1 The adsorption energy *(E_{ads})* at different adsorption sites and binding modes of electron donors 1OEt, 2OEt, 3OEt and 4OEt with (110) $Mg_{13}Cl_{26}.TiCl_3$-CH_2CH_3.....54

Table 4.2 Comparison of the *D1*, *D2* and *Ti*-C_α distances between the constraint and fully optimized structures of reactants, transition states, and products for the EA and EAS systems with different ED (*i.e.* 1OEt, 2OEt, 3OEt and 4OEt).....60

Table 4.4 Bond distances changed from reactant state (R) to transition state (TS) and product (P) for all systems running by GAUSSIAN09.....66

Table 4.3 The adsorption energy (E_{ads}), π-complex energy (ΔE_π), (intrinsic) activation energies (E_a) and apparent activation energies (E_{aa}) for the ethylene homopolymerization running by GASSIAN09 70

Table 4.5 The adsorption energies *(E_{abs})* at different adsorption sites and binding modes of (110) ED.$Mg_{13}Cl_{26}.TiCl_3$-CH_2CH_3 (i.e. ED1, ED2, ED2 and ED4) running by MS 73

Table 4.6 Bond distances changed from reactant (R) to transition state (TS) and product (P) of back insertion of ethylene for all systems running by GAUSSIAN09 83

Table 4.7 The (intrinsic) activation energies (E_a) and imaginary frequency values running by GAUSSIAN09.....85

Table 4.8 Bond distances changed from reactant state (R) to transition state (TS) and product (P) for back ethylene insertion from all systems running by GAUSSIAN09 86

LIST OF ABBREVIATEDS

BLYP	Beck Lee-Yang-Parr function
CCD	Chemical composition distribution
DFT	Density functional theory
ECP	Effective core potential
ED	Electron donor
GGA	Generalized gradient approximation
HDPE	High density polyethylene
LCAO	Linear combination of atomic orbital
LLDPE	Linear low-density polyethylene
LDA	Local density approximation
LSDA	Local spin-density approximation
MS	Material studio
MO	Molecular orbital
MW	Molecular weight
MWD	Molecular weight distribution
PBE	Perdew-Burke-Ernzerhof
PE	Polyethylene
PP	Polypropylene

จุฬาลงกรณ์มหาวิทยาลัย
Chulalongkorn University

PES	Potential energy scan
P	Product
QM	Quantum mechanic
R	Reactant
SCF	Self-consistent field
TS	Transition state
VWN	Vosko, Wilk and Nusair
ZNc	Ziegler-Natta catalyst

จุฬาลงกรณ์มหาวิทยาลัย
Chulalongkorn University

CHAPTER I
INTRODUCTION

1.1 Introduction of Ziegler-Natta catalyst

The original of heterogeneous Ziegler-Natta catalyst (ZNc) was discovered since 1953 in Germany for catalyzed α-olefin polymerization reaction: ethylene and propylene homopolymerization. One of scientific breakthrough from heterogeneous ZNc system is using transition-metal compounds (e.g. $TiCl_4$) in a numbery combination with trialkylaluminum (AlR_3) could polymerize ethylene to obtain the high product of linear ethylene homopolymerization, so-called high density polyethylene (HDPE) under the mild conditions of temperature and pressure. In 1954, at the Polytechnic of Milan, other scientific breakthroughs of homopolymerization of propylene were found again with the unexpected product when Natta applied Ziegler's concept to obtain the region and stereoselective polymerization into a partially crystalline and stereoregular so-called isotactic polypropylene (PP) product. These scientific breakthroughs, which allowed Ziegler and Natta to share the Nobel Prize in 1963, were quickly running into industrial realities by Hoechst and Montecatini, with the manufacture and commercialization of HDPE and isotactic PP, respectively. The development of catalysts related α-olefin polymerization technologies and product is still in progress ever since. Over the years, the property envelope of polymerization of α-olefin has been greatly expanded by the generation of improved the polymerization products that obtain the better products from the previously available materials. For example, polymerization of ethylene with another α-olefin comonomer e.g. 1-hexene has led to the synthesis of multiphase copolymers

offering and remarkable balance between rigidity, fluidity, transparency, impact strength etc. Initially, the product from α-olefin polymerization reaction obtained just a few thousand tons. At the present, the production of homopolymerization and copolymerization via heterogeneous ZNc system is approaching a global volume of 65 million tons and growing exponentially in time. This is not only due to the intrinsic properties and performances of these materials but especially to the availability of every more efficient, sophisticated and versatile catalyst systems, and resulting in manufacturing processes. Although in the middle of 1950s, studies of homogeneous ZNc system, titanocene, single-site catalyst has more recently been developed [1], which are based on late transition-metal complexes [2,3] or metallocenes [4-8] that offer a number of advantages over the conventional heterogeneous ZNc systems, but the heterogeneous ZNc system is still at the forefront of the scientific and industrial to account for the majority of global α-olefin polymer market share.

1.2 α-Olefin polymerization via heterogeneous Ziegler-Natta catalyst

1.2.1 Ethylene homopolymerization

The homopolymerization is defined as a polymerization of one type of α-olefin monomer such as ethylene, propylene. Due to the low price cost of polyethylene (PE) product, the worldwide annual total from polymerization of α-olefin production is approximately produced 19.6 and 31 million tons of linear low-density polyethylene (LLDPE), high-density polyethylene (HDPE), respectively. The product is widely used for packaging such as film, bags, sealing, bottles etc. Moreover, another important PE product is used for piping and tubing, because it has

a good chemical resistance and strength, thus, the reactions are highly influenced by the polymerization conditions, kinetics and catalyst. Polymer products that can be synthesized with ZNc is not only homopolymerization, a number of polymerization can be formed by this catalyst. Finally, this present work would investigate to the ethylene homopolymerization via heterogeneous ZNc system (**Figure 1.1**).

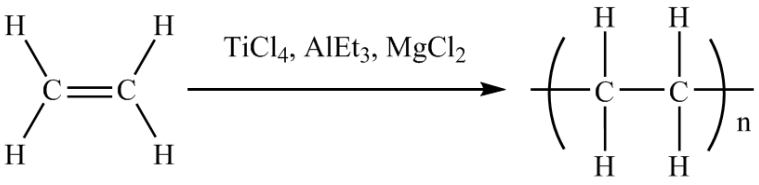

Figure 1.1 Ethylene homopolymerization catalyzed by heterogeneous ZNc

1.2.2 Ethylene/1-hexene copolymerization

The copolymerization is defined as the polymerization between two different kinds of monomers such as ethylene with another α-olefin comonomer e.g. propylene or 1-hexene etc. A wide range of copolymers can be synthesized using heterogeneous ZNc. Each polymerization products have its own distinct properties and an enormous range of different plastics can be synthesized through suitable choices of monomers, comonomer and reaction conditions. The copolymerization of ethylene introduced with other α-olefin monomers can form linear low-density polyethylene (LLDPE) product which leads to reduce the crystallinity and melting temperature. Consequently the product obtained will have a series of physical properties. Due to presence of multi active sites, linear low-density polyethylene (LLDPE) are formed with broad molecular weight distribution (MWD) and chemical composition distribution (CCD) [9]. If the comonomer is found to be highly enriched in fraction, product forming will

be formed in a low molecular mass which cause the unfavorable for CCD and poor polymer properties. Therefore, there are strong demands to improve the LLDPE and CCD of the product formed based on heterogeneous ZNc by broad MWD and narrow CCD [10-15]. This could be realized by modifying the copolymerization properties of heterogeneous ZNc. The modification of copolymerization properties can be related to the homopolymerization rates of the individual commoners which have distinct composition. Ethylene homopolymerization proceed significantly faster than those of other α-olefins, and as a result, the copolymer formed in the reaction of ethylene and another monomer will be made up mostly of ethylene. The reactivity of the monomers is not the only factor determining the composition of a copolymer. The reaction conditions, structure of the catalyst, identity of the cocatalyst, and particular combination of monomers have also been shown to be important. Therefore, in this work would also determine the ethylene/1-hexene copolymerization via heterogeneous ZNc system. (**Figure 1.2**)

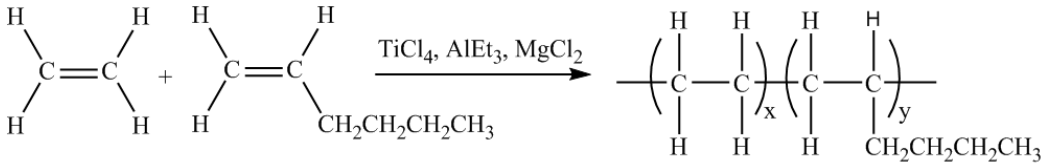

Figure 1.2 Ethylene/1-hexene copolymerization catalyzed by heterogeneous ZNc

1.3 Ziegler-Natta catalytic systems

Since the $TiCl_4/Al(Et)_3$ catalytic system was originally discovered, the α-olefin polymerization has been an enormous impact in the petrochemical industry. The conventional heterogeneous ZNc system consisting of $TiCl_4$ supported on a $MgCl_2$ substrate was later on found. However, many literatures reported many

possible structures of active centers in ZNc. A few general features of the active centers where is the α-olefin polymerization mechanism can be explained as follows:

i) The active centers are on the surfaces of catalyst surface particle

ii) The active centers contain Ti atoms

iii) The active centers are generated between Ti species ($TiCl_4$) in the catalyst and organomettallic co-catalyst ($AlEt_3$)

iv) At initial of of *α*-olefin polymerization reactions, the alkyl groups from the co-catalyst ($AlEt_3$) form the initial 'starting ends' of polymer chain

v) From the growing reaction of a polymer chain is an insertion reaction of the C=C double bond of a *α*-olefin monomer into the *Ti-C* bond in the active center.

Most other aspects of the polymerization mechanism and the chemical structure of the active centers are much less clear; some of them are often contested. Although extensive experimental studies on heterogeneous ZNc have been proposed the basic mechanism, however in this present work we try to fill this gap and density function theory (DFT) studies were undertaken in an attempt to model possible mechanism for insertion step mechanism.

จุฬาลงกรณ์มหาวิทยาลัย
Chulalongkorn University

1.3.1 Ziegler-Natta catalyst for ethylene homopolymerization system

The preparation method of the catalyst by mixing of $Mg(OEt)_2$ precursor with $TiCl_4$+$AlEt_3$+$SiCl_4$ which result in formation on active $MgCl_2$ crystalline and supported $TiCl_4$ and a Lewis base (an Electron Donor, ED, e.g $SiCl_m(OEt)_n$ when m +

n = 4) with formation of catalyst precursor. Finally, to generate active sites on the $MgCl_2$ surface, the pre-catalyst is activated by addition of trialkylaluminum ($AlEt_3$).

Characterization studies of $MgCl_2$ supported ZNc corresponding to the more stable (104) and less stable (110) $MgCl_2$ surface. However, calculations indicated that $TiCl_4$ coordination to the (104) $MgCl_2$ surface is rather weak or even unstable, whereas $TiCl_4$ coordination to the (110) surface is energetically quite favored [16,17]. Therefore, this present work was investigated the active catalyst as only (110) $MgCl_2$ surface.

In order to model active catalyst, Ti species on (110) $MgCl_2$ surface was generally considered. A wide variety of the $TiCl_4$ species on these surfaces were proposed, but that which have no Cl vacancies at the Ti atom are the most interesting since Raman spectroscopy shows that stable Ti complexes in the $TiCl_4/MgCl_2$ system include bound $TiCl_4$ molecules with Ti atoms in octahedral surroundings. There are known to be two stable $TiCl_4$ surface complexes corresponding to this condition: mononuclear Ti atom on the (110) $MgCl_2$ surface. The complexes may simultaneously exist on the activated $MgCl_2$ surface since they are located on the different $MgCl_2$ planes.

On the mechanism to improve by addition ED for polypropylene polymerization, the first microscopic proposal was made by Busico, Corradini, and their coworker.[18] They propose that (110) $MgCl_2$ surface are preferentially poisoned by selective adsorption of donors, which prevents the formation of the aspecific mononuclear Ti atom on the surface and increases the fraction of the isospecific dinuclear Ti atom on the 104 surface. Therefore, these will be suggested

that the active site catalyst structures are sensitive to ED may involve to polyethylene polymerization. Moreover, Busico *et. al* postulated a three-site model as a versatile active site image in $MgCl_2$-supported ZN-catalyst, which was modified by Terro *et. al* [19] In our calculation only one model describes the active site catalyst is (110) $MgCl_2$ surface supported mononuclear Ti atom with absence or presence of EDs ($SiCl_mOEt_n$, $m + n = 4$), O or donor, at the neighboring under coordinated metal sites: Mg. The idea is still evidenced by few aspects such as stronger adsorption on $TiCl_4$ on the 110 or 104 surfaces for ethylene polymerization. Many other aspects remain was not clarified such as energetic feasibility of the coadsorption of donors, steric interactions upon coadsorption and energy barriers.

1.3.2 Ziegler-Natta catalyst for ethylene/1-hexene copolymerization system

This presence work was emphasized the of ethylene/1-hexene copolymerization. The ethylene/1-hexene copolymerization in the classical ZNc system improved MWD dramatically by presence ED in the catalytic system was reported by Zhi Liu *et al.* [20]. In the conventional ZNc with ED, they found that the ED species adding in the reaction have different ability to increase the fraction of 1-hexene in the polymer chain product as in the order $Si(OEt)_4$ < $Si(OEt)_3(OiPr)$ < $Si(OEt)_3(OtBu)$ < $Si(OEt)_2(OiPr)(OtBu)$ (where, Et = ethyl, *i*Pr = isopropyl and *t*Bu = *tert*-butyl). Therefore, this aim of this work is investigated the different ability of 4 EDs in the ZNc system for ethylene/1-hexene copolymerization, adsorption energy, (intrinsic) activation energies with presence and absence of EDs by DFT calculation.

The model of active catalyst for ethylene/1-hexene copolymerization was used as the same as the ethylene homopolymerization as mentioned earlier: (110) $MgCl_2$ surface supported mononuclear Ti atom.

The aim of the present study is also to offer convincing conclusion on the ethylene insertion mechanism for electron donors to modify the ethylene homopolymerization performance of ZNc by DFT calculation. For this purpose, we have performed a reliable level and amount of DFT calculations to compare the obtained results of (intrinsic) activation energies (E_a) and the systems of presence and absence of electron donors, $SiCl_3OEt$, $SiCl_2(OEt)_2$, $SiCl(OEt)_3$ and $Si(OEt)_4$. DFT calculation was chosen, since this method gave the good agreement with the experimental E_a of α-olefin insertion among several methods.

จุฬาลงกรณ์มหาวิทยาลัย
Chulalongkorn University

CHAPTER II
THEORETICAL BACKGROUND

2.1 Character of Ziegler-Natta Species

The role of each species of classical ZNc system: $MgCl_2$ + $TiCl_4$ + $AlEt_3$ to the ethylene homopolymerization and ethylene/1-hexene copolymerization were considered in the molecular level. Additionally, to understand in the microscopic level of EDs included in the catalytic system were also considered here.

2.1.1 Characteristic of $MgCl_2$

The $MgCl_2$ using for heterogeneous ZNc can be used directly or prepared from its derivatives with chlorinating agent such as $Mg(OR)_2$ with $TiCl_4$, $SiCl_4$ [21]. The heterogeneous ZNc occur at the surface of $MgCl_2$ crystal where $TiCl_3$ supported on its surface as the active sites due to they have the similar crystal structure. The $MgCl_2$ surfaces have Cl-Mg-Cl consist of irregularly stacked like sandwich monolayer characterized by the presence of crystal surfaces that are consisted by Mg atoms with unsaturated coordination. The surfaces have been designated as (104) and (110) $MgCl_2$ for five and four coordinated to Cl atoms in the bulk, making these sites Lewis acidic (**Figure 2.1**) [22].

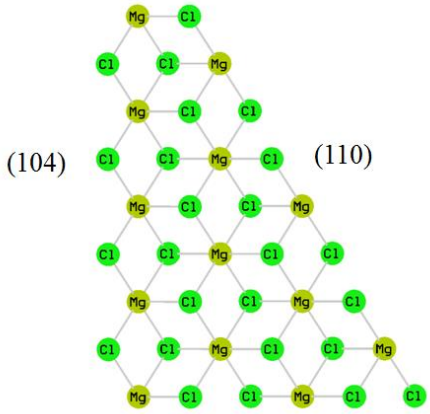

Figure 2.1 Model for a monolayer of $MgCl_2$ crystal showing the most probable surfaces

According to the α-olefin polymerization using ZNc occurs at the surface, the stability of two surfaces $MgCl_2$ should be discussed here, (110) and (104). Due to the Mg atoms in the bulk has 6 coordinatively octahedral Cl atoms, thus the (104) $MgCl_2$ is more stable than (110) $MgCl_2$ surfaces because the coordinated Cl atoms are 5 and 4 respectively [23,24]. Moreover, the degree of acidity of (110) $MgCl_2$ surface is more than (104) $MgCl_2$.

จุฬาลงกรณ์มหาวิทยาลัย
Chulalongkorn University

2.1.2 Characteristic of $MgCl_2$ supported $TiCl_4$

As mentioned earlier, the discovery of heterogeneous ZNc based on $MgCl_2$, or with its precursors e.g. $Mg(OR)_2$ (or other derivative transformed into $MgCl_2$ while preparing the catalyst) can be determined as a major breakthrough of both scientific and industrial. Initially with unexpectedly discovered, the $MgCl_2$ supported on $TiCl_4$ based on heterogeneous ZNc is considered.

Base on the scientific method, two main reasons of Mg^{2+} could support Ti(IV) (and Ti(III) in active form) in the molecular level was discovered. Firstly, the similar ionic radii of Mg^{2+} and Ti(IV) ions [18] (Pauling ionic radius: Mg^{2+} = 0.65 Å, Ti(IV) = 0.68 Å) and the isomorphism of the crystal structure of $MgCl_2$ (α and β forms) and the crystalline structure of $TiCl_3$ (γ and δ). Secondly, both Mg^{2+} and Ti(III) ions have the same octahedral geometry and similar bond lengths M-Cl (Mg-Cl = 2.57 Å and Ti-Cl = 2.51 Å) [25]. This is possible to make $TiCl_4$ adsorbed on the $MgCl_2$ surface where the α-olefin polymerization reaction occurred.

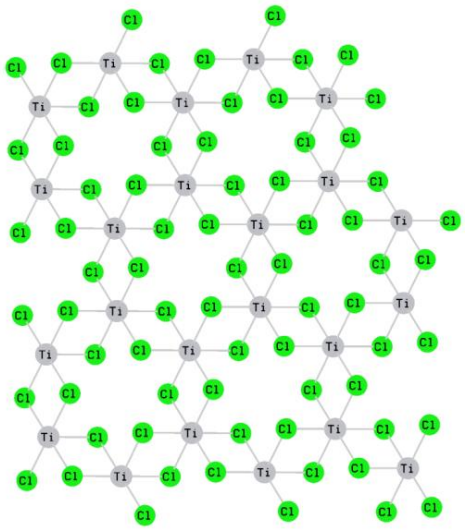

Figure 2.2 Model for a monolayer of a $TiCl_3$ crystal

According to the isomorphism of $MgCl_2$ with $TiCl_4$, $MgCl_2$ allowed the adsorption of $TiCl_4$ on the of $MgCl_2$ surface, the formation of catalytic sites, which are identical to those present on the surface of pure $TiCl_3$ (**Figure 2.3**) [26,27].

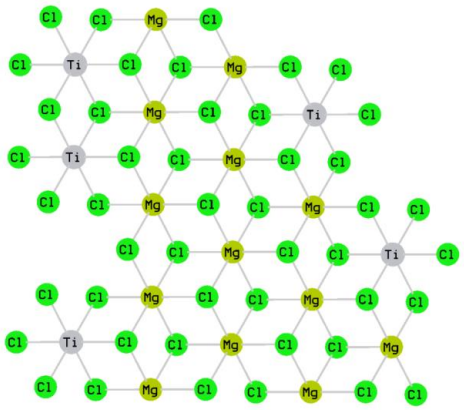

Figure 2.3 Dinuclear Ti(IV) species on the (104) $MgCl_2$ surface and great separated mononuclear Ti(IV) species on the (110) $MgCl_2$ surface

Brambilla *et al.* proposed the structure of the complexes formed by $TiCl_4$ molecule reacted with $MgCl_2$ during the precatalyst preparation from experiment. The $TiCl_4$ molecules can form the complexes with $MgCl_2$ surface both (110) and (104) $MgCl_2$ surfaces. The mononuclear ($TiCl_4$) and dinuclear Ti atom (Ti_2Cl_8) supported on both surfaces could be possible (**Figure 2.4**) [28].

The experimental from FT-Raman spectra evidences found that three different types of complexes were formed, model 1 (mononuclear Ti atom on (110) $MgCl_2$), model 2 (mononuclear Ti atom on (110) $MgCl_2$) and model 3 (dinuclear Ti atoms on (104) $MgCl_2$) (**Figure 2.5**).

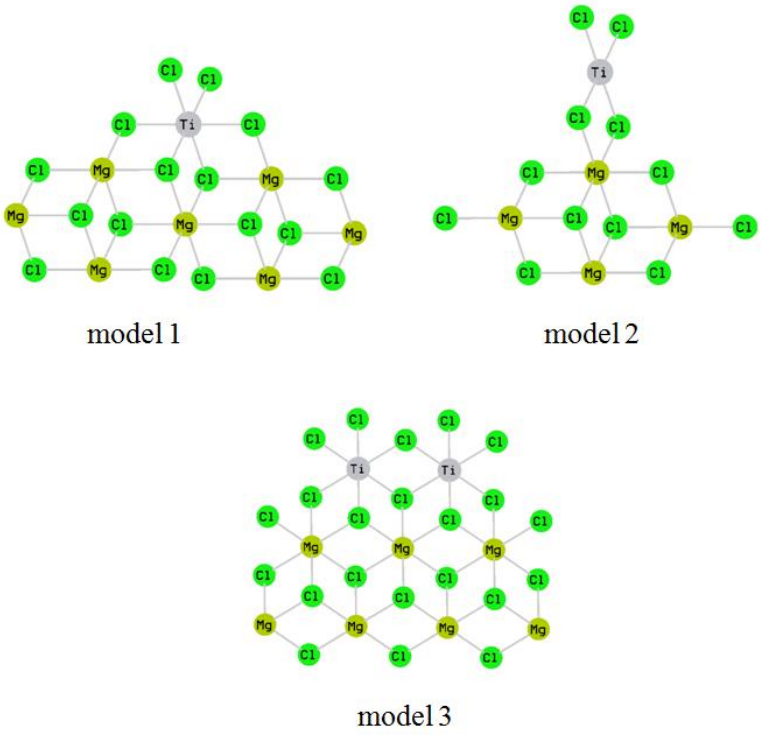

Figure 2.4 Models obtained from the Raman spectra evidences: $TiCl_4$ molecule absorbed on the (110) $MgCl_2$ surface in an octahedral coordination (model 1), $TiCl_4$ molecule absorbed on the (110) $MgCl_2$ surface in a tetrahedral coordination (model 2), dinuclear $TiCl_4$ species (Ti_2Cl_8) on the (104) $MgCl_2$ surface (model 3).

Chulalongkorn University

This observation from the experiment showed that the more stable complex of $TiCl_4$ is absorbed on (110) $MgCl_2$ crystallites surface (model1). From DFT quantum chemical calculations have been carried out on molecular models to predict the Raman spectra. The less stable and minority species could be the dinuclear Ti atom, Ti_2Cl_8 complexes on the (104) $MgCl_2$ surface (model 3). Quantum chemical energy calculations support these hypotheses because the mononuclear Ti atom species along (110) $MgCl_2$ surface was found to have higher complexation energy on $MgCl_2$ crystal

with respect to the dinuclear Ti atoms on the (104) $MgCl_2$ surface. The experimental observations can be summarized as follows:

i) during the milling process mononulcear and dinuclear Ti atom species are formed

ii) the mononuclear Ti atom ($TiCl_4$) easily complex along the (110) surface

iii) the dinuclear Ti atoms (Ti_2Cl_8) difficultly complex along the (104) surface

iv) the dinuclear Ti atoms (Ti_2Cl_8) are removed by washing with solvents

Therefore, the mononuclear species are the major complex of $TiCl_4$ with the $MgCl_2$ also in the ZNc systems. This present work use the catalytic model only (110) $MgCl_2$ surface absorbed with mononuclear Ti atom for both ethylene homopolymerization and ethylene/1-hexene polymerization.

Theoretical studies have suggested that $TiCl_4$ absorbs on both (110) and (104) $MgCl_2$ surfaces. The adsorption of $TiCl_4$ on the (110) surface of $MgCl_2$ is strong, while the adsorption on the (104) face is weak [16,29-31]. There are three possible active sites to describe the adsorption between $TiCl_4$ and $MgCl_2$. These models are designed as Corradini, edge and slope sites (**Figure 2.6**) [22,32,33]. In the Corradini model, the Ti atom has two bridging chlorine atoms and two surface chlorine atoms, making it five-coordinate ((104) $MgCl_2$ surface). The Corradini model has only one vacant site for monomer and base coordination. The edge site has two bridging chlorine atoms both bonded to a single Mg atom. The slope site involves five-coordinate Mg atoms, and Ti is bonded to two bridging chlorine atoms to form a four-coordinate active site. The slope model has two vacant sites after alkylation and is

suitable for the monomer and ED. The edge and Corradini sites involve four-coordinate Mg atoms ((110) $MgCl_2$ surface) and are more acidic than the slope sites, as they involve five-coordinate Mg atoms (104) surface.

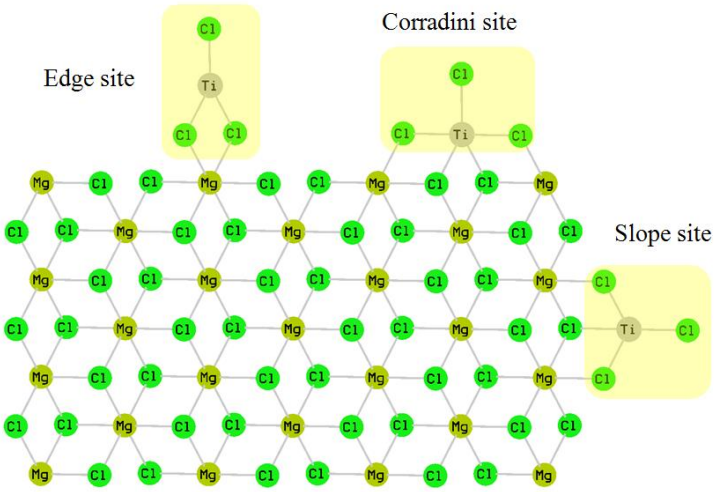

Figure 2.5 Active model of $TiCl_3$ supported on $MgCl_2$ surfaces

2.1.3 Characteristic of $MgCl_2.TiCl_4$ with AlR_3

The active site of $MgCl_2.TiCl_4$ was generated after mixing with an alkylating reducing species, such as trialkylaluminum, AlR_3 (R is alkyl group such as $AlEt_3$ (Et = $-CH_2CH_3$) [34,35] . The $TiCl_4$ molecule adsorbed on $MgCl_2$ surface are generally suggested to be activated by reduction with trialkylaluminum, $AlEt_3$ to become Ti(III) and to some degree of Ti(II) species located on (110) $MgCl_2$ surfaces (**Figure 2.7**).

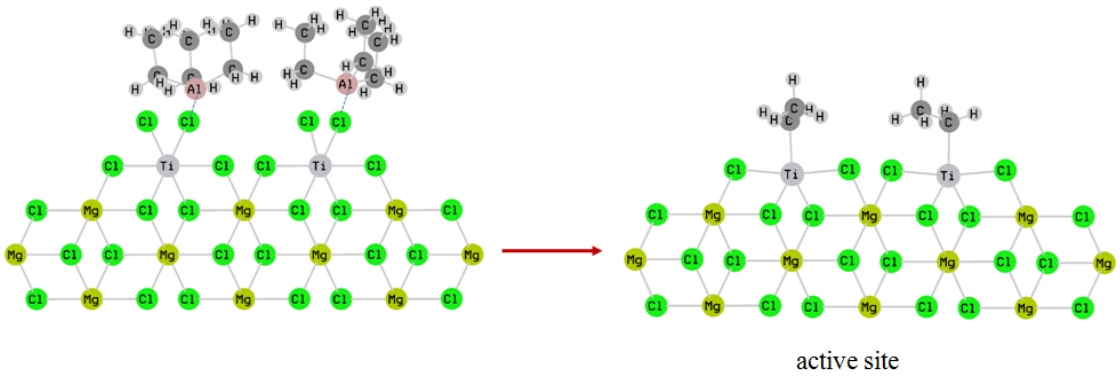

Figure 2.6 The possible reduction of Ti(IV) to Ti (III) active site by $AlEt_3$ on (110) $MgCl_2$ surface

From DFT calculation, Denis S. and Vladimir Z. has proposed the types of chemical reactions occur at the active center [36]; reduction, alkylation, and complexation of Ti species by trialkylaluminum compounds. As mentioned earlier, Ti atoms in an octahedral Cl coordination are the most preferable in the $MgCl_2$.$TiCl_4$ system, mononuclear $TiCl_4$ complex on the (110) $MgCl_2$ surface and dinuclear Ti_2Cl_8 complex on the (104) $MgCl_2$ surface can be considered as the most plausible precursors of active centers, and so reaction of such Ti species with trialkylaluminum must generate the basic variety of active centers in the catalyst. Interaction of the surface Ti(IV) species with trialkylaluminum includes the following processes: reduction of Ti(IV) species to Ti(III) and Ti(II) species, alkylation of Ti species with formation of Ti−C bonds, and complexing between the reduced Ti species and $AlCl_xR_{3-x}$ compounds

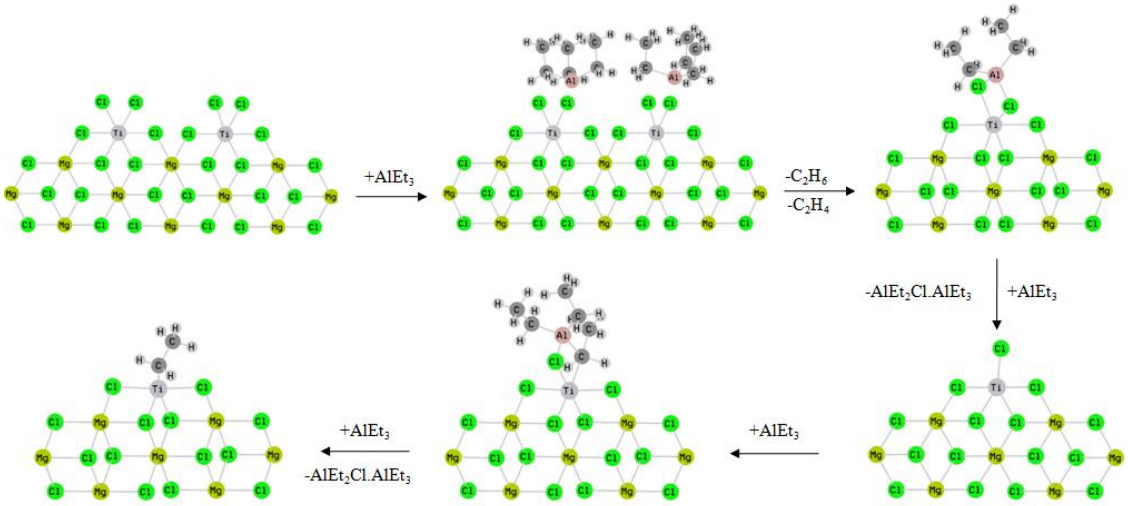

Figure 2.7 The possible mechanism for active site formation schematically illustrated mononuclear $TiCl_4$ species on the (110) $MgCl_2$ surface

They proposed that the most possible way of active center formation with $MgCl_2.TiCl_4$ after Ti(IV) reduced by mixing $AlEt_3$ can be postulated in **Figure 2.7**: firstly, Ti(IV) centers in six-coordinated Cl surroundings are reduced by $AlEt_3$ with formation of complexes $TiCl_3.AlEt_2Cl$; then $AlEt_3$ eliminates $AlEt_2Cl$ due to formation of complexes $AlEt_2Cl.AlEt_3$ and at the same time complexes $TiCl_3.AlEt_3$ and $TiCl_3.2AlEt_3$ are formed; finally $TiCl_3.2AlEt_3$ complexes are decomposed with formation of $TiCl_2$-Et species, the structures generally proposed as active sites for α-olefin polymerization. Finally, after mixing $MgCl_2.TiCl_4$ with $AlEt_3$ it became $MgCl_2.TiCl_2$-Et at the active center and readily for the next step: monomer of α-olefin begins to start react as the α-olefin polymerization reaction. Therefore, the discussion here focus only to the (110) $MgCl_2.TiCl_2$-CH_2CH_3 surface as a mononuclear titanium.

2.1.4 Characteristic of $MgCl_2/TiCl_4/AlR_3$/electron donor

Over the period of time, ZNc has been improved from the simple system $TiCl_4/MgCl_2$ species to $TiCl_4/MgCl_2$/electron donor (ED) system. The ED is a Lewis base that can be added during catalyst preparation (internal donors e.g. alkoxysilane, 1,3-diethers, aromatic esters) or possible mixed with a second electron donor with alkylating reducing species (AlR_3) (external donor e.g. succinate). In principle, ED can interact with $MgCl_2.TiCl_4$, $MgCl_2.TiCl_2$-CH_2CH_3, $TiCl_4$ and reducing agent (AlR_3) species in ZNc system. However, when ED interacts with Lewis acids e.g. AlR_3 and $TiCl_4$ species, in this case, the undesired by product is formed. Generally, the EDs have been assumed to stabilize the primary $MgCl_2$ crystal and/or to influence the distribution of $MgCl_2.TiCl_4$ complex in the final catalyst. In the other hand, the ED has to compete with $TiCl_4$ to coadsorb on the $MgCl_2.TiCl_4$ surfaces complex. This phenomenon possibly assumed that it leads to the stereoselectivity of homopolymerization of PP final product. Although the role of ED in homopolymerization mechanism of PP has widely mentioned from the literatures, for ethylene homopolymerization and ethylene/1-hexene copolymerization have rarely mentioned. Therefore, our research attempt to investigate the influence of ED effect to the two reactions: ethylene homopolymerization reaction and ethylene/1-hexene copolymerization, in the molecular level.

In the molecular level, all of EDs mentioned above have electron donor atoms at the Lewis basic site, mostly O atoms. Therefore, the site in which the donors can bind to the $MgCl_2.TiCl_2$-CH_2CH_3 surface is considered. Typically, it is believe that there are three binding modes in which oxygen atoms that can bind to $MgCl_2.TiCl_2$-CH_2CH_3 surface:

i) one Mg atom at the surface coordinated with one O atom from donor molecule, the ‘monodentate’ binding mode

ii) one Mg atom at the surface coordinated with two O atoms from donor molecule, the ‘bidentate’ binding mode, and

iii) two Mg atom the surface coordinated with two O atoms from donor molecule, the ‘bridging’ binding mode

The double head arrow curves as shown in **Figure 2.8** represent the possible binding modes at the $MgCl_2$ surfaces.

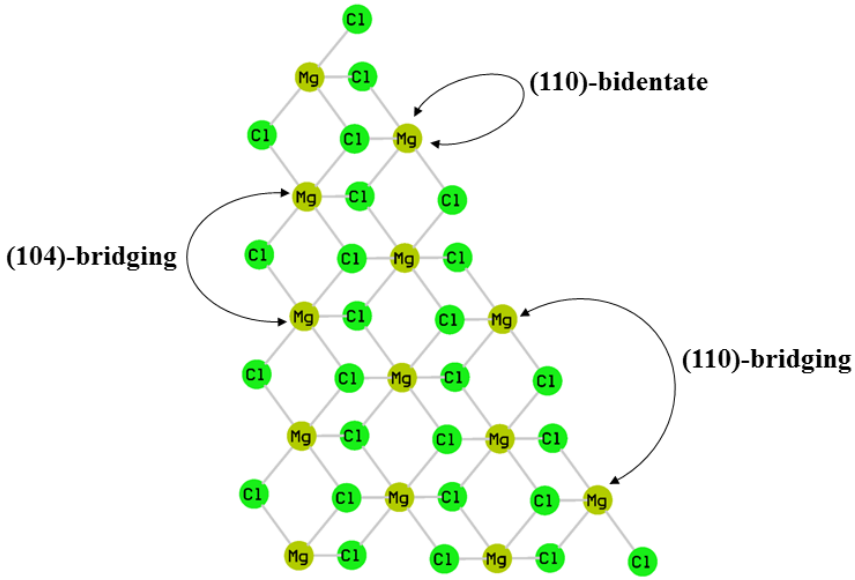

Figure 2.8 Possible binding modes at (110) and (104) $MgCl_2$ surfaces

2.2 α-Olefin polymerization mechanism

2.2.1 The mechanism of ethylene homopolymerization

Over the year, many literatures have been studying to clarify the mechanism of ethylene homopolymerization with classical ZNc, $MgCl_2.TiCl_4$ [29,37,38]. Nevertheless, due to the chemical complexity of the system where the exact nature of the active center is not yet fully understood, very few efforts have been devoted to clarify the mechanism of this reaction. Despite these difficulties, Cossee and Arlman have proposed a widely accepted mechanism [39-41]. While Cossee proposed that the active center model is an octahedrally coordinated Ti atom, Arlman proposed that the reaction occur at the vacancies presence on the surface of the crystal. The basic mechanism of the insertion step of polyethylene polymerization is shown in **Figure 2.9**. This ethylene insertion reaction mechanism is divided into 3 steps:

i) The dynamic ethylene molecule forms π-complex with *Ti-*C_α as a reactant (**R**),

ii) 4-center covalent transition state complex: *D1* (C1-C_α) and *D2* (C2-Ti) are forming while *Ti-*C_α is elongating as transition state complex (**TS**), and

iii) the ethylene completed insertion, product (**P**) is formed.

In this work, DFT calculations have been employed throughout to this study.

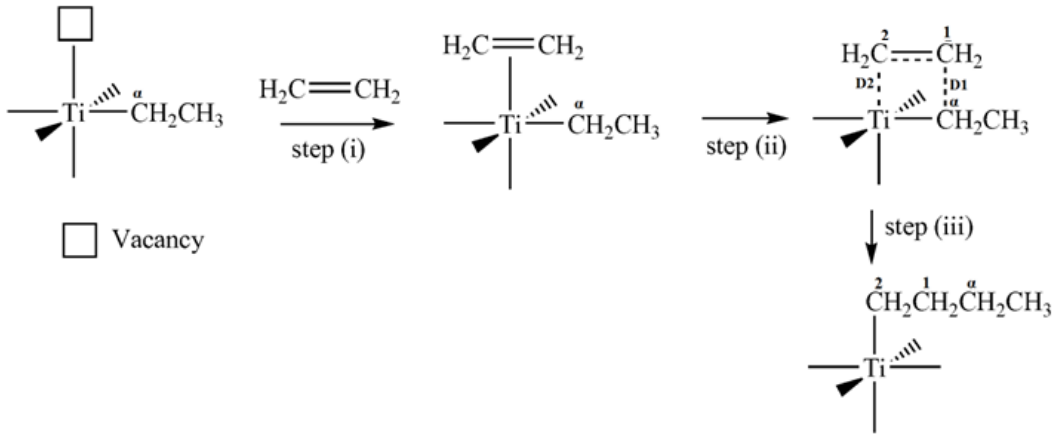

Figure 2.9 Reaction mechanism of ethylene insertion by classical ZNc derived by Cossee-Arlman mechanism

2.2.2 The mechanism of ethylene /1-hexene copolymerization

Overall copolymerization reaction between ethylene with 1-hexene is shown in **Figure 1.2**. For ZNc system, the active site of ZNc at surface was mentioned earlier. When ethylene and 1-hexene comonomer are formed product at the active center, over a dozen reaction pathways are possible due to the 1-hexene comonomer has significant possible orientation when approaching to growing chain at active center. The model examined in this present work is attempting to describe the experimentally observed relative to the insertion barriers of ethylene and 1-hexene. According to dynamic1-hexene molecule has much more steric than ethylene when they are approaching to the bulk growing chain at the active center, for example through an ED-complexed at catalyst surface adjacent to the Ti atom. Therefore, the modification of ED in the catalytic system should favor ethylene insertion over 1-hexene insertion. Therefore, the mechanism postulate for this work will focus to ethylene insertion over 1-hexene insertion which proposed by Cossee-Arlman

2.3 Introduction to quantum mechanics

In the late seventeenth century, physicists found that objects can be described as the rigid body particles with mass, $\boldsymbol{m}$. Their properties could be calculated according to classical mechanics such as

$$\boldsymbol{E_{kin} = \frac{1}{2}mv^2} \tag{2.1}$$

$$\boldsymbol{F = ma = \frac{dp}{dt} = \frac{d(mv)}{dt}} \tag{2.2}$$

where $\boldsymbol{E_{kin}}$ is kinetic energy, $\boldsymbol{F}$ is the force acting on particle, $\boldsymbol{v}$ is the velocity of the object, $\boldsymbol{p}$ is the momentum of the object, $\boldsymbol{t}$ is the time progresses

In the early twentieth century, it found that only classical mechanics alone cannot describe several phenomena especially for very small objects such as electrons and nuclei of atom and molecule. The behavior of such objects is explained by a set of laws call quantum mechanics (QM).

An understanding of the behavior of the objects, Schrödinger wave equation is usual formulation for solving QM problems or chemical problems. This equation is based on the concept of dual properties, all matter exhibits both wave-like and particle-like properties. According to Louis de Broglie suggested that the motion of very small particle might have a wave-like property aspect: that an particle of mass, $\boldsymbol{m}$, and speed $\boldsymbol{v}$ would have a wavelength, $\boldsymbol{\lambda}$, associate with it, where the linear momentum is $\boldsymbol{p}$.

$$\boldsymbol{\lambda = \frac{h}{mv} = \frac{h}{p}} \tag{2.3}$$

Where $\boldsymbol{h}$ is Plank's constant.

Hence, following this concept and mathematical description of the differential equation for the standing wave, Erwin Schrödinger proposed an equation that bears his name

$$\boldsymbol{\left(-\frac{h^2}{8\pi^2 m}\nabla^2 + \hat{V}\right)\Psi = E\Psi} \tag{2.4}$$

Here $\boldsymbol{\Psi}$ is the wave function, $\boldsymbol{\hat{V}}$ is the potential operator, $\boldsymbol{E}$ is the system energy, and $\boldsymbol{\nabla^2}$ is the Laplacian operator.

$$\boldsymbol{\nabla^2 = \frac{\partial^2}{\partial x^2} + \frac{\partial^2}{\partial y^2} + \frac{\partial^2}{\partial z^2}} \tag{2.5}$$

จุฬาลงกรณ์มหาวิทยาลัย
CHULALONGKORN UNIVERSITY

In abbreviation, the equation is written as

$$\boldsymbol{\hat{H}\Psi(r) = E\Psi(r)} \tag{2.6}$$

$$\boldsymbol{\hat{H} = \hat{T} + \hat{V}} \tag{2.7}$$

where $\boldsymbol{\hat{H}}$ is an Hamiltonian operator and $\boldsymbol{\hat{T}}$ is the kinetic operator

In mathematics, an equation of this form is called an eigenvalue equation. $\boldsymbol{\Psi}$ is called the eigenfunction and $\boldsymbol{E}$ is an eigenvalue. The goal of quantum chemical approaches is the approximate solution of the time-independent, non-relativistic Schrödinger eqaution:

$$\hat{H}\Psi_i(\vec{r}_1, \vec{r}_2, \ldots, \vec{r}_{N_e}, \vec{R}_1, \vec{R}_2, \ldots \vec{R}_M) = E_i\Psi_i(\vec{r}_1, \vec{r}_2, \ldots \vec{r}_{N_e}, \vec{R}_1, \vec{R}_2, \ldots \vec{R}_M) \quad (2.8)$$

where $\hat{H}$ is the Hamiltonian operator for a molecular system consisting of M nuclei and N_e electrons in the absence of magnetic or electric fields. $\hat{H}$ is a differential operator representing the total energy in atomic unit:

$$\hat{H} = -\frac{1}{2}\sum_{i=1}^{N_e}\nabla_i^2 - \frac{1}{2}\sum_{A=1}^{M}\frac{1}{M_A}\nabla_A^2 - \sum_{i=1}^{N_e}\sum_{A=1}^{M}\frac{Z_A}{r_{iA}} + \frac{1}{2}\sum_{i=1}^{N_e}\sum_{j=1}^{N_e}\frac{1}{r_{ij}} + \frac{1}{2}\sum_{A=1}^{M}\sum_{B=1}^{M}\frac{Z_A Z_B}{R_{AB}} \quad (2.9)$$

$$= \hat{T}_e + \hat{T}_N + \hat{V}_{ne} + \hat{V}_{ee} + \hat{V}_{nn} \quad (2.10)$$

Here, A and B run over the M nuclei while i and j denote the N_e electrons in the systems. The first term is the operator for the kinetic energy of electron($\hat{T}_e$). The second term is the operator for the kinetic energy of the nuclei ($\hat{T}_n$). The third term is potential energy of the attractions between the nuclei and the electron ($\hat{V}_{ne}$), r_{iA} being the distance between electrons i and nucleus A. The fourth term is potential energy of the repulsions between the electrons ($\hat{V}_{ee}$) , r_{ij} being the distance between electrons i and j. The last term is potential energy repulsions between the nuclei ($\hat{V}_{nn}$), R_{AB} being the distance between nuclei A and B with atomic number Z_A and Z_B.

The wave functions and energies of a molecule are found from Schrödinger equation:

$$\hat{H}\psi(\vec{r}, \vec{R}) = E\psi(\vec{r}, \vec{R}) \quad (2.11)$$

where $\vec{r}$ and $\vec{R}$ symbolize the electronic and nuclear coordinates, respectively. Hamiltonian on eq 2.8 is formidable enough to terrify any quantum chemist. Fortunately, a very accurate, simplifying approximation exists.

2.4 Born-Oppenheimer approximation

The Schrödinger equation is impossible to solve exactly with such complexity Hamiltonian. The Hamiltonian operator can be separated into two parts to reduce the complexity to a good approximation. Where one part describes the electronic motion and another part describes nuclear motion. This approximation is called Born-Oppenheimer approximation. Even the lightest nuclei, proton (^{1}H), weight roughly 1800 times more than an electron. Thus, the nuclei move much more slowly than the electrons. To compute electronic energy of these two motions, it is convenient to fix nuclear position. Thus, the nuclear kinetic energy term is taken to be independent of the electrons, the attractive electron-nuclear potential energy term is eliminated and the repulsive nuclear-nuclear potential energy term becomes a simply evaluate constant for a given geometry. Hence, the purely electronic Hamiltonian is taken to be

$$\hat{H}_{el} = \hat{T}_e + \hat{V}_{ne} + \hat{V}_{ee} \tag{2.12}$$

and the electronic motion Schrödinger equations is

$$(\hat{H}_{el} + \hat{V}_{nn})\psi_{el}(\vec{r}, \vec{R}) = E_{el}\psi_{el}(\vec{r}, \vec{R}) \tag{2.13}$$

when E_{el} is the electronic energy. Therefore, the electronic Schrödinger equation 2.10 may solve to the get a set of electronic wave functions and corresponding to the electronic energies. Moreover, the variable in 21.10 are electronic coordinates, $\hat{V}_{nn}$ is

not depended of these coordinate. Thus, to simplified the 2.10 we omitted $\hat{\boldsymbol{T}}_{\boldsymbol{N}}$ and $\hat{\boldsymbol{V}}_{\boldsymbol{nn}}$ term to obtain

$$\hat{\boldsymbol{H}}_{\boldsymbol{el}}\boldsymbol{\psi}_{\boldsymbol{el}}(\boldsymbol{r}) = \boldsymbol{E}_{\boldsymbol{el}}\boldsymbol{\psi}_{\boldsymbol{el}}(\boldsymbol{r}) \tag{2.14}$$

The total energy, $\boldsymbol{U}$ is given by

$$\boldsymbol{U} = \boldsymbol{E}_{\boldsymbol{el}} + \hat{\boldsymbol{V}}_{\boldsymbol{nn}} \tag{2.15}$$

However, the Schrödinger equations for electronic system can exactly be solved only for the one electron system. For many-electron systems, the approximation has to be applied.

2.5 Spatial orbital and spin orbitals

Consider one-electron wavefunction, it is not accurate electronic wavefunction to consider without spin. Spin of each electron must be included in the electronic wavefunction to satisfy a very important requirement. However, there is no spin in the solution of the Schrödinger equation. Under the orbital approximation, the electronic wave function can be constructed from the slater determinant of spin orbital.

Chulalongkorn University

Therefore, for an orbital of one-electron wave function denoted $\boldsymbol{\varphi}_{\mathbf{i}}(\mathbf{r})$ is a function of the position vector $\boldsymbol{r}$ and give details of an electron spatial distribution such that $|\boldsymbol{\varphi}_{\mathbf{i}}(\boldsymbol{r})|^2\boldsymbol{dr}$ is the probability of finding electron in the small proximity $\boldsymbol{dr}$ surrounding $\boldsymbol{r}$. To have such meaning, a set of spatial orbital satisfies the orthonormal condition

$$\int \boldsymbol{dr}\boldsymbol{\varphi}_{\mathbf{i}}^{*}(\boldsymbol{r})\boldsymbol{\varphi}_{\boldsymbol{j}}(\boldsymbol{r}) = \boldsymbol{\delta}_{\boldsymbol{ij}} \tag{2.16}$$

If the set of spatial orbitals $\{\boldsymbol{\varphi}_{\boldsymbol{i}}\}$ is completed, then any arbitrary function $\boldsymbol{f}(\boldsymbol{r})$ could be exactly expanded as

$$f(r) = \sum_{i=1}^{\infty} a_i \varphi_i(r) \tag{2.17}$$

An electron is necessary to specify its spin. The wavefunction for an electron that describes both its spatial distribution and its spin is a spin orbital, $\chi(x)$, where x indicates both space (r) and spin (ω)coordinate x.

$$\chi(x) = \begin{cases} \varphi(r)\alpha(\omega) \\ or \\ \varphi(r)\beta(\omega) \end{cases} \tag{2.18}$$

2.6 The Hartree-Fock approximation

According to orbital model is ultimate to be used successfully as the model for atom, molecule and solid state. Hartree-Fock approximation can search to solve the electronic Schrodinger equation for many-electron system by treating each electron moves in the average potential out the effect of other electrons and the nuclei. Due to the electron–electron repulsion term was taken as non-zero and Hatree-Fock approximation cannot treat the refine details of electronic structure theory that are caused by the instantaneous repulsion between electrons. Therefore, for many-electron (N) system, the Hatree-Fock approximation defined the ground state of the system by salter determinant.

$$\Psi = (N!)^{-1/2} \begin{vmatrix} \chi_i(x_1) & \chi_j(x_1) & \cdots & \chi_k(x_1) \\ \chi_i(x_2) & \chi_j(x_2) & \cdots & \chi_k(x_2) \\ \vdots & \vdots & \ddots & \vdots \\ \chi_i(x_N) & \chi_j(x_N) & \cdots & \chi_k(x_N) \end{vmatrix} \tag{2.19}$$

Where in the case of restricted closed-shell Hartree-Fock $N = 2n$

$$\Psi = (2n!)^{-1/2} \begin{vmatrix} \varphi_1(x_1)\alpha(x_1) & \varphi_1(x_1)\beta(x_1) & \varphi_2(x_1)\alpha(x_1) & \cdots \\ \varphi_1(x_2)\alpha(x_2 & \varphi_1(x_2)\beta(x_2) & \varphi_2(x_2)\alpha(x_2) & \cdots \\ \vdots & \vdots & \vdots & \cdots \\ \varphi_1(x_{2n})\alpha(x_{2n}) & \varphi_1(x_{2n})\beta(x_{2n}) & \varphi_2(x_{2n})\alpha(x_{2n}) & \cdots \end{vmatrix} \quad (2.20)$$

where $(2n!)^{-1/2}$ is the normalization constant

Although the system contains more than one electron system is no exact analytical solution from the Schrödinger equation, the standard numerical techniques can achieve approximate solutions. One approach in quantum chemistry is to build the total wave function from the linear combination of a set of orthogonal functions called 'basis function'. Basically, the basis set is referred to a set of atomic orbitals called "Linear Combination of Atomic Orbital to form Molecular Orbital (LCAO-MO). Therefore, the molecular orbital **i** (φ_i) can be built from k atomic orbitals (ϕ_k)

$$\varphi_i = \sum_{\mu=1}^{k} c_{\mu i}\phi_u \quad (2.21)$$

where $c_{\mu i}$ is the molecular coefficient.

To constructs a determinant wavefunction from a set of LCAO-MOs, the remains is to verify the molecular coefficient, $c_{\mu i}$. This could be achieved by optimizing the molecular wavefunction for a particular wavefunction for a particular system with the variation method. The procedure would guarantee that the exact energy obtained from energy eigenvalue is always an upperbound. Therefore, the lowest energy from the minimized set for molecular coefficients will give the best approximation to the exact wavefunction for the chosen basis set. The variation constraint leads to a set of algebraic equation (Roothaan-Hall) for $c_{\mu i}$ expressed in even more simply as matrices:

จุฬาลงกรณ์มหาวิทยาลัย
Chulalongkorn University

$$\boldsymbol{FC = SC\epsilon} \tag{2.22}$$

where $\boldsymbol{C}$ is the matrix of molecular coefficient, $\boldsymbol{F}$ is the Fock matrix which is the sum of a term representing the energy of a single electron in the field of the bare atomic nuclear and a term describing electron-electron repulsion within an averaged field of electron density, $\boldsymbol{S}$ is the matrix which describing the overlap of molecular orbitals and $\boldsymbol{\epsilon}$ is a diagonal matrix of orbital energies.

Since the terms with the Fock matrix $\boldsymbol{F}$ depend upon the electron density, which is turn, depends upon molecular wavefunction defined by the matrix of molecular coefficient, $\boldsymbol{C}$. The Roothan-Hall equation is nonlinear and must be solved by an iterative method so, it is called 'self-consistent field' (SCF) method. Leading to convergence of the SCF method, the minimum-energy molecular orbitals produce electric field which generates the same orbitals (hence, the self-consistency). However, each electron in Hatree-Fock approximation moves in an average field of other electron and nuclear thus, this approximation neglects electron correlation that can lead to the large deviation from exact values.

จุฬาลงกรณ์มหาวิทยาลัย
CHULALONGKORN UNIVERSITY

2.7 Density functional theory (DFT)

Density functional theory (DFT) is very famous for calculations of solid state physics since 1970 because its results for solid state systems agreed well with experiment data in many cases. Now, DFT is the most popular method for investigation of electronic structures in chemistry and physics. This theory is called density functional theory because this method to investigate the electronic structure by considering the properties of system by using functionals of electron density. The

DFT reduces the dimension of the electronic structure theory drastically. The only problem left is that the universal functional connecting to the electron density is still unknown. However, the major problems for recent functionals of DFT are the inability to systematically improve them and the poor description of van der Walls interactions.

The principle of DFT is based on two Hohenberg-Kohn theorems. The first theorem expresses that the ground state properties of a N-electron system are uniquely defined by the ground state electron density ($\boldsymbol{\rho}$). Thus, the ground state energy ($\boldsymbol{E_o}$) in the function of $\boldsymbol{\rho}$, written as $\boldsymbol{E_o = E_o[\rho]}$. However, this theorem did not propose the means to obtain the exact $\boldsymbol{\rho}$. The second theorem proves that the energy functional of the trial ground state density, $\boldsymbol{\tilde{\rho}}$, is an upperbound to the exact energy, $\boldsymbol{E_o}$.

$$\boldsymbol{E_{trial}[\tilde{\rho}] \geq E_o[\rho]} \tag{2.23}$$

However, this theorem still was not proposed how to compute the energy from the trial electron density. In 1965, Khon and Sham showed an idea to calculate the ground state energy based on the *N*-electron with non-interacting system for this system.

$$\boldsymbol{E_o[\rho] = T_s[\rho] + V_{ne}[\rho] + J[\rho] + E_{xc}[\rho]} \tag{2.24}$$

$$= -\frac{1}{2}\sum_{i=0}^{n}\langle \boldsymbol{\varphi_i}|\nabla^2|\boldsymbol{\varphi_i}\rangle + \sum_{\alpha}\int \frac{Z_\alpha \rho(1)}{|r_{1\alpha}|}\boldsymbol{d\vec{r}} + \frac{1}{2}\iint \frac{\rho(1)\rho(2)}{r_{12}}\boldsymbol{d\vec{r_1}d\vec{r_2}} + \boldsymbol{E_{xc}[\rho]} \tag{2.25}$$

where $\boldsymbol{\varphi_i}$ is Kohn-Sham orbital, $\boldsymbol{T_s[\rho]}$ is the kinetic energy functional for independent electron, $\boldsymbol{V_{ne}[\rho]}$ is the electron-nuclear attraction functional or external

potential, $\boldsymbol{J}[\boldsymbol{\rho}]$ is the coulomb interaction functional and $\boldsymbol{E_{xc}}[\boldsymbol{\rho}]$ is the exchange-correlation energy functional. $\boldsymbol{\rho}(\mathbf{1})$ can be expressed as

$$\boldsymbol{\rho} = \sum_{\boldsymbol{i=1}}^{\boldsymbol{n}} |\boldsymbol{\varphi_i}|^{\mathbf{2}} \tag{2.26}$$

The final term in eq 2.24 , the exchange-correlation energy functional, is the only term that is still unknown. The first simple and good approximation is to assume that the density is a slowly varying function. It means that the density is local and can be treated as a uniform electron gas. For local density approximation, LDA, the exchange-correlation energy functional ($\boldsymbol{E_{xc}^{LDA}}[\boldsymbol{\rho}]$) can be written as

$$\boldsymbol{E_{xc}^{LDA}}[\boldsymbol{\rho}] = \int \boldsymbol{\rho}\,(\boldsymbol{r})\boldsymbol{\varepsilon_{xc}}\big(\boldsymbol{\rho}(\boldsymbol{r})\big)\boldsymbol{dr} \tag{2.27}$$

when $\boldsymbol{\varepsilon_{xc}}\big(\boldsymbol{\rho}(\boldsymbol{r})\big)$ is the exchange-correlation energy per particle of a uniform electron gas of density $\boldsymbol{\rho}(\boldsymbol{r})$. This term can be split in to exchange ($\boldsymbol{\varepsilon_x}$) and ($\boldsymbol{\varepsilon_c}$) contributions.

$$\boldsymbol{\varepsilon_{xc}}\big(\boldsymbol{\rho}(\boldsymbol{r})\big) = \boldsymbol{\varepsilon_x}\big(\boldsymbol{\rho}(\boldsymbol{r})\big) + \boldsymbol{\varepsilon_c}\big(\boldsymbol{\rho}(\boldsymbol{r})\big) \tag{2.28}$$

The exchange functional part is first given by Dirac formula and has been developed by Slater (S) in 1972. The correlation functional part, which is purely dynamical correlation, has been parameterized from the quantum Monte Carlo results by Vosko, wilk and Nusair (VWN). This approximation can be extended to the unrestricted open shell system and it is called the "local spin-density approximation" or LSDA.

$$\boldsymbol{E_{xc}^{LSDA}}[\boldsymbol{\rho_\alpha}\boldsymbol{\rho_\beta}] = \int \boldsymbol{\rho}\,(\boldsymbol{r})\boldsymbol{\varepsilon_{xc}}\left(\boldsymbol{\rho_\alpha}(\boldsymbol{r}), \boldsymbol{\rho_\beta}(\boldsymbol{r})\right)\boldsymbol{dr} \tag{2.29}$$

To improve over the LSDA approach, the non-uniform electron gas must be considered. The first derivative of the electron density has been included to the exchange and correlation functionals. Such the approach is known as the "Generalized Gradient Approximation" (GGA) or non-local approximation.

$$E_{xc}^{GGA}[\rho_\alpha \rho_\beta] = \int \rho(r)\varepsilon_{xc}\left(\rho_\alpha(r), \rho_\beta(r), \nabla\rho_\alpha(r), \nabla\rho_\beta(r)\right) dr \qquad (2.30)$$

Using GGA, improved results for molecular geometries and ground-state energies are obtained. In particular, the most widely used GGA functional for the solid state system is the Perdew-Burke-Ernzerhof (PBE) exchange-correlation functional, a direct GGA parameterization, because it can give reasonable bond length and good lattice constants in bulk solid. Although DFT results are usually accurate for most systems, there is no systematically way for improving these functionals. Thus, the current DFT approach cannot estimate the error of the calculation without comparing to other methods or experimental results.

2.8 Basis sets

The beset set is defined by a set construct the molecular orbital of basis functions from a linear combination of atomic orbitals approximate from the molecular wavefunctions. The molecular orbital is a main tool to explain atomic and molecular system, thus, they are center of atom. Due to the atomic orbitals are Slater type orbitals that decayed exponentially with distance from the nucleus with difficult to calculate analytically of the overlap and 2-electron integrals with slater type orbitals, it lead to simpler integral to minimize the computational cost by using Gaussian-type orbitals instead. On the other hand, the basis function which gives numerical values on an atomic-centered spherical-polar mesh can be applied which is

called “numerical basis set”. For the numerical basis set, the radial part is obtained by solving the atomic DFT equations numerically. In addition, a reasonable level of accuracy is usually obtained by using about 300 radial points from the nucleus to an outer distance of 10 Bohr. A set of cubic spline for each of the 300 sections are stored radial functions thus, the radial part is pricewise analytic. The use of exact DFT spherical atomic orbitals has several advantages. The molecule can be dissociated exactly to its constituent atoms. The basis set superposition effects has been minimized. Therefore, it can give the excellent results even for weak bonds. The most simple of the molecular orbitals operate only one basis function for each atomic orbital up to the valence orbitals. These basis set is minimal basis set still cannot describe well in most cases since; the exponent has only one value. This effect lead to an inability to explain differently charge distribution on atom and the size of orbital cannot be changed in the different environment. To increase the flexibility, the basis set is decontracted. When two or more basis functions are used to describe each atomic orbital cannot be changed in the different environment. To increase the flexibility, the basis set is decontracted. When two or more basis functions are used to describe each atomic orbital, the basis set is called the extended basis set. In the split-valence basis set, two functions (or more) are required for description of the atomic orbital in the valence space, while orbitals for inner core electrons are treated with single function. Examples of the split-valence basis set are SVP, 6-31G and DN basis sets. Nevertheless, the extended basis still gives the unsophisticated results in the case of high polar of high strain systems. Since, the flexibility on the shape of orbitals is needed to be included. The higher angular momentum functions are added to increase the flexibility of the orbitals. This expansion is called polarization function. For

example, DN basis set is added with single d function on all non-hydrogen atoms and DND basis set is formed. DNP basis set is expanded from DND by including a p function on hydrogen atom.

CHAPTER III
CALCULATION DETAIL

3.1 Model of active Ziegler-Natta catalyst structure

The first microscopic proposal made by Busico, Corradini, and coworker indicated the coordination numbers of 5 for Mg atoms on 104 $MgCl_2$ surface and 4 for Mg atoms on 110 $MgCl_2$ surface [22,42-44]. The calculation from Busico *et al.* reported that $TiCl_4$ has stronger interaction on 110 surfaces with bearing species ($TiCl_4$) than on 104 surface with dinuclear species (Ti_2Cl_8) [18]. Moreover, the active site models of Tebikie *et al.* found that $TiCl_3$ has stronger binding than $TiCl_4$ to the $MgCl_2$ surfaces. Therefore, the oxidation state for Ti active site was set to be +3 instead of +4. Busico *et al.* postulated a three-site model as a versatile active site image in $MgCl_2$-supported ZNc; slope, edge, Corradini, which was modified by Terro *et al*. In this work, the model of titanium configuration relevant to the Corradini model was chosen (**Figure 3.1a**).

จุฬาลงกรณ์มหาวิทยาลัย
Chulalongkorn University

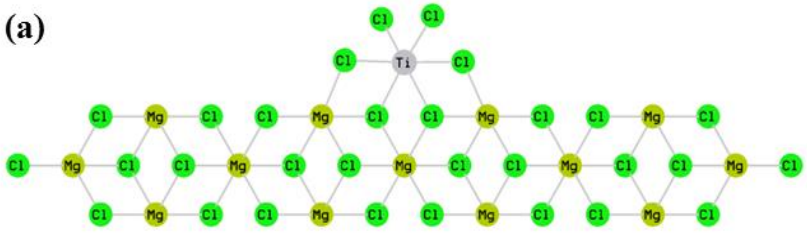

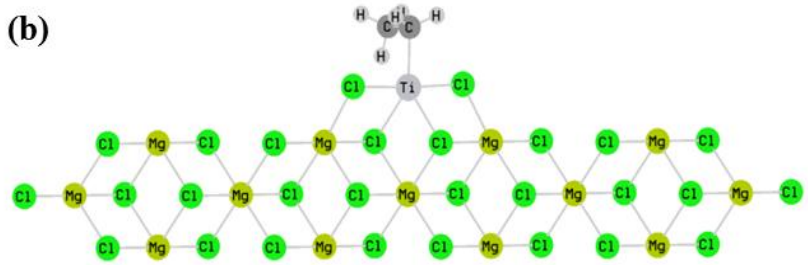

Figure 3.1 Titanium configuration relevant as the Corradini model (**a**) and reduction form : Ti(III), $TiCl_2$-CH_2CH_3 **(b)**

In our calculation, only one model as (110) $MgCl_2$ surface supported mononuclear titanium, $TiCl_4$ ($MgCl_2$.$TiCl_4$) was chosen to investigate the coadsorption sites with ED. Since the active site was alkylated by $AlEt_3$, the active site model was $MgCl_2$.$TiCl_2$-CH_2CH_3 (**Figure 3.1b**).

3.2 Electron donor systems

3.2.1 Electron donors for ethylene homopolymerization

Our developed catalytic system was prepared by mixing of $Mg(OEt)_2$ with $TiCl_4$ + $AlEt_3$. Moreover, adding $SiCl_4$ in the catalytic system found that the activity of the catalyst was increased significantly. To determine the effect of $SiCl_4$ to the catalytic system two systems are divided as EA (absence $SiCl_4$) and EAS (presence $SiCl_4$). According to the procedure of catalyst preparation, we can only carefully summarize the possible complexes to create active site as follow the for EA and EAS systems.

For EA system, when mixing $Mg(OEt)_2$ with $TiCl_4$, $TiCl_4$ acts as a chlorinating agent to generate $MgCl_2$. Besides, $Ti(OEt)_xCl_y$ (when $x + y = 4$) was also possibly generated (eq. 3.1) [22]. Adding $Al(Et)_3$ as alkylating reducing species will possibly reduce Ti(IV) to Ti(III) to generate active site of catalyst $MgCl_2.TiCl_2$-CH_2CH_3 (eq. 3.2).

$$Mg(OEt)_2 + 2TiCl_4 \rightarrow MgCl_2.TiCl_4 + Ti(OEt)_xCl_y \quad (\text{when } x + y = 4) \qquad 3.1$$

$$MgCl_2.TiCl_4 + Al(CH_2CH_3)_3 \rightarrow MgCl_2.TiCl_2\text{-}CH_2CH_3 \qquad 3.2$$

For EAS system, the same procedure as EA catalyst preparation is routinely conducted. Nevertheless, at the first step, $SiCl_4$ substance is initially added to $Mg(OEt)_2$ before $TiCl_4$ which lead to the various complexes formation showing in the eq. 3.3. We assume that $SiCl_4$ acts as chlorinating agent as the same role as $TiCl_4$ [22]. Therefore, $Si(OEt)_mCl_n$ and $Ti(OEt)_xCl_y$ were generated at the same manner (eq. 3.4).

$$2Mg(OEt)_2 + SiCl_4 \rightarrow 2MgCl_2 + Si(OEt)_mCl_n (\text{when } m+n = 4) \qquad 3.3$$

$$MgCl_2 + 2TiCl_4 + Mg(OEt)_2 \rightarrow 2MgCl_2.TiCl_4 + Ti(OEt)_xCl_y \quad (\text{when } x+y = 4) \qquad 3.4$$

$$MgCl_2.TiCl_4 + Al(Et)_3 \rightarrow MgCl_2.TiCl_2\text{-}CH_2CH_3 \qquad 3.5$$

Applying the same polymerization condition, the EAS is found to be more active than that of the conventional EA catalyst. The adding of $SiCl_4$ is somehow affecting the polymerized activities. To investigate the role of EDs in EAS, we believe that alkoxy group with silicon $Si(OEt)_mCl_n$ ($m + n = 4$) and titanium $Ti(OEt)_xCl_y$ ($x + y = 4$), generated during the procedure could coadsorb at the surface of catalyst. Although two ED species were generated, many reports shown that alkoxysilane was successful in broadening the molecular weight distribution of the

obtained polymer. Therefore, the role of 4 alkoxysilane with different number of alkoxy groups to silicon: $Si(OEt)_4$, $Si(OEt)_3Cl$, $Si(OEt)_2Cl_2$ and $Si(OEt)Cl_3$ are investigated.

3.2.2 Electron donors for ethylene/1-hexene copolymerization

The model of catalyst for ethylene/1-hexene copolymerization, the (110) $MgCl_2$ surface, $Mg_{13}Cl_{26}.TiCl_2$-CH_2CH_3 cluster has been used as a model of ethylene homopolymerization. Introducing ED in the ethylene/1-hexene copolymerization can increase broad molecular weight distribution (MWD) and high molecular weight products, Zhi Liu *et al.* [20] reported that the ZNc system with alkoxysilane group highly impact the rang of MWD product. Experiment data revealed that the ability of EDs can increase the wide MWD in the order $Si(OEt)_4$ < $Si(OEt)_3$(O*i*Pr) < $Si(OEt)_3$(O*t*Bu) < $Si(OEt)_2$(O*t*Bu)(O*i*Pr). Therefore, to describe the different role of different ED to enhance the catalytic system, this all four EDs have been a studied for ethylene/1-hexene copolymerization for this present work.

จุฬาลงกรณ์มหาวิทยาลัย
CHULALONGKORN UNIVERSITY

3.3 Geometry optimization

The geometry optimization search for alkyl conformation at active surface catalyst and the adsorption energy calculations were carried out using the density functional theory (DFT) calculations with a spin doublet manner of all systems in the $DMol^3$ package (Accelrys Inc.) Material studio version 5.5 (MS) [45]. $DMol^3$ instructs that the numerical basis sets are designed to minimize the basis sets superposition error [46]. The other numerical parameters include the convergence

tolerance, density of the integration grid and real-space cut off radius was set to those the ‘medium accuracy’. The energy and force convergence criteria for geometry optimization were set to 0.01255 kcal/mol and 2.51004 kcal/mol.Å, respectively. The exchange-correlation Perdew-Burke-Ernzerhof (PBE) functional [47] and a double numerical polarized (DNP) basis set [46] were employed with effective core potentials. The frozen-cores used for calculation are [Ar] for Ti, [Ne] for Mg and Cl, [He] for C.

On the other hand, to calculate the (intrinsic) activation energy and apparent activation energy, all geometries were carried out using the GAUSSIAN 09 program with PBE functional and 6-31G(d, p) basis set for C, H, O, Mg and Cl, and LANL2DZ basis set and ECP function for Ti atom [48].

3.3.1 Conformation Search for alkyl group

The $TiCl_4$ supported by (110) $MgCl_2$ surface was modeled as active Zeigler-Natta catalyst (ZNc). The appropriate active models consist of neutralized form of $MgCl_2$ and $TiCl_3$. The cluster model contains $MgCl_2$ with Mg:Cl ratio of 1:2 and active catalytic $TiCl_3$ site with oxidation state of Ti(III). Note that the numbers of $MgCl_2$ unit were arbitrarily chosen. According to the most stable mononuclear Ti atom with the model of Corradini site (110) $MgCl_2$ complex was chosen. Therefore, our model was chosen by the 13 units of (110) $MgCl_2$ surface support mononuclear Ti which was reduced by $Al(Et)_3$ as active oxidation state Ti(III), corresponding to $Mg_{13}Cl_{26}.TiCl_2\text{-}CH_2CH_3$. The $MgCl_2$ cluster has been kept rigid to preserve the structure as in the bulk crystal, whereas the rotation of $TiCl_2\text{-}CH_2CH_3$ has been

optimized to obtain the optimal conformation. The *Ti-C* bond distance is believed to change when the ethylene insertion reaction occurs. The optimum conformation of -CH_2CH_3 bound to Ti(III) on the catalyst surface was observed (see the label for dihedral angles Cl_1-Ti_2-C_α-C_β in **Figure 3.2**).

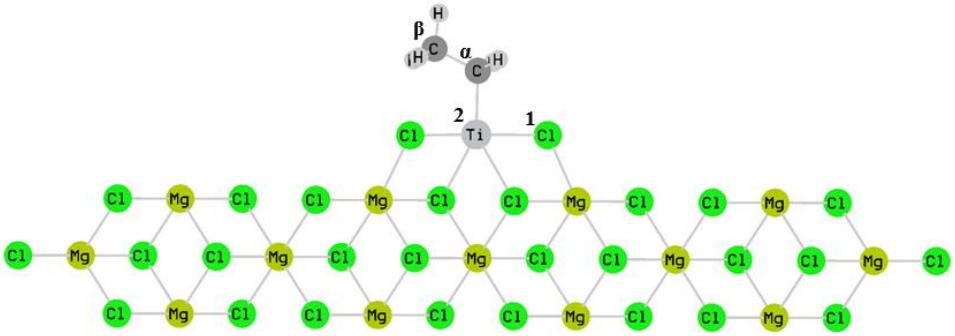

Figure 3.2 Assignment of four atoms for dihedral angles for (101) $Mg_{13}Cl_{26}.TiCl_2$-CH_2CH_3

3.3.2 $MgCl_2$/Donor coadsorption

The geometries of $Si(OEt)_mCl_n$ ($m + n = 4$) on $Mg_{13}Cl_{26}.TiCl_2$-CH_2CH_3 (EAS system) was modeled to observe the effect of these EDs at the insertion step of ethylene homopolymerization. The different binding modes, *i.e.*, nomodentate, bidentate and bridging have been determined (**Figure 3.4a-c**). Adsorption energy (E_{ads}) of the ED on catalyst surface was computed based on the following equation:

$$\boldsymbol{E_{ads} = E_{D.cpx} - E_D - E_{cat}} \qquad (3.6)$$

where $\boldsymbol{E_{D.cpx}}$ the energy of donor complex, $\boldsymbol{E_{cat}}$ the energy of active catalyst, and $\boldsymbol{E_D}$ the energy of donors.

The two groups of electron donor were investigated adsorption energy are $Si(OEt)Cl_3$, $Si(OEt)_2Cl_2$, $Si(OEt)_3Cl$, $Si(OEt)_4$, (so-called 1OEt, 2OEt, 3OEt, 4OEt) for ethylene homopolymerization and $Si(OEt)_4$, $Si(OEt)_3(O\textit{t}Bu)$, $Si(OEt)_3(O\textit{i}Pr)$ and $Si(OEt)_2(O\textit{t}Bu)(O\textit{i}Pr)$ so-called ED1, ED2, ED3 and ED4, respectively, for ethylene/1-hexene copolymerization (**Figure 3.3**). The coadsorption of ED at the two Mg sites (*A* and *B*) were indicated at the plausible location of Mg on (110) $MgCl_2$ surfaces supported $TiCl_2$-CH_2CH_3 (**Figure 3.4a**). The interaction between O atom of ethoxy group and Mg atoms which has a partial negative charge and positive charge, respectively, is electronic interaction supposed to be preferential mode of interaction. The O atom(s) from different ED can bind with different possible modes, *i.e.* monodentate, bidentate and bridging modes (**Figure 3.4a-c**).

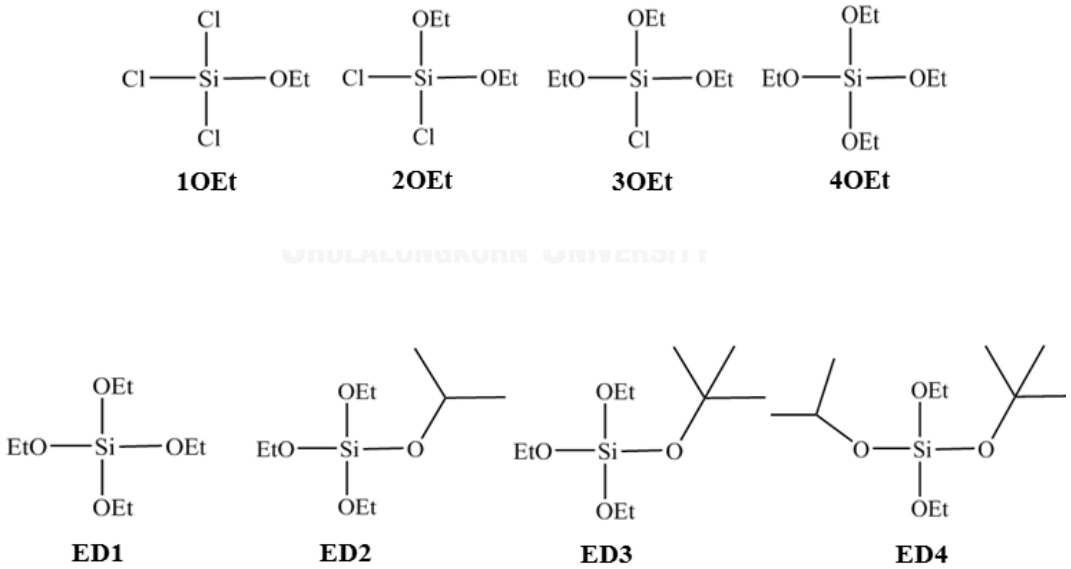

Figure 3.3 Structure of electron donors considered in this investigation for ethylene homopolymerization and ethylene/1-hexene copolymerization

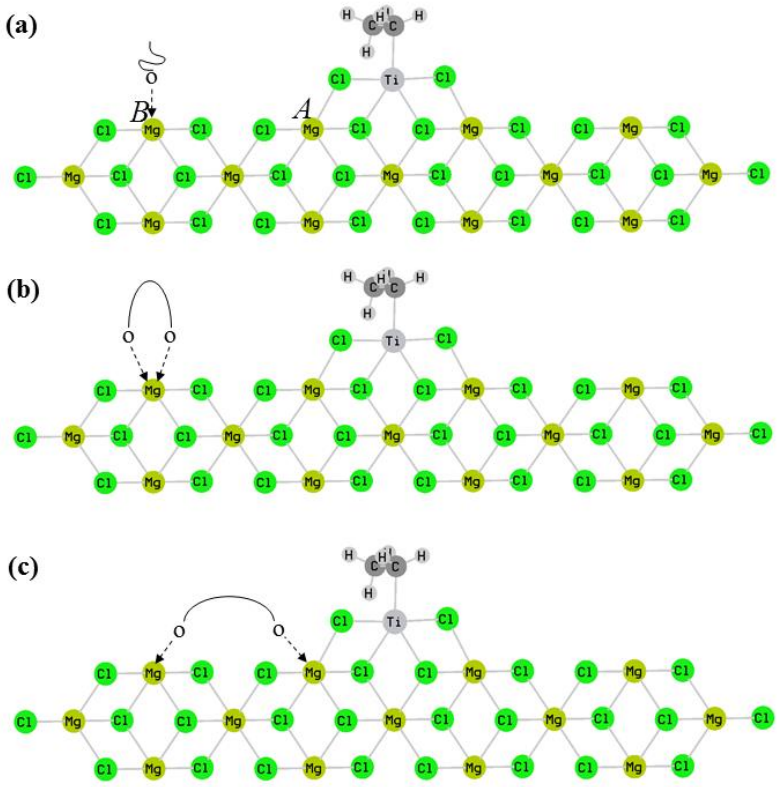

Figure 3.4 Label the adsorption sites at the (110) $Mg_{13}Cl_{26}.TiCl_2$-CH_2CH_3 surface **(a)** binding modes of electron donors to Mg atom: monodentate (**a**), bidentate (**b**) and bridging (**c**)

จุฬาลงกรณ์มหาวิทยาลัย
Chulalongkorn University

3.3.3 Insertion of ethylene

After the model of coadsorption sites of ED at the specific surface of $MgCl_2.TiCl_2CH_2CH_3$ was considered, the insertion of ethylene monomer was investigated. Although the active center is complicated, Arlman and Cossee have proposed a widely acceptable general mechanism (**Figure 2.9**). At the active center, the metal is bounded by four chlorine atoms which connect the Ti to the bulk of the crystal and an alkyl group which develops into the growing chain, while the last coordination position is occupied at each polymerization step by an incoming

ethylene monomer molecule. Various theoretical studies have been elucidated to the clarification of the elementary steps, however, all the considered systems always focused on the insertion on a simple Ti-CH_2CH_3 bond (step *iii*) [49-58] (**Figure 2.9**). However, in order to examine the influence of ED occur during the reaction, the energy barrier of ethylene insertion reaction in step *iii* was considered. The key for the ZNc is $MgCl_2$ supported $TiCl_4$ and the ED of alkoxysilane group with the largest absence of clear answer for how is the combination of alkoxysilane coadsorb with $MgCl_2$ can increase the catalytic properties of Ti active site. Thus, this work aims to investigate theoretically of the ethylene insertion step and the energies with presence and absence ED of two reactions, ethylene homopolymerization and ethylene/1-hexene copolymerization.

3.3.3.1 Ethylene insertion for ethylene homopolymerization

Generally, Ti-CH_2CH_3 and ethylene can grow the chain by insertion reaction to with a reaction pathway R→TS→P . In this study, the chemical reaction pathway with insertion of CH_2=CH_2 to Ti-CH_2CH_3 were approximated by linear potential energy scan (PES) at the relative energy maxima along the reaction coordinate, the C1- C2 distance for insertion into *Ti-*C_α. The reaction coordinate was scanned over *D1* (C1- C_α): 1.8 – 3.0 Å and *D2* (Ti-C2): 1.4-3.4 Å with the interval of 0.2 Å (**Figure 3.5a**). All geometries were optimized by MS. This is useful for the detail of reaction pathway that can be considered from bond shortening and bond elongating pathway. The PES map could guide us to perceive the structures of i) **R** (reactant) which form a π-complex between CH_2=CH_2 and Ti-CH_2CH_3, ii) **TS**

(transition state) which form a 4 center activated complex, and ii) **P** (product) with the formed *D1* and *D2*.

3.3.3.2 Ethylene insertion for ethylene/1-hexene copolymerization

To investigate the role of alkoxysilane electron donors affect to copolymerization ethylene/1-hexene reaction, insertion of CH_2=CH_2 has to be observed. To estimate barrier of ethylene insertion continuously, we performed ethylene comonomer insertion step into Mg_2Cl_{26}-$TiCl_2$-HE, where H is 1-hexene and E denotes ethylene. The issue of regioselectivity and reactivity of 1-hexene comonomer has minor effect for copolymerization reaction of 1-hexene comonomer due to the large proportion of ethylene in the polymer chain.

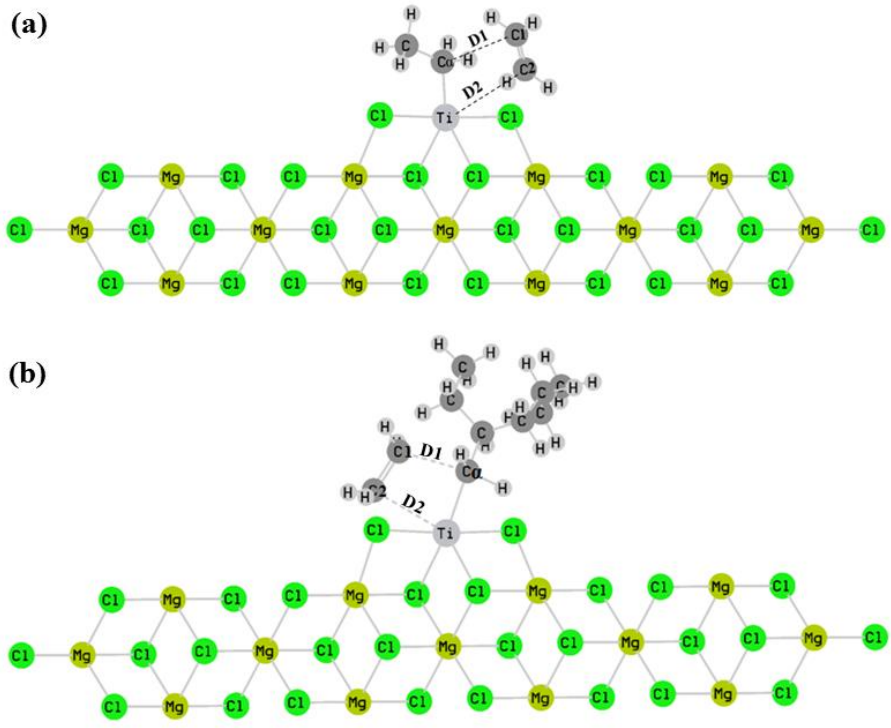

Figure 3.5 Definitions of the two intermolecular distances (*D1* and *D2*) between the incoming ethylene and the (110) $MgCl_2$ surface where the atoms (C_α, Ti, C1 and C2) involved in the ethylene insertion reaction are labeled for homopolymerization **(a)** and copolymerization **(b)**

3.4 The reaction barrier

All of the geometries in the chemical reaction pathway, R→TS→P for ethylene insertion for both reactions: ethylene homopolymerization and ethylene/1-hexene copolymerization were running GASSIAN09. To obtain the reaction barriers for the presence and absence of ED, the (intrinsic) activation energy (E_a) was computed using the equation 3.7:

$$\boldsymbol{E_a = E_{TS} - E_{\pi cpx}} \tag{3.7}$$

where $\boldsymbol{E_{TS}}$ is transition activated complex energy, $\boldsymbol{E_{\pi cpx}}$ is reactant complex energy (**R**).

จุฬาลงกรณ์มหาวิทยาลัย
Chulalongkorn University

CHAPER IV
RESULTS AND DISCUSSION

4.1 Ethylene homopolymerization

4.1.1 Conformation of ethyl group

To find the most stable ethyl conformation on Ti-CH_2CH_3 at the growing chain, the Cl_1-Ti_2-C_α-C_β dihedral angles was rotated every 20^o from 20^o to 180^o. The relative potential energy and the optimum geometrical structures are shown in **Figure 4.1**. From the relative potential energy of the rotational scan, the minimum is reached at 100^o. This growing chain was further optimized and then the optimum dihedral angle is found at ~89^o. The geometrical structure shows that the methyl end of ethyl group is pointed out of catalyst support. The less repulsive effect between the methyl end and atoms of catalyst support lead to energetically minimum structure. This optimum conformation is used to be the starting structure for the ethylene insertion study in the next step.

จุฬาลงกรณ์มหาวิทยาลัย
Chulalongkorn University

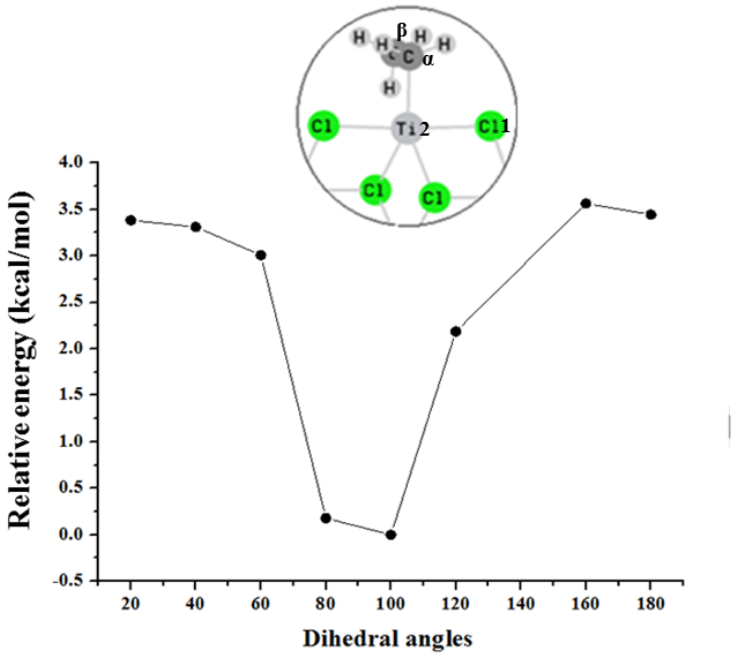

Figure 4.1 Relative energy profile vs dihedral angles of ethyl on (110) $MgCl_2$ surface and optimum structure (inset)

4.1.2 $MgCl_2$/donor coadsorption

The coadsorption of EDs; $Si(OEt)Cl_3$, $Si(OEt)_2Cl_2$, $Si(OEt)_3Cl$ and $Si(OEt)_4$ with the two Mg sites (*A* and *B*) were indicated at the plausible location of Mg on (110) $MgCl_2$ surfaces supported $TiCl_2$-CH_2CH_3 (**Figure 3.4a**). Since 1OEt has one oxygen atom, the binding with Mg site can be only monodentate binding mode. All possible binding modes are possible for other three EDs. The adsorption energies computed from equation 3.6 are shown in **Table 4.1**.

Table 4.1 The adsorption energy *(E_{ads})* at different adsorption sites and binding modes of electron donors 1OEt, 2OEt, 3OEt and 4OEt with (110) $Mg_{13}Cl_{26}$.$TiCl_3$-CH_2CH_3

Systems	Binding sites (Mg)	Mode of Binding	Adsorption energies (E_{ads}) (kcal/mol)
1OEt	*A*	monodentate	-5.88
	B	monodentate	-21.05
2OEt	*A*	monodentate	-7.71
		bidentate	-5.72
	B	monodentate	-24.57
		bidentate	-30.98
	AB	bridging	-4.94
3OEt	*A*	monodentate	0.93
		bidentate	0.89
	B	monodentate	-22.74
		bidentate	-28.58
	AB	bridging	-4.91
4OEt	*A*	monodentate	-2.81
		bidentate	0.79
	B	monodentate	-20.41
		bidentate	-33.7
	AB	bridging	-3.28

It found that the preferential mode for 1OEt complex at Mg-*B* has the lower energy than that of Mg-*A* by ~15 kcal/mol. In case of 2OEt complex, the bidentate mode is more energetically favored than the monodentate mode at Mg-*B*, but trend is reversed at Mg-*A*. However, adsorption energy of both binding modes at Mg-*B* atom

is more energetically favored than the monodentate mode at Mg-*A* due to the steric effect between the ethyl ends.

Similarly, the bidentate mode at Mg-*B* has the lowest E_{ads} for 3OEt and also 4OEt complexes. On the other hand, the bridging mode of 2OEt, 3OEt and 4OEt at Mg-*AB* have the highest in energies due to the short distance of two O bridging atoms of O-Si-O from all EDs (2.44 Å) cannot coordinate to the two Mg atoms on the catalyst surface (Mg-Mg distance = 6.31 Å).

The E_{ads} of bidentate mode for all OEt-complexes is 4EOt < 2EOt ~ 3EOt. This agrees with that of Lee J. W. and Jo W. H.[64]. The optimized structures of bidentate mode at Mg-*B* atom for all ED.$Mg_{13}Cl_{26}$.$TiCl_3$-CH_2CH_3 complexes are shown in **Figure 4.2a-d**. The bond distances between two ethoxy O atoms and Mg-*B* is in the reverse order of the corresponding adsorption energies. The Mg-O bond distances are in order of 4OEt (2.19/2.22 Å) ~ 3OEt (2.19/2.21 Å) < 2OEt (2.28/2.24 Å). It can be indicated that adsorption energy of ED-omplexes does not depend on the increasing number of OEt group in $Si(OEt)_mCl_n$.

จุฬาลงกรณ์มหาวิทยาลัย
CHULALONGKORN UNIVERSITY

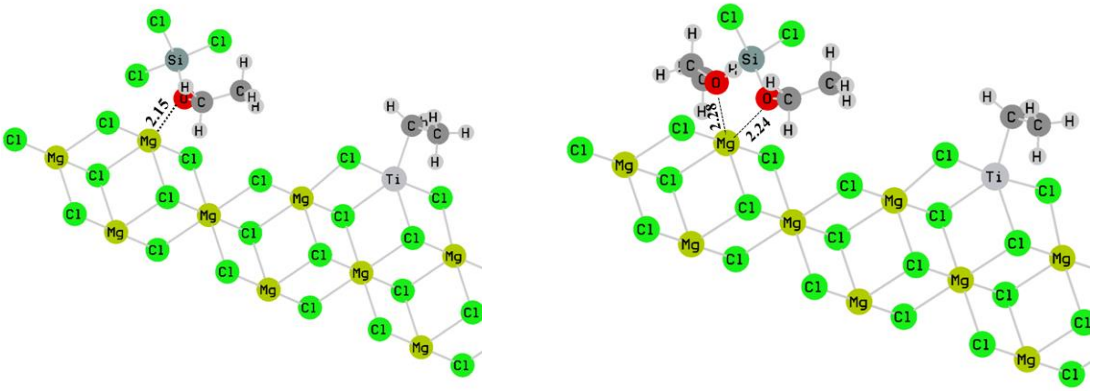

(a) **(b)**

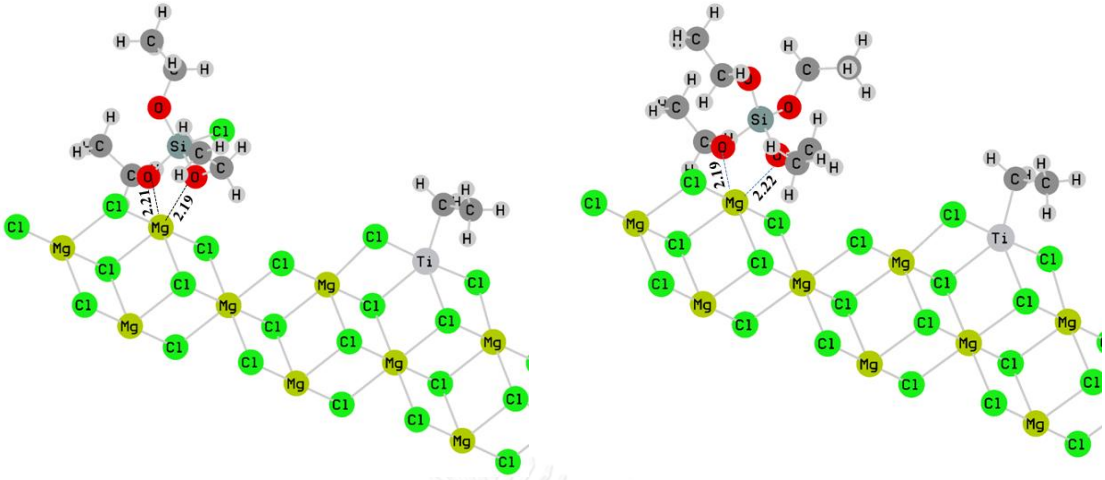

(c) **(d)**

Figure 4.2 The lowest adsorption energy binding mode structures of (110) ED.$Mg_{13}Cl_{26}$.$TiCl_2$-CH_2CH_3 complexes: 1OEt(**a**), 2OEt(**b**), 3OEt(**c**) and 4OEt(**d**)

4.1.3 Insertion of ethylene

A dynamic CH_2=CH_2 molecule begins to form a complex at the vicinity of the Ti site, a π-complex (**R**) is practically formed. In this work, the ED is expected to indicate reaction pathway through the preferential coordination of such donor onto the $MgCl_2$ surface. To check this assumption, the ethylene insertion reaction pathway with EA and EAS were investigated by PES through R →TS →P.

EA system

The PES for the 4-center covalent TS formation of EA system is plotted relative to the R species as shown in **Figure 4.3a**. The PES map indicates the pseudo-

concerted mechanism of ethylene insertion. Generally, concerted reaction was defined as while one bond is breaking another bond is forming at the same time. From the PES map, *D1* and *D2* bond distances at local energy minima was started from the R at *D1* of 3.2 Å and *D2* of 2.6 Å. The *D1* was initially decreased from 3.2 Å to 2.6 Å while the *D2* of 2.6 Å was kept constant. Consequently, TS structure was formed where *D1= D2* = 2.2 Å. Afterwards, the reduction of *D1* alone had led to a formation of the stable P at *D1* of 1.6 Å. Overall, the pseudo-concerted mechanism of ethylene was defined as the *D1* and *D2* bond distances are not initially decreased at the same time at R → TS→ P states.

It can be seen that two local energy minima corresponding to the R and P were detected with a single approximate TS along the minimum energy pathway. **Figure 4.3a** shows the simplified overall relative energy profile along the chemical reaction pathway extracted from PES. It is suggested that the ethylene insertion was exothermic reaction which agreed with the experiment [59]. The newly product formed is ~13 kcal/mol more stable than the reactants.

Chulalongkorn University

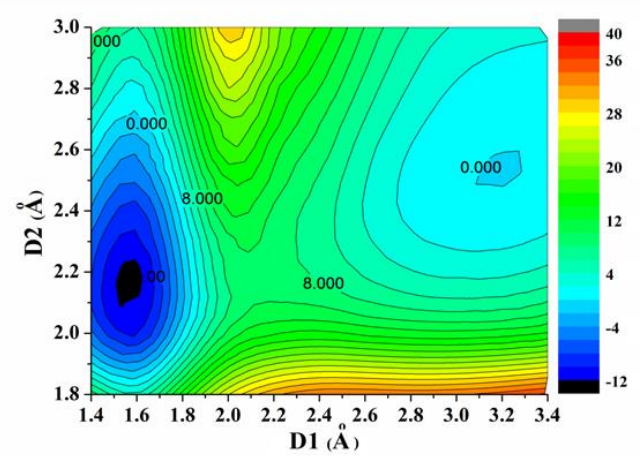

(a)

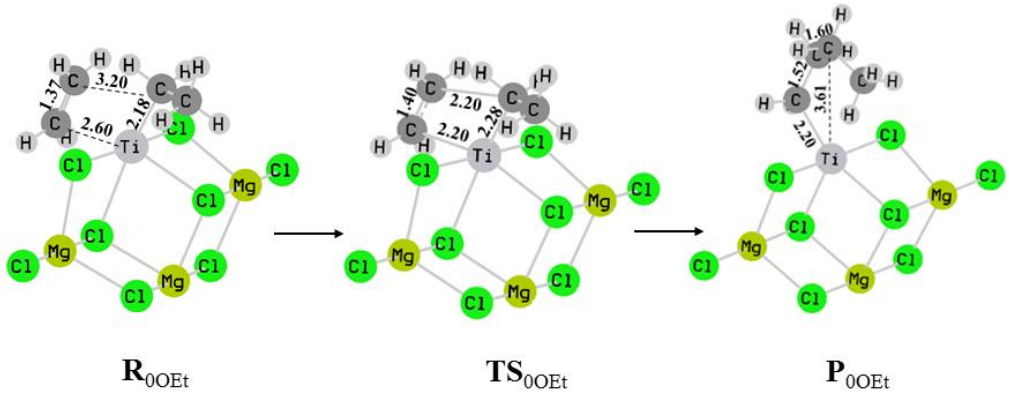

(b)

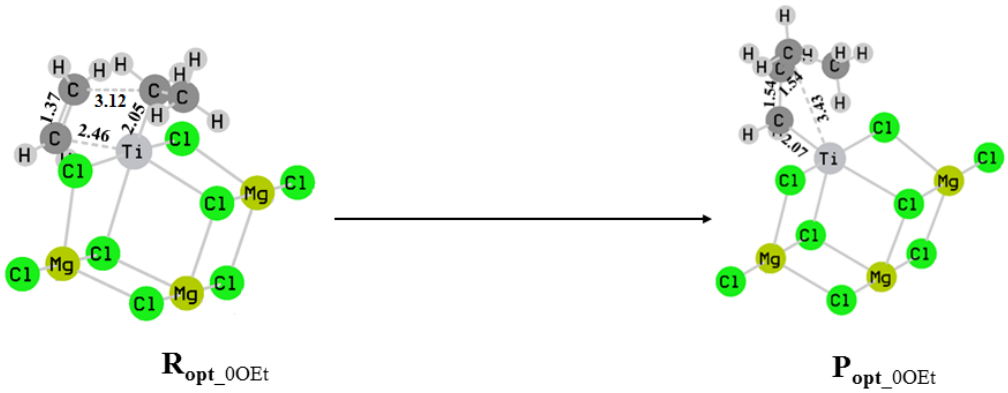

(c)

Figure 4.3 PES for ethylene insertion of EA system and covalent complex formation (**a**), The geometries of reactant (R), transition state complex (TS) and product (P) determined from PES of the EA system (**b**), Fully optimized structures of reactant and product for the EA system (**c**) running by MS

Figure 4.3b shows the partial optimized geometries of R, TS and P. It shows that the hybridization of two carbon atoms on ethylene (*i.e.* C1 and C2) were

gradually changed from sp^2 (reactant) to sp^3 (product), indicating by the increasing of bond length from 1.37 to 1.52 Å. The two forming bond distances decreased from 3.20 to 1.60 Å and 2.60 to 2.20 Å for *D1* and *D2*, respectively, during the reaction process. Meanwhile, the *Ti*-C_α distance gradually increased from 2.19 to 3.58 Å. The R and P structures taken from PES were then fully optimized **Figure 4.3c**. The obtained structures for both reactant and product were closed to those of PES with a small change in distances within 0.01 Å. Moreover, all distances of R, TS, P complexes obtained here were agreed with many works [38,60,61]. Their works were suggested the detail only bond distances from each state complex but PES map from our work can investigate the details of all bond distance between R and TS complex and TS and P complex.

EAS system

The PES of EAS systems with different 4 EDs of 1OEt, 2OEt, 3OEt and 4OEt complexes are shown in **Figure 4.4a-d.** The *D1*, *D2* and *Ti*-C_α of these two local minima for the EA and EAS systems from both partial and fully optimizations are summarized and compared in **Table 4.2** and the optimized structures are shown in **Figures 4.5-4.8**. Moreover, with presence and absence of ED, the hybridization of C1 and C2 atoms of the incoming ethylene was detected to change from sp^2 to sp^3. Note that the three important distances of optimized structures for all systems were almost unchanged when compared to the constraint distances. As the PES maps of ethylene insertion are flat along the reaction coordinate , such the linear scan was believed to be accurate enough for the identification TS complex to investigate chemical reaction

pathway R→ TS→P [43]. The energy maxima mostly obtained in the *D1*/*D2* distances range of 2.10-2.30 Å were agreed with ref. [29,38].

Table 4.2 Comparison of the *D1*, *D2* and *Ti*-C_α distances between the constraint and fully optimized structures of reactants, transition states, and products for the EA and EAS systems with different ED (*i.e.* 1OEt, 2OEt, 3OEt and 4OEt)

Systems		**Reactant**					
		***D1* (Å)**		***D2* (Å)**		***Ti*-C_α(Å)**	
		Const[a]	Opt[b]	Const	Opt	Const	Opt
EA	**0OEt**	3.20	3.2	2.60	2.6	2.2	2.2
EAS	**1OEt**	3.20	3.2	2.60	2.5	2.2	2.2
	2OEt	3.20	3.2	2.60	2.5	2.2	2.2
	3OEt	3.20	3.2	2.60	2.5	2.2	2.2
	4OEt	3.20	3.1	2.60	2.5	2.2	2.2
		Product					
EA	**0OEt**	1.60	1.5	2.20	2.2	3.6	3.6
EAS	**1OEt**	1.60	1.5	2.20	2.2	3.7	3.6
	2OEt	1.60	1.5	2.20	2.2	3.6	3.6
	3OEt	1.60	1.5	2.20	2.2	3.6	3.6
	4OEt	1.60	1.5	2.20	2.1	3.6	3.6

[a] *Constraint structures* [b]*Fully optimized structures*

Chulalongkorn University

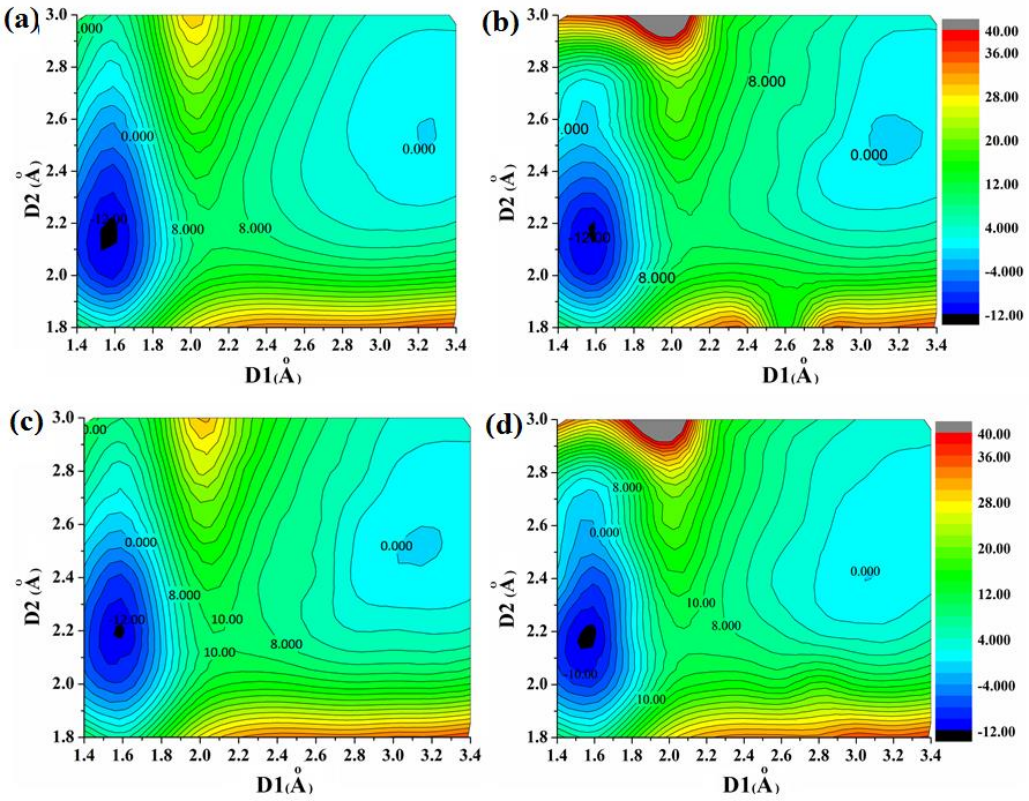

Figure 4.4 PES of the ethylene insertion for the EAS systems with presence electron donors:1OEt(**a**), 2OEt(**b**), 3OEt(**c**) and 4OEt(**d**)

Although the four PESs were somewhat different, two local energy minima with the minimum energy pathway were determined and the pseudo-concerted mechanism for the ethylene insertion was likely suggested for ethylene homopolymerization. The mechanism of the electron donors involve in the insertion reaction from PES suggested that four-centered pseudo-concerted is possible (**Figure 4.4a-d**.

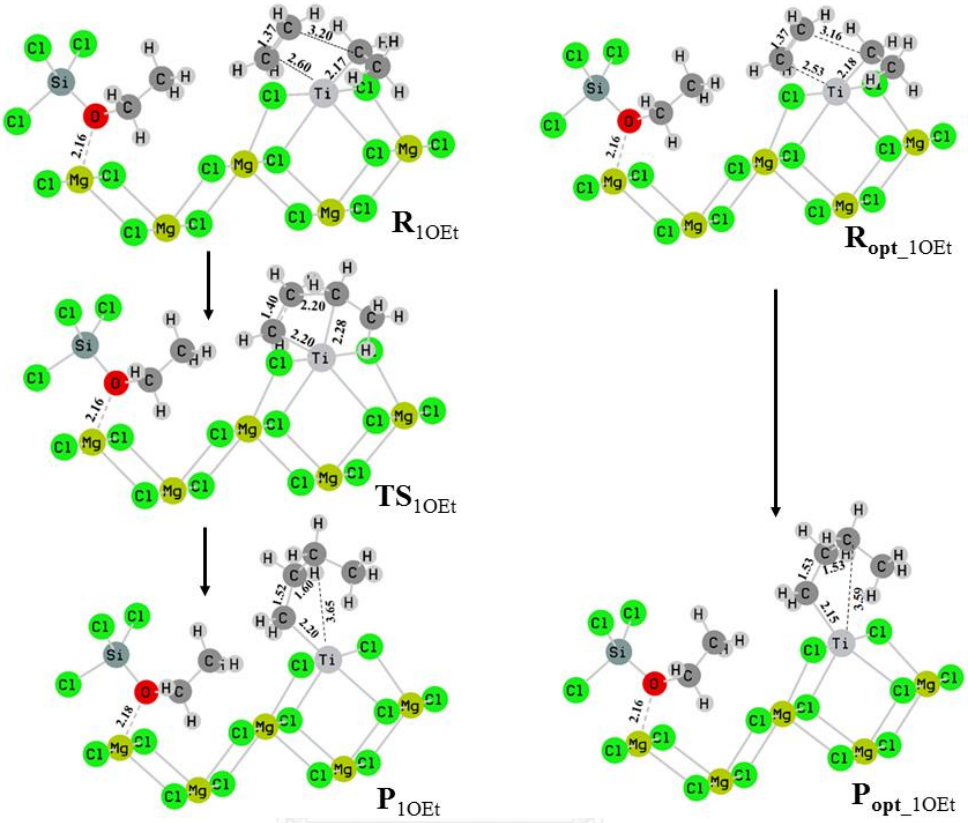

Figure 4.5 The (**a**) constraint and (**b**) fully optimized structures of reactant (R), transition state complex (TS) and product (P) taken from PES for 1OEt running by MS

จุฬาลงกรณ์มหาวิทยาลัย
CHULALONGKORN UNIVERSITY

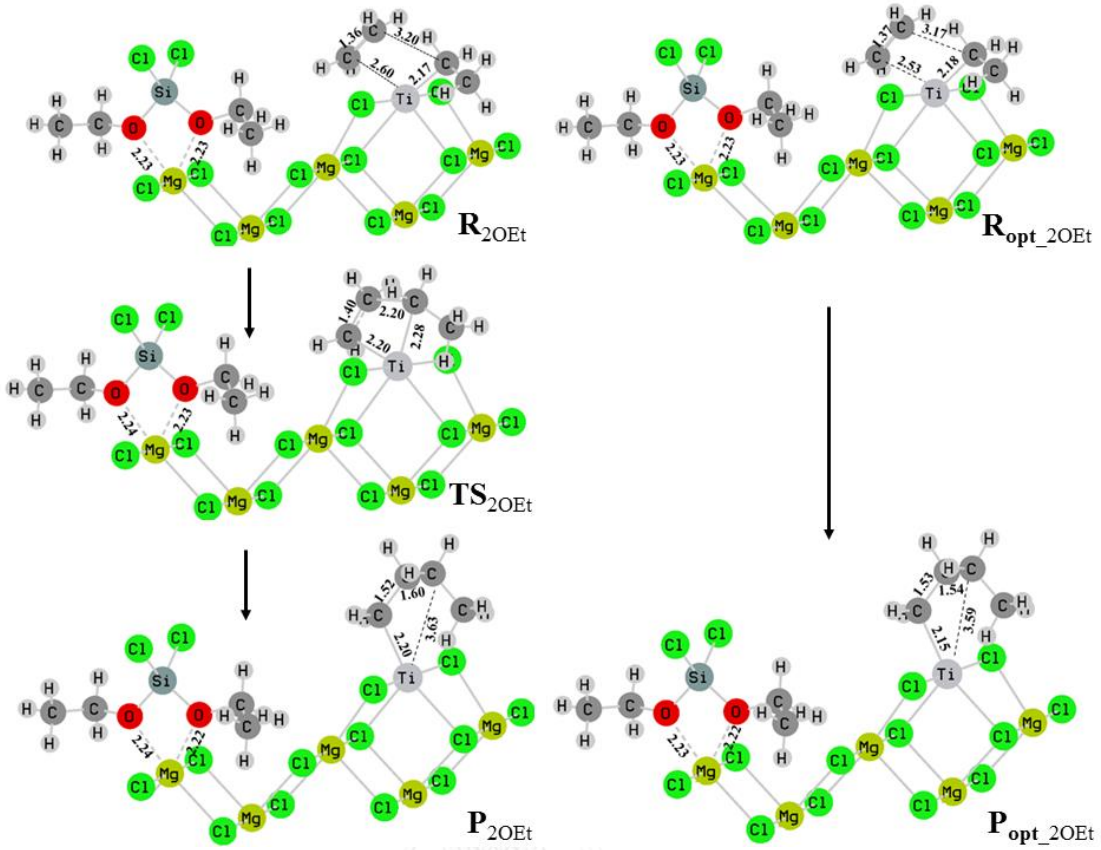

Figure 4.6 The (**a**) constraint and (**b**) fully optimized structures of reactant (R), transition state complex (TS) and product (P) taken from PES for 2OEt running by MS

Chulalongkorn University

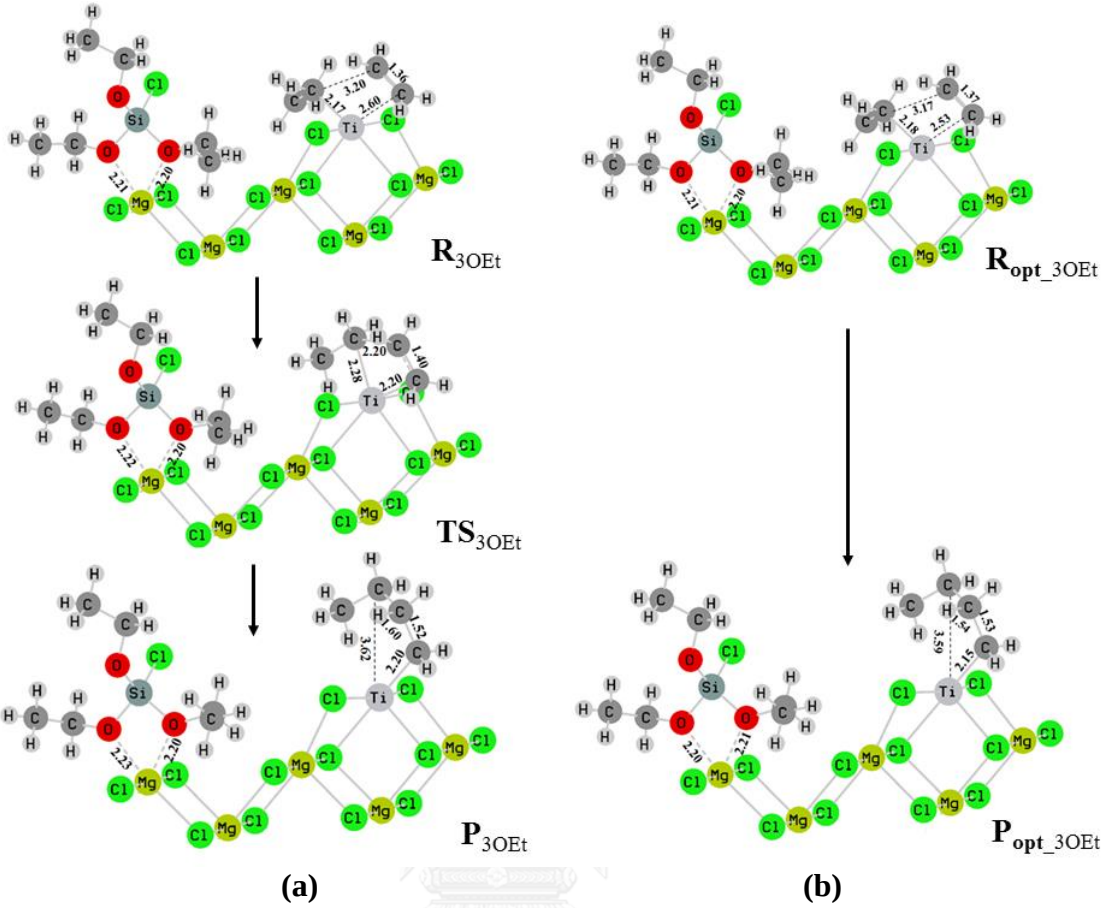

Figure 4.7 The (**a**) constraint and (**b**) fully optimized structures of reactant (R), transition state complex (TS) and product (P) taken from PES for 3OEt running by MS

จุฬาลงกรณ์มหาวิทยาลัย
Chulalongkorn University

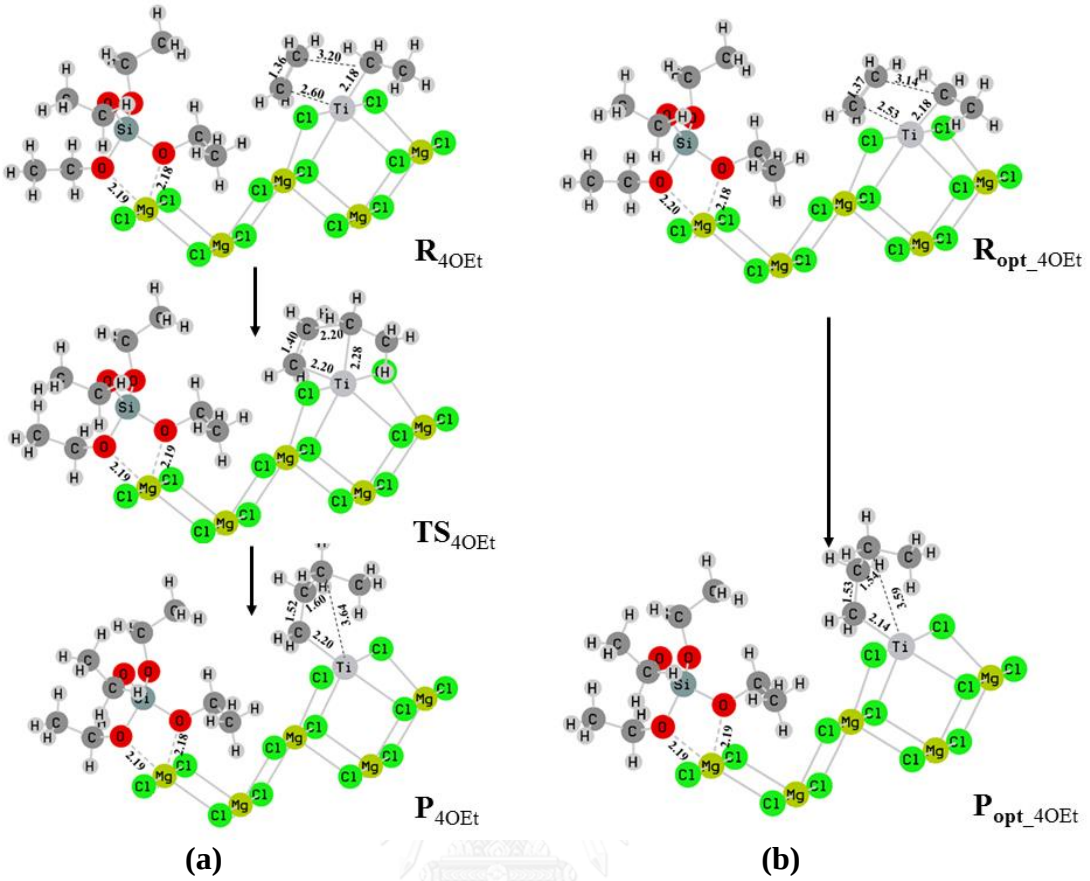

Figure 4.8 The (**a**) constraint and (**b**) fully optimized structures of reactant (R), transition state complex (TS) and product (P) taken from PES for 4OEt running by MS

จุฬาลงกรณ์มหาวิทยาลัย
Chulalongkorn University

To obtain the E_a, TS structure with one minus imaginary were searched by GUASSIAN09. The TS states with one imaginary frequency revealed the transition state of reaction coordinate whereas the structures were shown in **Figures 4.9-4.10**. The result of E_a values computed by eq. 3.7 from all systems is given in **Table 4.3**. Surprisingly, it is found that the EAS systems has similar energy barrier to the EA system. This indicated that presence of EDs in the ZNc is not significantly decreased the E_a for ethylene homopolymerization at ethylene insertion reaction step.

The results of bond distances changed from the reaction progress R →TS →P, obtained from GASSIAN09 (**Table 4.4**) were almost the same as those running by MS that in PES maps (**Table 4.2**).

Table 4.3 Bond distances changed from reactant state (R) to transition state (TS) and product (P) for all systems running by GAUSSIAN09

Systems	**Reaction States**	**Bond distances (Å)**			
		D1	***D2***	***C1-C2***	***Ti-C_α***
0OEt	R	3.12	2.46	1.37	2.05
	TS	2.24	2.22	1.4	2.24
	P	1.54	2.07	1.54	3.43
1OEt	R	3.12	2.46	1.37	2.06
	TS	2.24	2.22	1.4	2.24
	P	1.54	2.07	1.54	3.44
2OEt	R	3.12	2.46	1.37	2.06
	TS	2.25	2.22	1.4	2.24
	P	1.54	2.06	1.53	3.55
3OEt	R	3.12	2.46	1.37	2.06
	TS	2.27	2.23	1.39	2.24
	P	1.54	2.06	1.53	3.54
4OEt	R	3.11	2.46	1.37	2.06
	TS	2.25	2.22	1.4	2.24
	P	1.54	2.07	1.54	3.45

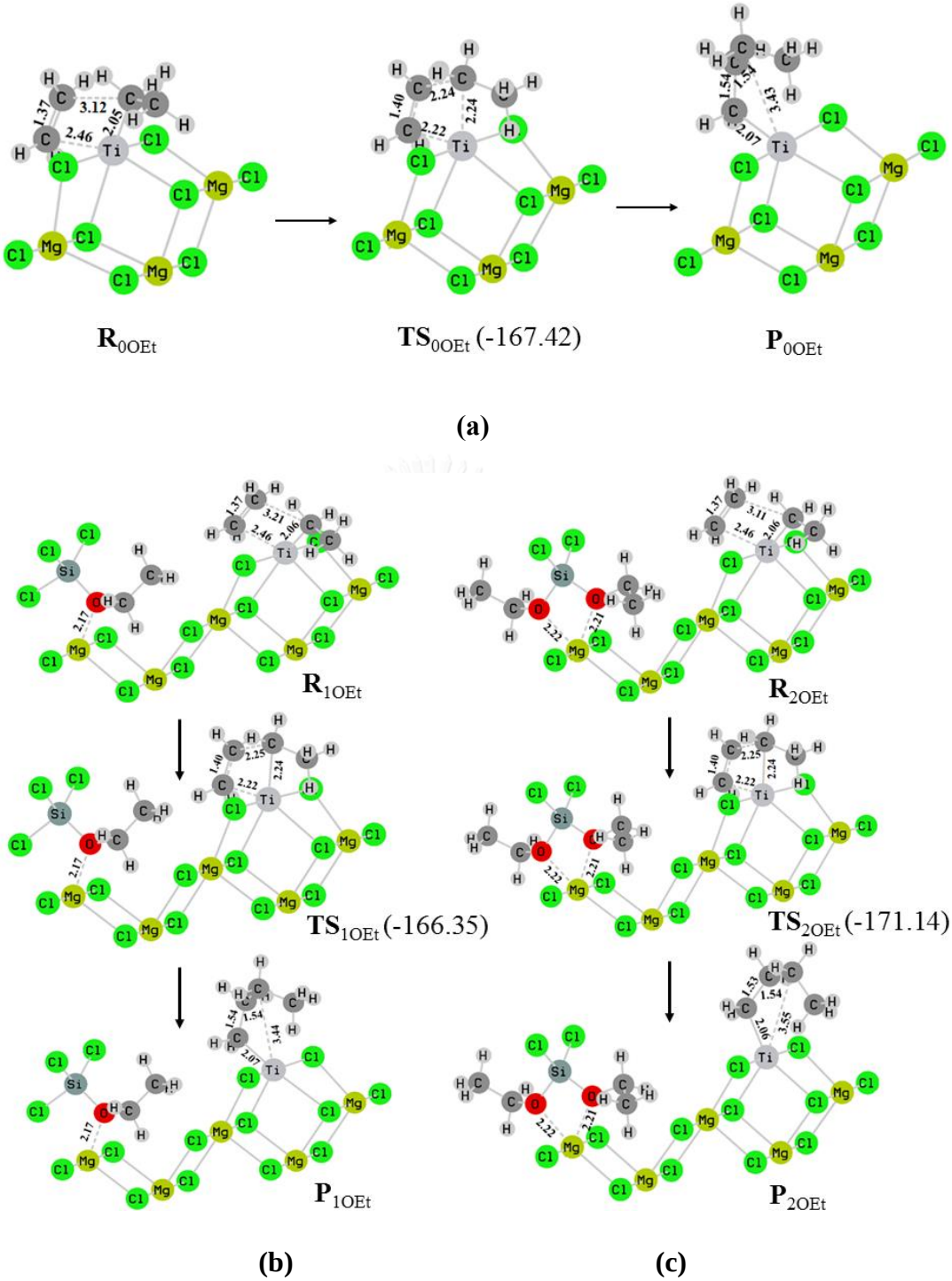

Figure 4.9 The optimized structures of reactant (R), transition state complex (TS) and product (P) for **(a)** the 1OEt system **(b)** the 1OEt and (**c**) 2OEt systems running by GAUSSIAN09

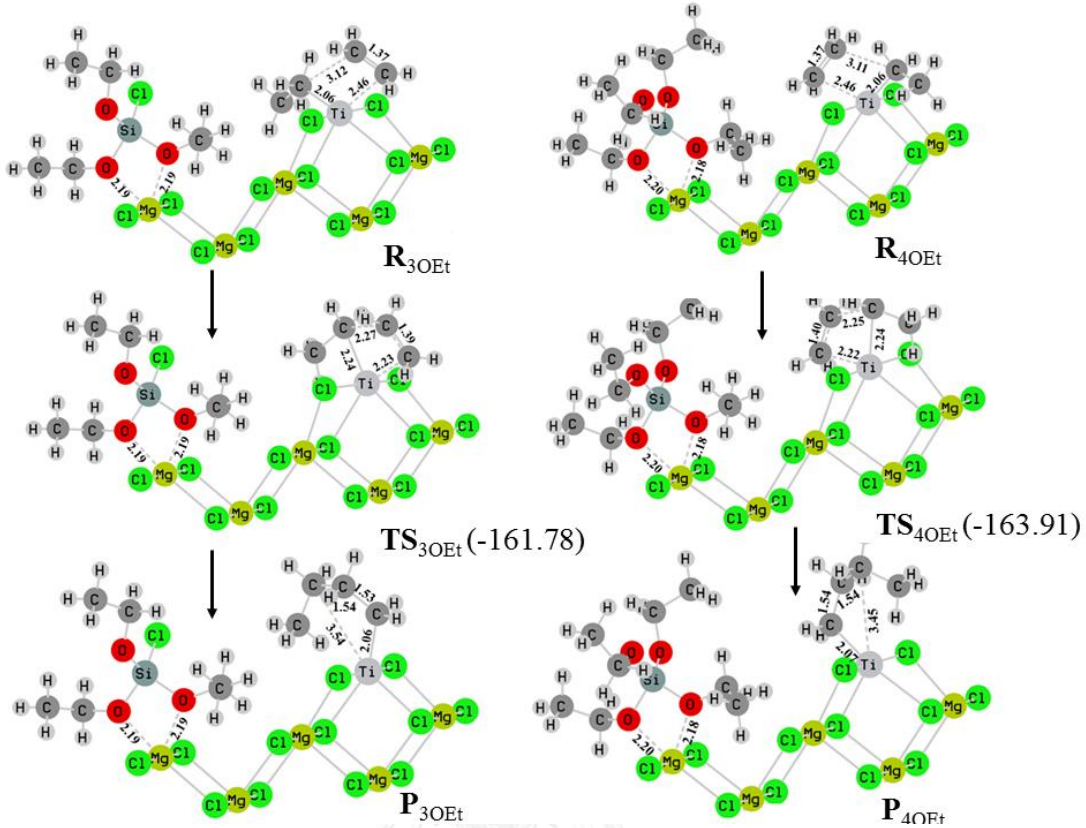

Figure 4.10 (a) The optimized structures of reactant (R), transition state complex (TS) and product (P) for the 3OEt and 4OEt systems running by GAUSSIAN09.

จุฬาลงกรณ์มหาวิทยาลัย
CHULALONGKORN UNIVERSITY

According to presence $SiCl_4$ in the ZNc system can increase the catalyst activity of ethylene homopolymerization, 4 EDs generated in the EAS system were not decreased the E_a values significantly different. This indicates that the number of OEt generated in the catalytic system is not significantly affect the energy barrier of the ethylene insertion reaction. The only E_a is not complete energy to respect system. In chemistry, E_a is the minimum enegy needed to cause a chemical reaction. A chemical reaction between two substances occurs only when molecules of one

collides with a molecule. However, the E_a of complex reactions is a combination of the activation energies of the elementary stages. This concept was called 'apparent' activation energy and used in addition to the true activation energy. In our case, 3 substances involved for the chemical reaction pathway: active catalyst, electron donor molecule, ethylene molecule. The apparent activation energy (E_{aa}) must be considered. To obtained the energy, this is computed by each elementary step

step i) adsorption energy ($\boldsymbol{E_{ads}}$) from complexation between active catalyst with electron from eq. 3.6

$$\boldsymbol{E_{ads} = E_{D.cpx} - E_D - E_{cat}} \quad (1)$$

step ii) π-complex energy ($\boldsymbol{\Delta E_{\pi}}$) from complexation between electron donor complex with ethylene molecule

$$\boldsymbol{\Delta E_{\pi} = E_{\pi cpx} - E_{D.cpx} - E_{eth}} \quad (2)$$

where $\boldsymbol{\Delta E_{\pi cpx}}$ is reactant complex energy, $\boldsymbol{E_{eth}}$ is dynamic ethylene molecule energy.

step iii) (instrinsic) activation energy ($\boldsymbol{E_a}$) from eq. 3.7

$$\boldsymbol{E_a = E_{TS} - E_{\pi cpx}} \quad (3)$$

Finally, apparent activation energy was computed by summation of eq. (1) + (2) and 3

$$\boldsymbol{E_{aa} = E_{ads} + \Delta E_{\pi} + E_a} \quad (4)$$

The results of E_{aa} values given in **Table 4.3** shown that the presence of all EDs (EAS) in the ZNc system has the lower E_{aa} than the absence ED (EA). Therefore, the role of EDs in the ZNc system to increase the catalyst activities is not significantly decreased the energy barrier at the insertion step, but for the 3 substances

complex system, stabilization of active complex from ED, E_{ads} and π-complexes energy (ΔE_{π}) must be included.

Table 4.4 The adsorption energy (E_{ads}), π-complex energy (ΔE_{π}), (intrinsic) activation energies (E_a) and apparent activation energies (E_{aa}) for the ethylene homopolymerization running by GASSIAN09

Systems	E_{ads}(kcal/mol)	ΔE_{π} (kcal/mol)	E_a (kcal/mol)	E_{aa}(kcal/mol)
ED0	*	-21.55	6.06	-15.49
ED1	-19.09	-13.60	6.04	-26.64
ED2	-29.32	-13.53	5.75	-37.09
ED3	-31.55	-15.03	6.05	-40.52
ED4	-34.41	-18.89	5.78	-47.52

In case of EAS system, the E_{aa} for insertion reaction of all ED-complexes can be found at -26.64, -37.09, -40.52 and -47.52 kcal/mol for 1OEt, 2OEt, 3OEt and 4OEt complexes, respectively (**Table 4.3**). The energy is decreased from -26.63 kcal/mol in 1OEt system to –47.52 kcal/mol in 4OEt system. The highest E_{aa} is observed for 1OEt while the lowest is found in 4OEt system. In case of 1OEt, its high E_{aa} is in accordance to those of its weakest adsorption interaction while the lowest E_{aa} for 4OEt is due to the strongest adsorption interaction. The results can be confirmed here that mixing of $Mg(OEt)_2$ with $SiCl_4$ can be possibly generated 4 types of ED: $Si(OEt)_4$, $Si(OET)_3Cl$, $Si(OEt)_2Cl_2$, $SiOEtCl_3$ lead to lowering the apparent energy barrier of the insertion reaction step of ethylene homopolymerization reaction

catalyzed by ZNc. It's seen that the completed chlorination ($Si(OEt)_4$ donor complex has the most ability to enhance the catalyst activity for this system.

4.2 Ethylene/1-hexene copolymerization

The coadsorption of ED1, ED2, ED3 and ED4; $Si(OEt)_4$, $Si(OEt)_3(O\textit{i}Pr)$, $Si(OEt)_3(O\textit{t}Bu)$ and $Si(OEt)_2(O\textit{i}Pr)(O\textit{t}Bu)$ with the two Mg sites (*A* and *B*) were indicated at the plausible location of Mg on (110) $MgCl_2$ surfaces supported $TiCl_2$-CH_2CH_3 . The interaction between O atom of ethoxy and Mg atoms which has a partial negative charge and positive charge, respectively, is electronic interaction supposed to be preferential mode of interaction. The O atom(s) from different four ED can also bind with different possible modes, *i.e.*, monodentate, bidentate and bridging modes.

4.2.1 $MgCl_2$/Donor coadsorption

Due to the asymmetric tetrahedral of OR groups bonded to silicon central atom of ED2, ED3 and ED4, the bidentate mode at Mg-*B* can possibly bind with a different pair of 2 O atoms from different OR groups. We denoted OR_1/OR_3 as a bidentate mode at Mg-*B* (**Figure 4.11**): OR_1 is denoted orientation at the same side to the R group at Ti active site, and OR_3 is denoted orientation at opposite side. The adsorption energies computed from eq. 3.6 are given in **Table 4.5**.

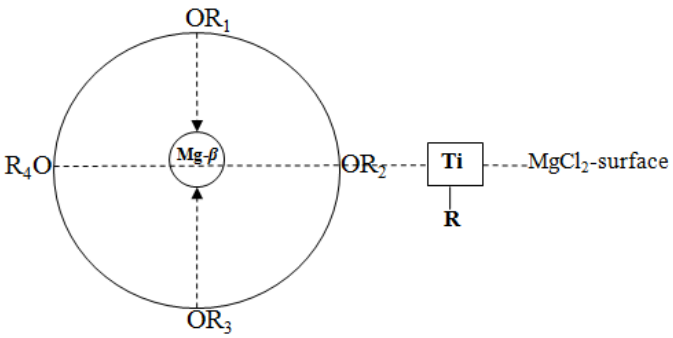

Figure 4.11 Label the bidentate mode at Mg-*B* on the (110) $MgCl_2$ surface (denoted OR_1/OR_3)

It is found that the preferential mode for all ED-complexes is bidentate mode at Mg-*B* site. The strongest bidentate mode, (OR_1/OR_3) related to the lowest adsorption energies are -33.7, -52.01, -53.12, -53.49 kcal/mol for ED1(OEt/OEt), ED2(OEt/O*i*Pr), ED3(OEt/OEt) and ED4(OEt/O*t*Bu) complexes, respectively. This result shows that forming bidentate mode by two different OR groups leads to the different ability of coadsorption. The weakest adsorption bidentate mode is found in ED1 (OEt/OEt) complex and the strongest is found in ED4 (OEt/O*t*Bu) complex. Thus, increasing the number of carbon at bidentate OR groups led to the lower adsorption energy.

Although the same bidentate OEt/OEt of the ED1 and ED3 found in the complexes, the lower E_{ads} of -19.42 kcal/mol has found in ED3 (**Figure 4.12b**). Therefore, the orientation of two uncoordinated OR_2/OR_4 group must be cared: ED1 (OEt/OEt), ED3(OEt/O*i*Bu). The lowest E_{ads} of ED3 is due to the larger of O*i*Bu at OR4 caused of stronger adsorption coadsorption.

Finally, the adsorption energies of bidentate mode for ED4 ~ED3 ~ ED2 complexes are quite similar but the highest energy is found in ED1 complex. All of the optimized structures of bidentate mode at Mg-*B* atom for ED2, ED3 and ED4: ED.$Mg_{13}Cl_{26}$.$TiCl_3$-CH_2CH_3 complexes are shown in **Figure 4.12a-c**.

To consider the bond distances between O atom from two OR1/OR3 group and Mg-*B*, we found that the Mg--O bond distances for ED4 (2.15/3.09 Å) ~ ED3(2.19/2.17 Å) < ED2 (2.18/2.17 Å) (**Figure 4.12a-c**). All of this ED-complexes structures corresponding to the lowest adsorption energy have been using to the next step, ethylene insertion.

Table 4.5 The adsorption energies *(E_{abs})* at different adsorption sites and binding modes of (110) ED.$Mg_{13}Cl_{26}$.$TiCl_3$-CH_2CH_3 (i.e. ED1, ED2, ED2 and ED4) running by MS

Systems	**Mg-site**	**Mode of Binding**	**O*R* groups**	**Adsorption energy (E_{ads}) (kcal/mol)**
ED1	*A*	monodentate	Et	-2.81
		bidentate	Et_Et	0.79
	B	monodentate	Et	-20.41
		bidentate	Et_Et	-33.7
	A_B	bridging	Et_Et	-3.28
ED2	*A*	monodentate	*i*Pr	-24.01
		monodentate	Et	-19.17
		bidentate	Et_Et	-22.57
		bidentate	Et_*i*Pr	-17.62
	B	monodentate	Et	-46.79
		monodentate	*i*Pr	-48.15
		bidentate	Et_*i*Pr	-52.01
		bidentate	Et_Et	-38.93

	A_B	bridging	Et_Et	-23.91
		bridging	*i*Pr_Et	37.14
		bridging	Et_*i*Pr	-19.22
ED3	*A*	monodentate	Et	-23.44
		monodentate	*t*Bu	-20.02
	B	monodentate	*t*Bu	-24.36
		monodentate	Et	-31.59
		bidentate	Et_*t*Bu	-50.61
		bidentate	Et_Et	-53.12
	A_B	bridging	*t*Bu_Et	-20.91
		bridging	Et_*t*Bu	-22.81
		bridging	Et_Et	-17.08
ED4	*A*	monodentate	*i*Pr	-22.77
		monodentate	Et	-24.38
		monodentate	*t*Bu	-23.47
	B	monodentate	*i*Pr	-26.24
		monodentate	*t*Bu	-23.64
		monodentate	Et	-43.58
		bidentate	Et_*i*Pr	-43.06
		bidentate	Et-*t*Bu	-53.49
		bidentate	Et_Et	-34.83
		bidentate	But_*i*Pr	-48.18
	A_B	bridging	*i*Pr_Et	-24.07
		bridging	Et_Et	-43.34
		bridging	*t*But_Et	-21.85
		bridging	Et_*t*But	-42.64
		bridging	Et_*i*Pro	-25.61

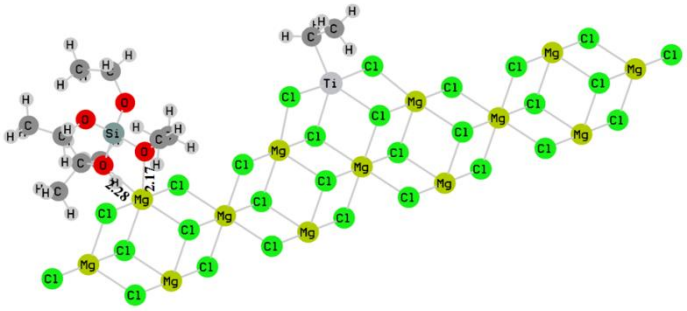

(a)

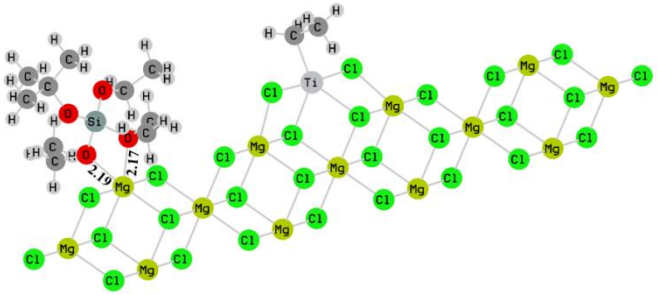

(b)

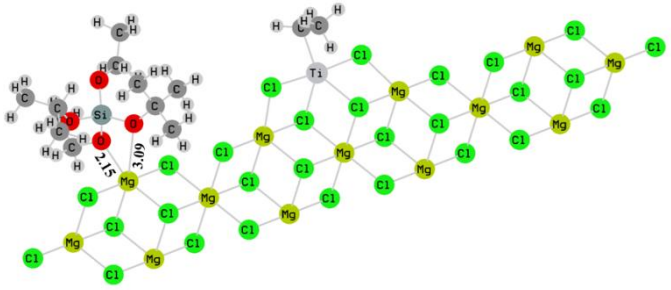

(c)

Figure 4.12 The most stable structures of (110) ED.$Mg_{13}Cl_{26}$.$TiCl_2$-CH_2CH_3 complexes :(**a**) ED2, (**b**)ED3, (**c**) ED4

4.2.2 Ethylene insertion

From the experiment result found that the fraction of 1-hexene molecule in the polymer chain product from ethylene/1-hexene copolymerization improved by presence of four alkoxysilane groups. The percent yield of triad distribution, EHE was increased in the presence of ED4 > ED3 > ED2 > ED1. Therefore, in the absence (ED0) and presence of EDs, 5 complexes were investigated: ED0, ED1, ED2, ED3 and ED4. The insertion of dynamic ethylene molecule (E) to Ti-HE (where Ti-HE = Ti-$CH_2CH(CH_2CH_3)$(*n*-Bu)) was the elementary reaction step used to investigate.

4.2.2.1 Conformation of alkyl group

We start to study this part by linear energy scan the conformation of alkyl group, -$CH_2CH(CH_2CH_3)$(*n*-But) or -HE at the growing chain where each dihedral angles Cl_1-Ti_2-C_α-C_β on the catalyst surface are labeled in the **Figure 4.13a (**inset**)**. To find the most stable conformation of -HE, dihedral angles were rotated every 20^o in the direction from 20^o to 180^o. The relative potential energy and the optimum geometrical structure are shown in **Figure 4.13b-c**. From the relative potential energy of the rotation scan, the minimum is reached at 100^o. This growing chain was further optimized and then the optimum dihedral angle is found to be at ~107^o. The geometrical structure shows that the C_α-C_β oriented out of $MgCl_2$ surface (**Figure 4.13c**). This optimum conformation is used to be the starting structure for the ethylene insertion study in the next step.

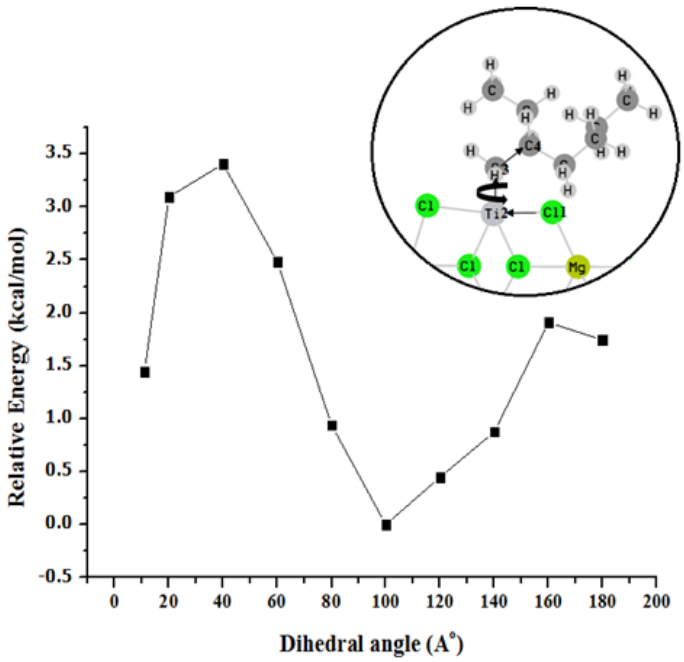

(a)

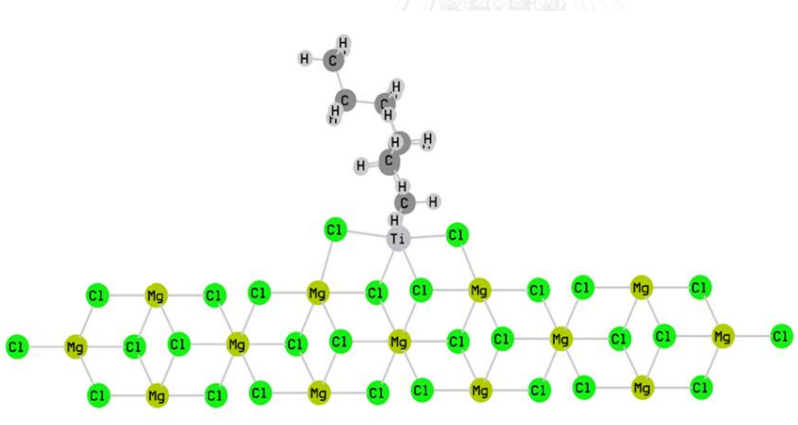

(b)

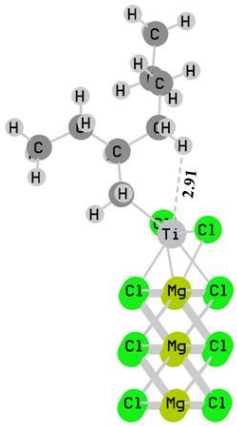

(c)

Figure 4.13 Relative energy profile vs dihedral angles of $–CH_2CH_2(CH_2CH_3)$(*n*-But) on (110) $MgCl_2$ surface and assignment of four atoms for dihedral angles for (110) $Mg_{13}Cl_{26}.TiCl_2$- $CH_2CH(CH_2CH_3)$(*n*-But) surfaces (inset) **(a)**, Fully optimized geometry of (110) $Mg_{13}Cl_{26}.TiCl_2$- $CH_2CH(CH_2CH_3)$(*n*-But) front view (**b)**, side view (**c)** running by MS

4.2.2.2 PES for absence of electron donor

We started to guess all bond distances *D1*/*D2* of R, TS and P substances by constructing PES map of ED0 system (running by MS). The local energy minima along the PES map indicated that the mechanism of ethylene (E) insertion to Ti-HE is pseudo-concerted mechanism (**Figure 4.14a).** The geometries of R→TS→ P complexes taken from the PES map with the constraint bond distance *D1*/*D2* are shown in **Figure 4.14b-1**. The constraint and fully optimized bond distances in **Figure 4.14b-2** showed the slightly different about ~0.1 Å. Therefore, to investigate the chemical reaction pathway of 5 systems running by GAUSSIAN09, the initial distances *D1*/*D2* for R, TS and P complexes are (3.20/2.60 Å), (2.20/2.20 Å) and (1.60/2.20 Å), respectively.

จุฬาลงกรณ์มหาวิทยาลัย
Chulalongkorn University

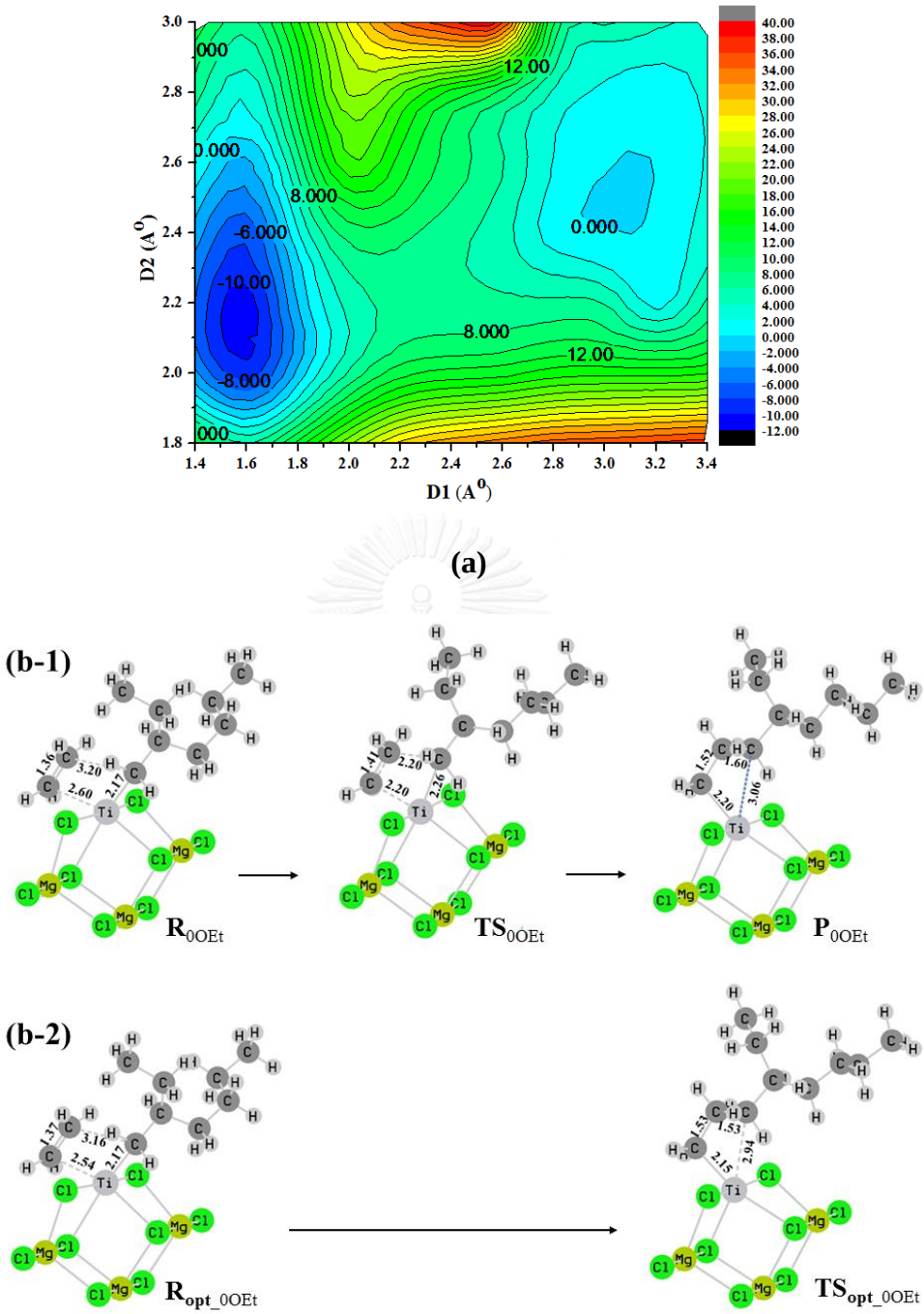

Figure 4.14 (a) Potential energy surface for ethylene insertion of ED0 (110)-$MgCl_2$ and covalent complex formation**,** **(b-1)** The constraint distance of reactant (R), transition state complex (TS) and product (P) taken from PES and **(b-2)** fully optimized structures of reactant (R_{opt}) and product (P_{opt}) running by MS

4.2.2.3 Ethylene insertion to Ti-HE

According to the most stable ED-complexes catalyst was used as initial, the different of two OR groups bidentate mode,(OR_1/OR_3) at Mg-*B* can possibly affect to the incoming ethylene molecule. Thus, the two possibilities of ethylene insertion were varied as back and front side insertion (**Figure 4.15a-b**). All geometries in the chemical reaction pathway with all systms: R→TS→P, were optimized by runing GAUSSIAN09.

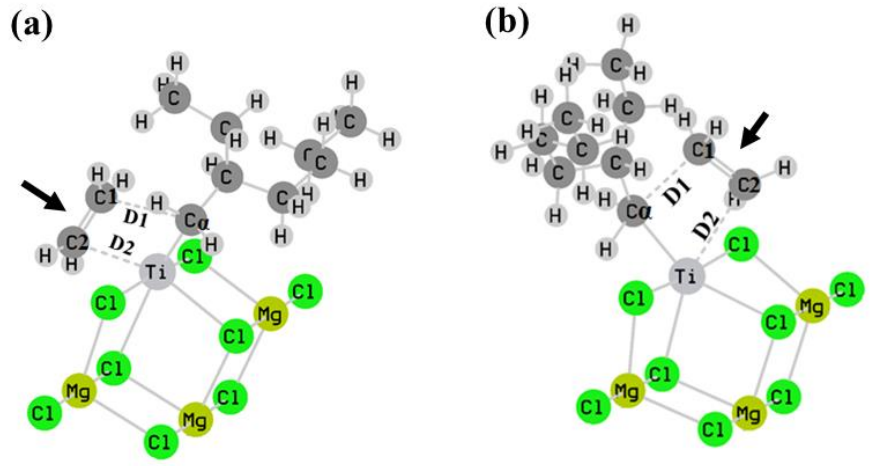

Chulalongkorn University

Figure 4.15 Definitions of the two intermolecular distances (*D1* and *D2*) between the incoming ethylene and the (110) $MgCl_2$.$TiCl_2$-$CH_2CH(CH_2CH_3)$(*n*-Bu) surface where the atoms (C_α, Ti, C1 and C2) involved in the ethylene insertion reaction are labeled (**a)** back (**b**) front

Back Insertion

At the initial π-complex or R complex, the incoming ethylene molecule forming a stable π-complexs at the *Ti-*C_α active site was considered. We found the two possible orientation of *C1-C2* double bond to *Ti-*C_α bond of π-complex were formed: parrallel and orthogonal. The ED1 π-complex alone was found the orthogonal orientataion (**Figure 4.17**), while the ED0, ED2, ED3 and ED4 π-complexes were parralleled orientation (**Figure 4.16, 4.18-4.20**). This two possible orienatation of ethylene insertion at the R state were also found from Mauro Boero *et al.* work [29]. They proposed that it can switch the orientation by little or no barrier existses between them.

The bond distances *D1*/*D2* at the R states were also determined. In case of stable ED0, ED2, ED3 and ED4 π-complexes, the bond distances of *D1* is 3.12 to 3.16 Å and *D2* is 2.46 to 2.47 Å. Furthermore, the bond distances of stable ED1 orthogonal π-complexe are 2.46 Å for C1-Ti and 2.47 Å for C2-Ti (**Table 4.6**). Moreover, the bond distances of SiO--Mg kept small changed within ~0.01 Å from the ED-complexes to the π-complexes. This indicated that the ED have been binding on the (110) $MgCl_2$ surface catalyst along this two state.

Next, the TS complexes were considered. Although the orientation of incoming ethylene molecule of ED1 system at the R complex is orthogonal, it is turned to the parallel orienatation at TS state as a 4-center covalent bond finally (**Figure 4.17**). For ED0, ED2, ED3 and ED4, all TS complexes are formed 4-center covalent bonds (**Figures 4.16, 4.18-4.21**). To confirm TS structure, one frequecy imaginary from all systems were labeled in **Figures 4.16-4.21**. The bond distances

changed from R→TS are given in **Table 4.6**. The TS-complexes are formed by decreasing *D1*/*D2* and increaing *Ti*-C_α/*C1*-*C2* bond distances. We found that the distances of *D1* is 2.34-2.24 Å, *D2* is 2.22-2.27 Å, *Ti*-C_α is 2.12-2.24 Å and *C1*-*C2* is 1.39-1.40 Å in all cases.

Lastly, the P complexes were determined. **Figures 4.17-4.20** and **Table 4.6** are shown all geometries and bond distances changed from R → TS → P complexes. From R→P complexes, they show that the hybridization of two carbon atoms on ethylene (*i.e.* C1 and C2) were gradually changed from sp^2 (reactant) to sp^3 (product), indicating by the increasing of bond length from ~1.37 to ~1.52 Å. Additionally, *D1* and *D2* bond distances decreasing from R→ P of ED0, ED2, ED3 and ED4 systems are ~3.12 → ~1.55 Å and ~2.56 → ~2.07 Å, respectively. For R→P of ED1 π-complex, (C1-Ti) is changed from 2.46 →2.27 Å and (C2-Ti) is changed from 2.47 Å to (C2-C_α) 2.34 Å. Meanwhile, for all systems, the *Ti*-C_α distance gradually increased from ~2.19 to ~3.58 Å.

จุฬาลงกรณ์มหาวิทยาลัย
Chulalongkorn University

Table 4.6 Bond distances changed from reactant (R) to transition state (TS) and product (P) of back insertion of ethylene for all systems running by GAUSSIAN09

Systems	**Substances**	**Bond distances (Å)**					
		C1-Ti	*C2-Ti*	*D1*	*D2*	*C1-C2*	*Ti-*C_α
ED0	R			3.12	2.46	1.37	2.05
	TS			2.24	2.22	1.4	2.24
	P			1.54	2.07	1.54	3.43
ED1	R	2.47	2.46	*	*	1.37	2.02
	TS	2.27	2.49	2.34	2.27	1.39	2.12
	P	*	*	1.55	2.05	1.54	2.77
ED2	R			3.26	2.5	1.37	2.07
	TS			2.3	2.25	1.4	2.14
	P			1.55	2.05	1.54	2.76
ED3	R			3.15	2.46	1.37	2.07
	TS			2.34	2.27	1.39	2.12
	P			1.54	2.05	1.54	2.76
ED4	R			3.16	2.47	1.37	2.06
	TS			2.34	2.27	1.39	2.12
	P			1.55	2.05	1.54	2.76

จุฬาลงกรณ์มหาวิทยาลัย
CHULALONGKORN UNIVERSITY

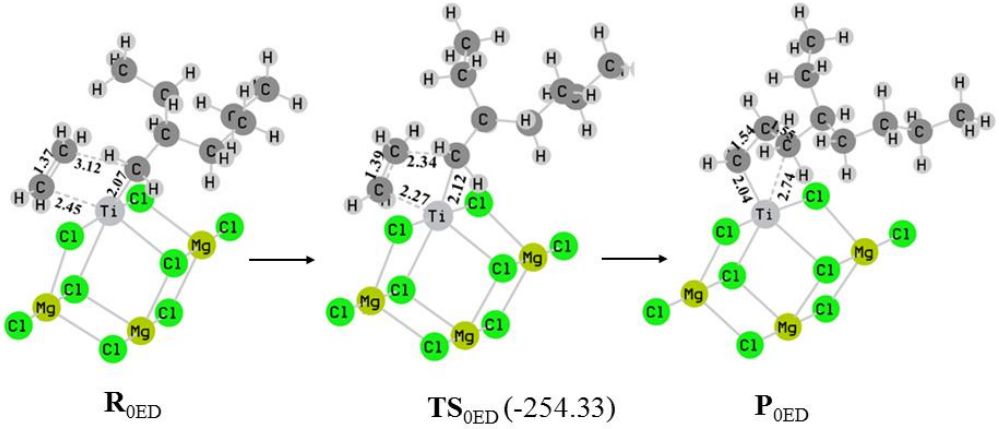

Figure 4.16 The various states of the ethylene insertion of **ED0** system. The approaching of an ethylene to the Ti active center on $Mg_{13}Cl_{26}.TiCl_2.CH_2CH(Et)$(*n*-But) (**$R_{ED0}$**), the π-complex form as the reactant state, (**TS_{ED0}**) the 4-center covalent bond shortening and elongation as the transition state and (**P_{ED0}**) the product state running by GASSIAN09

To overcome the TS energy, the (instrinsic) activation energies, E_a computed by eq.3.6 were obtained in **Table 4.7**. We found that the E_a values was decreased as ED0 > ED1 > ED2 > ED3 > ED4, respectively. These results was agreed well with experimental data.

Table 4.7 The (intrinsic) activation energies (E_a) and imaginary frequency values running by GAUSSIAN09

Systems	Ethylene insertion	E_a (kcal/mol)	imaginary frequency (cm^{-1})
ED0	*	7.04	-254.33
ED1	*back*	6.74	-254.56
	Front	5.83	-196.76
ED2	*back*	5.14	-171.85
	Front	4.96	-268.36
ED3	*back*	5.77	-252.18
	Front	3.85	-207.89
ED4	*back*	3.17	-256.38
	Front	3.57	-206.71

**back and front has the same geometry*

Front insertion

Next, we investigated the ethylene molecule insertion to the front of Ti-HE. Interestingly, the orientation of *C1-C2* double bond of incoming ethylene molecule to the *Ti-*C_α bond for ED3 and ED4 complex at the R state are orthogonal (**Figures 4.20-4.21**) while ED0, ED1, ED2 are parallel. All bond distances from R $\rightarrow$ TS $\rightarrow$ P complexes are given in **Table 4.8**. The bond decreasing and increasing of *D1*, *D2*, *C1-C2* and *Ti-*C_α in **Table 4.8** are confirmed the chemical reaction. The E_a values of ethylene insertion to the front side of Ti-HE is in the order ED4 < ED3 < ED2 < ED1 < ED0 complexes, respectively (**Table 4.7**). This result was agreed well with the

experimental data. This result shows that the ethylene insertion to the Ti-HE was activated by the presence of ED to the ZNc system.

Table 4.8 Bond distances changed from reactant state (R) to transition state (TS) and product (P) for back ethylene insertion from all systems running by GAUSSIAN09

Systems	**States**	**Bond Distances (Å)**					
		C1-Ti	***C2-Ti***	***D1***	***D2***	***C1-C2***	***Ti-C_α***
ED1	R	*	*	3.14	2.46	1.37	2.04
	TS	*	*	2.26	2.22	1.4	2.06
	P	*	*	1.55	2.04	1.54	2.78
ED2	R	*	*	3.13	2.46	1.37	2.04
	TS	*	*	2.28	2.24	1.4	2.06
	P	*	*	1.56	2.82	1.55	2.57
ED3	R	2.42	2.46	*	*	1.37	2.04
	TS	*	*	2.23	2.22	1.4	2.06
	P	*	*	1.55	2.04	1.54	2.82
ED4	R	2.43	2.47	*	*	1.37	2.04
	TS	*	*	2.24	2.22	1.4	2.06
	P	*	*	1.54	2.04	1.54	2.84

We can summarize and explain the ethylene insertion for all 4 ED complexes that the E_a for both sides insertion is in the order of ED4 < ED3 < ED2 < ED1 < ED0. This can conclude that in the presence of EDs can enhance the activity of ZNc system. However, among the presence EDs system, the favorable of incoming ethylene insertion to the front and back to the Ti-C active center was different. The energy barrier for back/front side ethylene insertion of ED1, ED2, ED3 and ED4 systems can be found (6.74/5.83), (5.14/4.96), (5.77/3.85) and (3.17/3.57) kcal/mol, respectively.

This result is shown that the incoming ethylene insertion is favor in the front side for the ED1, ED2 and ED3 systems. Contrary, the back side insertion is favor for ED4 system. The highest barrier is found in ED1 system (back side insertion) while the lowest is found in ED4 system (back side insertion). In case of ED1, its highest energy barrier is in accordance to those of its weakest adsorption interaction. For the lowest barrier of ED4 is corresponded to the strongest adsorption of ED4. For ED2 and ED3 complexes, ethylene insertion are favor to the front side of Ti-C accordance to the less steric repulsion between dynamic ethylene molecules and OEt (OR_3) moiety of the coadsorbed donor part **Figure 4.18-4.19**. The high E_a values of ED1 and ED2 complexes indicated the less favorable of ethylene insertion for both direction to the Ti-C active center. However, ED3 has the moderate active catalyst due to the significant low E_a, 3.85 kcal/mol from the front side ethylene insertion compared to the front side, 5.77 kcal/mol.

จุฬาลงกรณ์มหาวิทยาลัย
Chulalongkorn University

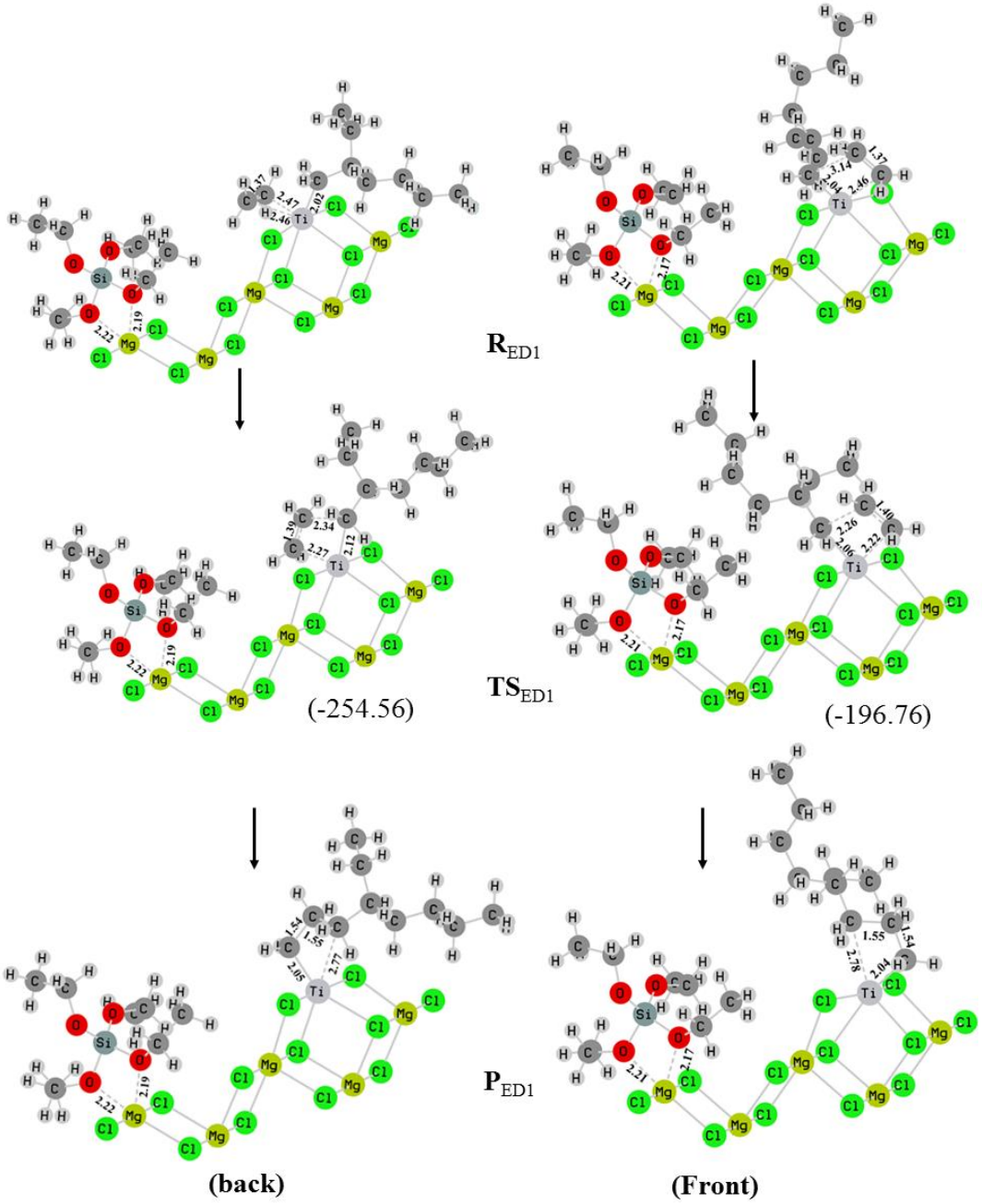

Figure 4.17 The various states of the back and front ethylene insertion of ED1 system. The approaching of an ethylene to the Ti active center on $Si(OEt)_4.Mg_{13}Cl_{26}.TiCl_2.CH_2CH_2(CH_2CH_3)$(*n*-Bu) complex, the π-complex form as the reactant state ($\mathbf{R}_{ED1}$), the 4-center covalent bond transition state ($\mathbf{TS}_{ED1}$) and as the product state ($\mathbf{P}_{ED1}$) running by GAUSSIAN09

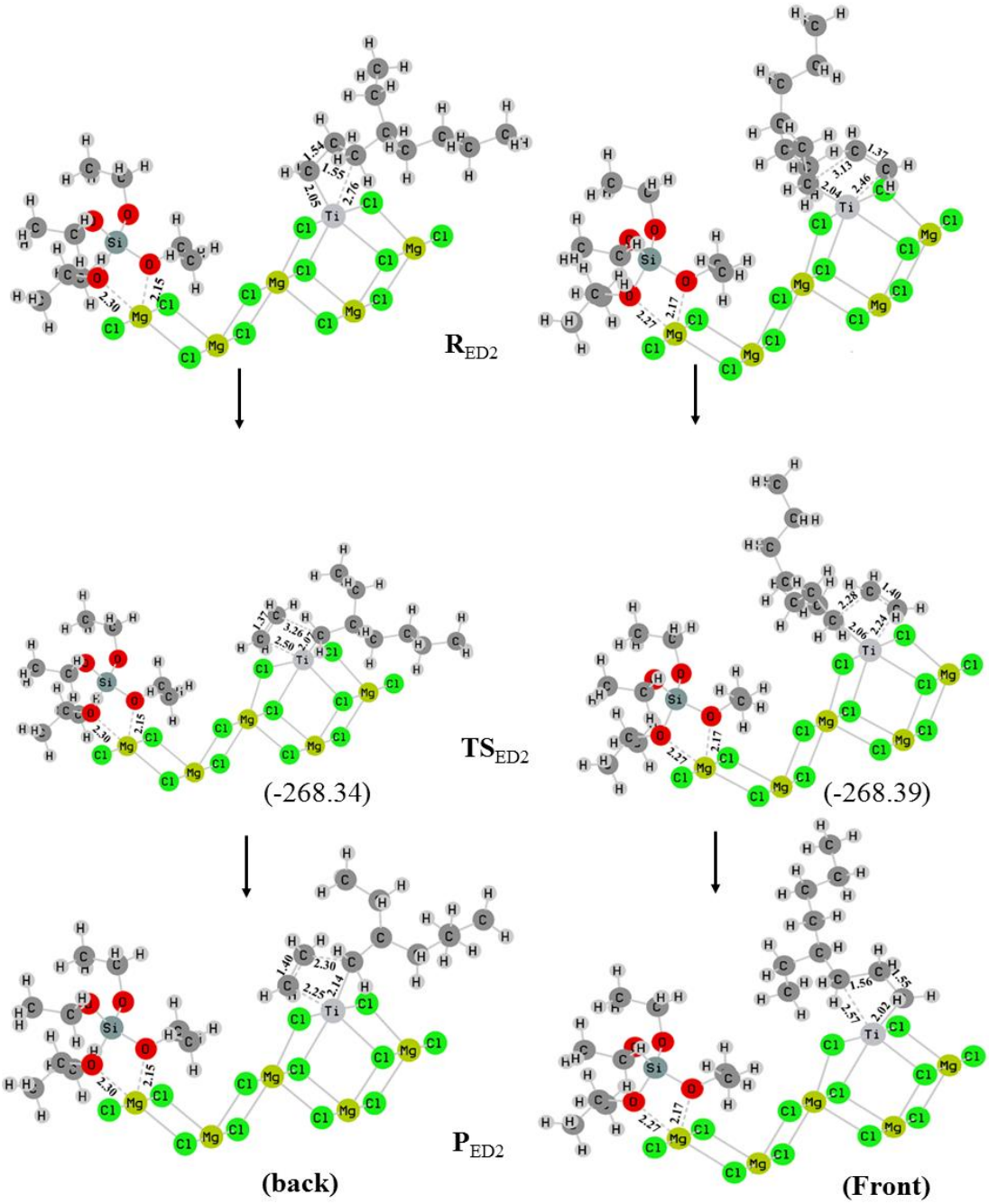

Figure 4.18 The various states of the back and front ethylene insertion of ED2 system. The approaching of an ethylene to the Ti active center on $Si(OEt)_3(OiPr).Mg_{13}Cl_{26}.TiCl_2.CH_2CH_2(Et)(n\text{-}Bu)$ complex, the π-complex form as the reactant state ($\mathbf{R}_{ED2}$), the 4-center covalent bond as the transition state ($\mathbf{TS}_{ED2}$) and as the product state ($\mathbf{P}_{ED2}$) running by GAUSSIAN09

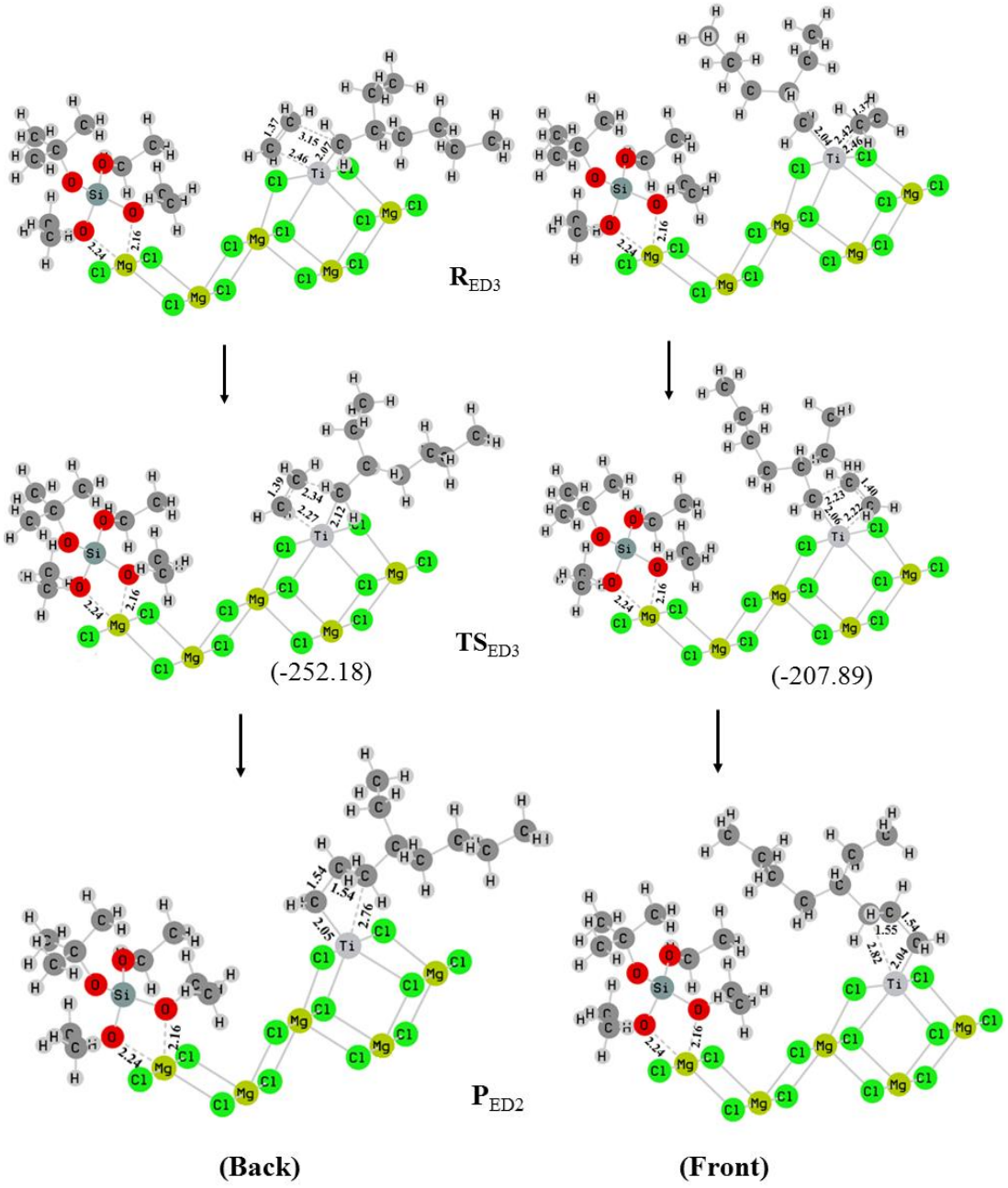

Figure 4.19 The various states of the back and front ethylene insertion of **ED3** system. The approaching of an ethylene to the Ti active center on $Si(OEt)_3(OtBu).Mg_{13}Cl_{26}.TiCl_2.CH_2CH_2(CH_2CH_3)(n\text{-}Bu)$ complex, the π-complex form as the reactant state ($\mathbf{R}_{ED3}$), the 4-center covalent bond as the transition state ($\mathbf{TS}_{ED3}$) and as the product ($\mathbf{P}_{ED3}$) running by GASSIAN09

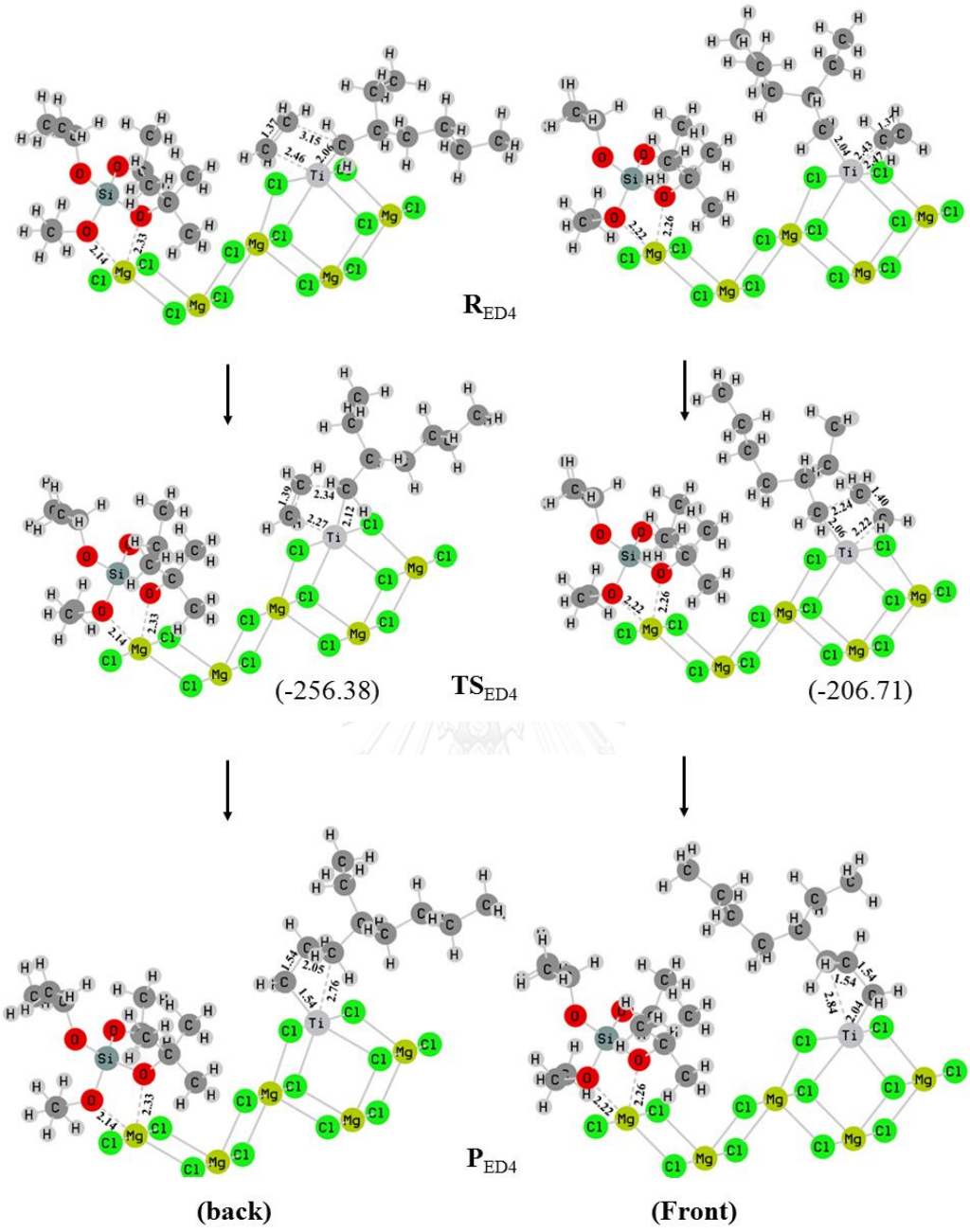

Figure 4.20 The various states of the back and front ethylene insertion of **ED4** system. The approaching of an ethylene to the Ti active center on $Si(OEt)_2(O\textit{t}Bu)(O\textit{i}Pr).Mg_{13}Cl_{26}.TiCl_2.TiCl_2.CH_2CH_2(CH_2CH_3)(\textit{n}\text{-}Bu)$ complex, the π-complex form as the reactant state ($\mathbf{R}_{ED4}$), the 4-center covalent bond as the transition state ($\mathbf{TS}_{ED4}$) and as the product state ($\mathbf{P}_{ED4}$) running by GAUSSIAN09

CHAPTER V
CONCLUSIONS

The DFT calculations have been carried out to investigate the ethylene insertion pathway using Ziegler-Natta catalyst with presence and absence of electron donors for ethylene homopolymerization and ethylene/1-hexene copolymerization on the (110) $MgCl_2$ surface.

For ethylene homopolymerization, the adsorption energy (E_{ads}) was that $Si(OEt)_4$ molecule is the strongest coadsorbed on (110) $MgCl_2$ surface. The bidentate mode is more preferential than those of monodentate and bridging modes for the rest coadsorbed molecules. The results from PES map indicated that the reaction mechanism of ethylene insertion is pseudo-concerted mechanism. The (intrinsic) activation energy indicated that in the presence and absence of all electron donors had a similar energy barrier. However, the apparent activation energy (E_{aa}) with the presence of all electron donors was lower than the absence of electron donor. In the presence electron donor, the E_{aa} was decreased in order of, $Si(OEt)Cl_3$, $Si(OEt)_2Cl_2$, $Si(OEt)_3Cl$ and $Si(OEt)_4$, respectively. Therefore, we assumed that within the presence of electron donors, the completed chlorination, $Si(OEt)_4$, is the most active electron donor for the ethylene homopolymerization in the Ziegler-Natta catalytic system.

For ethylene/1-hexene copolymerization, the adsorption energy was shown that all electron donors have the preferential coadsorption bidentate mode on (110) $MgCl_2$ surface. The two preferential oxygen atoms for $Si(OEt)_4$, $Si(OEt)_3(O\textit{i}Pr)$, $Si(OEt)_3(O\textit{t}Bu)$, $Si(OEt)_2(O\textit{t}Bu)(O\textit{i}Pr)$ are (OEt/OEt), (OEt/*i*Pr), (OEt/OEt) and

OEt/O*i*Bu), respectively. The strongest coadsorption was in $Si(OEt)_2(O$*t*$Bu)(O$*i*$Pr)$ donor. The PES map for the absence of electron donor revealed that the mechanism of ethylene insertion to Ti-HE is pseudo-concerted reaction. The ethylene insertion to Ti-HE shows that the C-C double bond orientation was possibly form a π-complex in either orthogonal or parallel to the Ti-C active site. According to experimental data, $Si(OEt)_2(O$*t*$Bu)(O$*i*$Pr)$ has the most active catalyst to enhance the fraction of 1-hexene molecule in the polymer chain more than $Si(OEt)_3(O$*t*$Bu)$, $Si(OEt)_3(O$*i*$Pr)$ and $Si(OEt)_4$, respectively. Not surprise that the lowest E_a found in the presence of $Si(OEt)_2(O$*t*$Bu)(O$*i*$Pr)$ with the corresponding to the highest adsorption energy. Moreover, the geometry of $Si(OEt)_2(O$*t*$Bu)(O$*i*$Pr)$ complex along the reaction pathway structures revealed that the dynamic ethylene molecule is strongly favor insertion to the both side of Ti-C at the active center. However, for $Si(OEt)_3(O$*t*$Bu)$ donor complex , the dynamic ethylene insertion is significant favor only from the less repulsion between ethylene molecule and steric alkoxy bidentate coadsorbed donor (OEt). For the least active catalyst $Si(OEt)_4$ donor was explained by the highest barrier which corresponding to the lowest coadsorption energy.

Chulalongkorn University

REFERENCES

[1] Breslow, D. S.; Newburg, N. R. *Journal of the American Chemical Society* **1957**, *79*, 5072-5073.

[2] Britovsek, G. J. P.; Bruce, M.; Gibson, V. C.; Kimberley, B. S.; Maddox, P. J.; Mastroianni, S. *et al. Journal of the American Chemical Society* **1999**, *121*, 8728-8740.

[3] Ittel, S. D.; Johnson, L. K.; Brookhart, M. *Chemical Reviews* **2000**, *100*, 1169-1204.

[4] Möhring, P. C.; Coville, N. J. *Journal of Organometallic Chemistry* **1994**, *479*, 1-29.

[5] Brintzinger, H. H.; Fischer, D.; Mülhaupt, R.; Rieger, B.; Waymouth, R. M. *Angewandte Chemie International Edition in English* **1995**, *34*, 1143-1170.

[6] Alt, H. G.; Köppl, A. *Chemical Reviews* **2000**, *100*, 1205-1222.

[7] Coates, G. W. *Chemical Reviews* **2000**, *100*, 1223-1252.

[8] Resconi, L.; Cavallo, L.; Fait, A.; Piemontesi, F. *Chemical Reviews* **2000**, *100*, 1253-1346.

[9] Kissin, Y. V.; Mink, R. I.; Nowlin, T. E. *Journal of Polymer Science, Part A: Polymer Chemistry* **1999**, *37*, 4255-4272.

[10] Yamamoto, K.; Ishihama, Y.; Sakata, K. *Journal of Polymer Science Part A: Polymer Chemistry* **2010**, *48*, 3722-3728.

[11] Small, B. L.; Brookhart, M.; Bennett, A. M. A. *Journal of the American Chemical Society* **1998**, *120*, 4049-4050.

จุฬาลงกรณ์มหาวิทยาลัย
Chulalongkorn University

[12] J. P. Britovsek, G.; C. Gibson, V.; J. McTavish, S.; A. Solan, G.; J. P. White, A.; J. Williams, D. *et al. Chemical Communications* **1998**, 849-850.

[13] Wang, L.; Ren, H.; Sun, J. *Journal of Applied Polymer Science* **2008**, *108*, 167-173.

[14] Ma, L.; Sheng, Y.; Huang, Q.; Zhao, Y.; Deng, K.; Li, J. *et al. Journal of Polymer Science Part A: Polymer Chemistry* **2008**, *46*, 33-37.

[15] Chen, X.; Liu, D.; Wang, H. *Macromolecular Reaction Engineering* **2010**, *4*, 342-346.

[16] Monaco, G.; Toto, M.; Guerra, G.; Corradini, P.; Cavallo, L. *Macromolecules* **2000**, *33*, 8953-8962.

[17] Taniike, T.; Terano, M. *Macromolecular Rapid Communications* **2007**, *28*, 1918-1922.

[18] Busico, V.; Corradini, P.; De Martino, L.; Proto, A.; Savino, V.; Albizzati, E. *Die Makromolekulare Chemie* **1985**, *186*, 1279-1288.

[19] Liu, B.; Nitta, T.; Nakatani, H.; Terano, M. *Macromolecular Chemistry and Physics* **2003**, *204*, 395-402.

[20] Liu, Z.; Zhang, X.; Huang, H.; Yi, J.; Liu, W.; Liu, W. *et al. Journal of Industrial and Engineering Chemistry* **2012**, *18*, 2217-2224.

[21] Smith, G. M.; Tirendi, C. F.; Amata, R. J.; Band, E. I. *Inorganic Chemistry* **1993**, *32*, 1161-1166.

[22] Giannini, U. *Die Makromolekulare Chemie* **1981**, *5*, 216-229.

จุฬาลงกรณ์มหาวิทยาลัย
Chulalongkorn University

[23] Credendino, R.; Busico, V.; Causa, M.; Barone, V.; Budzelaar, P. H. M.; Zicovich-Wilson, C. *Physical Chemistry Chemical Physics* **2009**, *11*, 6525-6532.

[24] Busico, V.; Causà, M.; Cipullo, R.; Credendino, R.; Cutillo, F.; Friederichs, N. *et al. The Journal of Physical Chemistry C* **2008**, *112*, 1081-1089.

[25] Barbé, P.; Cecchin, G.; Noristi, L. In *Catalytical and Radical Polymerization*; Springer Berlin Heidelberg: 1986; Vol. 81, p 1-81.

[26] Ziegler, K. *Angewandte Chemie* **1964**, *76*, 545-553.

[27] Natta, G. *Chim. Ind. (Milan)* **1964**, *46*.

[28] Ettore, G.; Di, D. G.; Ermanno, S.; Paolo, G.; Adolfo, M.; Montedison: 1972.

[29] Boero, M.; Parrinello, M.; Terakura, K. *Journal of the American Chemical Society* **1998**, *120*, 2746-2752.

[30] Seth, M.; Margl, P. M.; Ziegler, T. *Macromolecules* **2002**, *35*, 7815-7829.

[31] Seth, M.; Ziegler, T. *Macromolecules* **2003**, *36*, 6613-6623.

[32] Puhakka, E.; Pakkanen, T. T.; Pakkanen, T. A. *Surface Science* **1995**, *334*, 289-294.

[33] Corradini, P. B., Vincenzo; Fusco, Roberto; Guerra, Gaetano *Gazzetta Chimica Italiana* **1983**, *113*, 9-10.

[34] Chien, J. C. W.; Bres, P. L. *Journal of Polymer Science Part A: Polymer Chemistry* **1986**, *24*, 2483-2505.

จุฬาลงกรณ์มหาวิทยาลัย
Chulalongkorn University

[35] Magni, E.; Somorjai, G. A. *Catal Lett* **1995**, *35*, 205-214.

[36] Stukalov, D. V.; Zakharov, V. A. *The Journal of Physical Chemistry C* **2009**, *113*, 21376-21382.

[37] Bahri-Laleh, N.; Nekoomanesh-Haghighi, M.; Mirmohammadi, S. A. *Journal of Organometallic Chemistry* **2012**, *719*, 74-79.

[38] Cavallo, L.; Guerra, G.; Corradini, P. *Journal of the American Chemical Society* **1998**, *120*, 2428-2436.

[39] Cossee, P. *Journal of Catalysis* **1964**, *3*, 80-88.

[40] Arlman, E. J.; Cossee, P. *Journal of Catalysis* **1964**, *3*, 99-104.

[41] Arlman, E. J. In *Proc. Int. Congr. Catal. 3rd* 1964; Vol. 2, p 957.

[42] Busico, V.; Causa, M.; Cipullo, R.; Credendino, R.; Cutillo, F.; Friederichs, N. *et al. The Journal of Physical Chemistry C* **2008**, *112*, 1081-1089.

[43] Correa, A.; Piemontesi, F.; Morini, G.; Cavallo, L. *Macromolecules* **2007**, *40*, 9181-9189.

[44] Boero, M.; Parrinello, M.; Weiss, H.; Hüffer, S. *Journal of Physical Chemistry A* **2001**, *105*, 5096-5105.

[45] Studio, M. In *Materials Studio*; release 5.5 ed.; Accelrys Software San Diego, CA, 2009.

[46] Delley, B. *The Journal of Chemical Physics* **1990**, *92*, 508-517.

[47] Perdew, J. P.; Burke, K.; Ernzerhof, M. *Physical Review Letters* **1996**, *77*, 3865-3868.

จุฬาลงกรณ์มหาวิทยาลัย
Chulalongkorn University

[48] Dolg, M.; Wedig, U.; Stoll, H.; Preuss, H. *The Journal of Chemical Physics* **1987**, *86*, 866-872.

[49] Fujimoto, H.; Yamasaki, T.; Mizutani, H.; Koga, N. *Journal of the American Chemical Society* **1985**, *107*, 6157-6161.

[50] Sakai, S. *The Journal of Physical Chemistry* **1991**, *95*, 175-178.

[51] Sakai, S. *The Journal of Physical Chemistry* **1991**, *95*, 7089-7093.

[52] Sakai, S. *The Journal of Physical Chemistry* **1994**, *98*, 12053-12058.

[53] Jensen, V. R.; Borve, K. J.; Ystenes, M. *Journal of the American Chemical Society* **1995**, *117*, 4109-4117.

[54] Armstrong, D. R.; Perkins, P. G.; Stewart, J. J. P. *Journal of the Chemical Society, Dalton Transactions* **1972**, 1972-1980.

[55] Novaro, O.; Chow, S.; Magnouat, P. *Journal of Catalysis* **1976**, *41*, 91-100.

[56] Giunchi, G.; Clementi, E.; Ruiz-Vizcaya, M. E.; Novaro, O. *Chemical Physics Letters* **1977**, *49*, 8-12.

[57] Novaro, O.; Blaisten-Barojas, E.; Clementi, E.; Giunchi, G.; Ruiz-Vizcaya, M. E. *The Journal of Chemical Physics* **1978**, *68*, 2337-2351.

[58] Fujimoto, H.; Koga, N.; Fukui, K. *Journal of the American Chemical Society* **1981**, *103*, 7452-7457.

[59] Vasile, C. *Handbook or polyolefins*; 2 ed. Romania, 2000.

จุฬาลงกรณ์มหาวิทยาลัย

[60] Bernardi, F.; Bottoni, A.; Miscione, G. P. *Organometallics* **1998**, *17*, 16-24.

[61] Mukhopadhyay, S.; Kulkarni, S. A.; Bhaduri, S. *Journal of Molecular Structure: THEOCHEM* **2004**, *673*, 65-77.

จุฬาลงกรณ์มหาวิทยาลัย
Chulalongkorn University

APPENDIX

จุฬาลงกรณ์มหาวิทยาลัย
Chulalongkorn University

VITA

Biography: Mr.Sutiam Kruawan

Date of Birth: 16 October 1978

Place of Birth: Surin, Thailand

Education

1983-1988 Primary school at Pratoonayong School, Surin

1989-1991 Secondary school at Taelsiriwittaya School, Surin

1992-1994 High school at Surawittayakarn School, Surin

1995-1998 B.Sc. in Chemistry at Mahasarakham Univeristy, Mahasarakham

2004-2006 M.Sc in Chemistry at Chulalongkorn University, Bangkok, thesis: ‘Synthesis of Indoaniline derived calix[4]arenes as alkali cation sensors’

since 2009 Ph. D. study at the Department of chemistry, Chulalongkorn University, Bangkok

จุฬาลงกรณ์มหาวิทยาลัย
Chulalongkorn University